1986

A Theoretical And Experimental Investigation Of Coke Gasification In A Batch Reactor

Esmail R. Monazam

INFORMATION TO USERS

While the most advanced technology has been used to photograph and reproduce this manuscript, the quality of the reproduction is heavily dependent upon the quality of the material submitted. For example:

- Manuscript pages may have indistinct print. In such cases, the best available copy has been filmed.

- Manuscripts may not always be complete. In such cases, a note will indicate that it is not possible to obtain missing pages.

- Copyrighted material may have been removed from the manuscript. In such cases, a note will indicate the deletion.

Oversize materials (e.g., maps, drawings, and charts) are photographed by sectioning the original, beginning at the upper left-hand corner and continuing from left to right in equal sections with small overlaps. Each oversize page is also filmed as one exposure and is available, for an additional charge, as a standard 35mm slide or as a 17"x 23" black and white photographic print.

Most photographs reproduce acceptably on positive microfilm or microfiche but lack the clarity on xerographic copies made from the microfilm. For an additional charge, 35mm slides of 6"x 9" black and white photographic prints are available for any photographs or illustrations that cannot be reproduced satisfactorily by xerography.

Monazam, Esmail R.

A THEORITICAL AND EXPERIMENTAL INVESTIGATION OF COKE GASIFICATION IN A BATCH REACTOR

West Virginia University PH.D. 1986

PLEASE NOTE:

In all cases this material has been filmed in the best possible way from the available copy. Problems encountered with this document have been identified here with a check mark ✓.

1. Glossy photographs or pages _____
2. Colored illustrations, paper or print _____
3. Photographs with dark background _____
4. Illustrations are poor copy _____
5. Pages with black marks, not original copy ✓
6. Print shows through as there is text on both sides of page _____
7. Indistinct, broken or small print on several pages ✓
8. Print exceeds margin requirements _____
9. Tightly bound copy with print lost in spine _____
10. Computer printout pages with indistinct print _____
11. Page(s) _____ lacking when material received, and not available from school or author.
12. Page(s) _____ seem to be missing in numbering only as text follows.
13. Two pages numbered _____. Text follows.
14. Curling and wrinkled pages _____
15. Dissertation contains pages with print at a slant, filmed as received ✓
16. Other _____

_____

_____

University
Microfilms
International

A THEORITICAL AND EXPERIMENTAL INVESTIGATION OF COKE GASIFICATION IN A BATCH REACTOR

DISSERTATION

Submitted to the Graduate School

of

West Virginia University

In Partial Fulfillment of the Requirements for

The Degree of Doctor of Philosophy

by

Esmail R. Monazam
M.S M.E

Morgantown

West Virginia

1986

ACKNOWLEDGMENT

I would like to express my sincere appreciation, gratitude and thanks to my advisor Dr. Eric K. Johnson who has guided me throughout the course of this research with his wisdom, patience and encouragement. I would also like to extend my deep appreciation to Dr. John W. Zondlo for his invaluable remarks and help during the course of this study. Appreciation also is extended to the other members of the committee including Dr. Eugene V. Cilento, Dr. Charles F. Stanley, Dr. Massood Ramezan, and Dr. John T. Jurewicz for their help, and expert criticism.

The author wishes to express his thanks to the Energy Research Center for their financial support during the first three years of this project and to the Mechanical & Aerospace Engineering Department for their financial support during the fourth and final year.

The author is extremely grateful to James W. Collins for his help and numerous contributions to this dissertation, and to Sherry D. Carder for her brilliant and tireless typing of the dissertation manuscript.

Special thanks are extended to Mehdi Haeri and his wife Barbra Haeri. Their friendship and support were essential to the completion of this dissertation and were much appreciated.

Finally, I want to acknowledge my family, especially my mother and father. You have been a source of love, motivation and inspiration. I love you all very much!

ABSTRACT

A computer model has been developed to simulate the char-gasification process occurring in the gasification component of a crossflow coal gasifier. This process corresponds to the batch gasification process in a combustion pot. Temperature and concentration profiles along the gasifier were obtained by solving the material and energy balances.

In order to obtain the data necessary for evaluating and improving the computer model, an experimental system was developed to obtain data for the char-gasification process in the combustion pot. The results show that the gasification rate strongly depends on the air flow rate and that the reactivity of the char has a strong effect on the output gas composition.

The results from the computer model were compared with available literature data on the fixed-bed gasifier and the experimental data obtained from this study, and were found to be in good agreement.

A sensitivity analysis was performed on the input parameters (heat transfer coefficient, void fraction, particle diameter, and reactivity factor coefficients) of the computer model. The results show the importance of the input parameters in predicting the desired gas composition and total process time.

TABLE OF CONTENTS

LIST OF TABLES

LIST OF FIGURES

NOMENCLATURE

a - contact area between solid and gas per unit volume of bed

$$a = \frac{6(1-\epsilon)}{d_p} \qquad (cm^2/cm^3)$$

a_{ij} - molar stoichiometric coefficient of reactant gas species j in recation i

A - pre-exponential factor for K_s of C-O$_2$ reaction

A_b - cross-sectional area of the bed (cm^2)

A_g - total flow area of the gas in the bed (cm^2)

A_s - total surface area of the solid in the bed (cm^2)

A'_t - transfer area per unit depth of the bed (cm)

b_{ij} - molar stoichiometric coefficient of product gas species j in reaction i

C_{pg} - specific heat of gas (cal/g ^{o}K)

C_s - specific heat of solid (cal/g^{o}K)

D - diffusivity (cm^2/sec)

d_p - particle diameter (cm)

E - activation energy (cal/mol)

h - the convective heat transfer between gas and solid (cal/cm sec ^{o}K)

h_n - the empirical heat transfer coefficient for nonreactive systems (cal/cm sec ^{o}K)

h_o - initial guess value for the step size (cm) or (sec)

H_j - total enthalpy of gas species j (cal/gm)

$\hat{H}_j$ - molar enthalpy of gas species j (cal/g-mol)

ΔH_5 - heat of reaction of water-gas shift reaction (cal/gm)

K_{ash} - ash diffusion rate constant (gm/cm^2.sec.atm)

k_e - local effective heat conductivity of gas species (Kj/sec-cm-$^\circ$K)

K_{eq} - equilibrium constant

K_o - pre-exponential factor for equilibrium constant

K_g - gas film reaction rate constant (gm/cm^2.sec.atm)

K_{over} - overall kinetic constant, defined by Eq. (3.16)

K_s - surface reaction rate constant (gm/cm^2.sec.atm)

K_v - volumetric reaction rate (gmol/sec-cm^3)

$\dot{m}''_g$ - local mass flux of gas species (gm/sec cm^2)

$\tilde{M}_c$ - molecular weight of carbon (gm/gm-mole)

$\dot{M}''_G$ - gasification rate (gm/sec cm^2)

$\dot{M}''_j$ - total mass flux of gas species j (gm/sec cm^2)

$\tilde{MW}_j$ - molecular weight of gas species j (gm/gm-mole)

N - total number of gas species involved in gasification reactions

$P_j - P_j^*$ - effective partial pressure of j-component (atm)

P_t - total pressure (atm)

$\dot{R}''_i$ - reaction rate of reaction i (gm/sec-cm^2)

$\dot{R}''_1$ - rate of char-oxygen reaction

$\dot{R}''_2$ - rate of char-steam reaction

$\dot{R}''_3$ - rate of char-carbon dioxide reaction

$\dot{R}''_4$ - rate of char-hydrogen reaction

$\dot{R}''_5$ - water-gas shift reaction rate (gmol/sec-cm^2)

R_p - particle radius (cm)

r_c - core radius (cm)

r_s - solid radius (cm)

$\bar{R}$ - gas constant (cal/mol $^\circ$K)

t - time (sec)

T_g - gas phase temperature ($^\circ$K)

T_m - mean temperature ($^\circ$K)

T_s - solid phase temperature (^oK)

U_g, U_s - internal energy of gas and solid respectively (cal/gm K)

$\forall$ - volume of particle (cm^3)

V_g - gas velocity (cm/sec)

X_c - carbon conversion

x - damping coefficient

y - system axis (cm)

Z - molar ratio of carbon monoxide to carbon dioxide

% - percentage by volume in section 7.3.5

Greek letters

γ_{ij} - mass stoichiometric coefficient of reactant gas species j in reaction i

δ - the change in variables (section 7.3.5)

ϵ - void fraction between gas and solid

ζ - proportional factor for the gas-solid heat transfer coefficient of the coke bed

η_1 - reactivity factor coefficient for K_s of char-carbon dioxide reaction

η_2 - reactivity factor coefficient for K_s of char-steam reaction

λ - fractional contribution of the energy released from the water-gas shift reaction to the ash products of solid phase

μ - viscosity of local gas (gm/sec-cm)

ν_{ij} - mass stoichiometric coefficient of product gas species j in reaction i

ξ - fraction of the particle radius which is occupied by unreacted char

ρ_g - gas density (gm/cm^3)

ρ_s - solid density (gm/cm^3)

ϕ - mechanism factor

$\Tau$ - total burning time (min)

Subscripts

b - refered to bed

c - refered to particle's core

g - refered to gas phase

i - ith gas-solid reactions

ij - refered to gas species j in reaction i

j - refered to gas species

o - reference point

s - refered to solid phase

Superscripts

" - per unit area

' - per unit depth

. - per unit time

~ - per unit mole

1. MODELING AND SIMULATION OF CROSSFLOW COAL GASIFICATION

1.1 Introduction

The gasifier is the heart of any coal gasification process and has a significant influence on the economics of the process. According to an economic study conducted by the Bureau of Mines (1), nearly 30% of the total capital cost of a large capacity gasification plant is required for the gasifiers. When considering the large expenditures required for the initial investment, the importance of optimizing the gasifier design becomes clear. Thus, this is the primary motive for many gasification modeling and simulation studies. Because the economics of the entire coal gasification process depends heavily on the gasifier's performance, considerable effort has been given to developing accurate models for the various gasification processes.

At present, commercial coal gasification systems are size limited in that the commercial gasification systems have only been successfully operated upto a maximum fuel consumptions rate. Thus, in order to supply a large quantity of gases from coal, it has been necessary to employ a large number of coal gasification reactors. The apparent advantage of a crossflow coal gasification system is that it is not size

limited, as very large systems of this type have been operating in the taconite industry without any apparent size limitation effects having been observed. Thus one or two crossflow reactors could represent a significant cost reduction over other gasification processes currently in use.

When compared with the different types of gasification processes, crossflow coal gasification has not received a significant amount of attention. The crossflow coal gasification concept represents an old technology that may have the potential to become the most acceptable gasification process in the future, due to recent technological developments.

The basic sketch illustrating the crossflow coal gasifier is shown in Figure 1.1. The coal is shown entering the pyrolysis chamber as the the surface of the coal is ignited by a gas flame, thus establishing a combustion zone. As the combustion zone travels downward through the bed of coal, the hot gases produced will gasify the coal. When the combustion zone approaches the protective mineral matter layer (limestone, crushed bricks, etc), two options are possible. One, the combustion zone may consume the remaining carbon in the pyrolysis chamber or two, the traveling bed could enter the steam-char reaction chamber. The last chamber cools the ash and provides heated air for the process.

FIGURE 1.1: CROSSFLOW COAL GASIFICATION

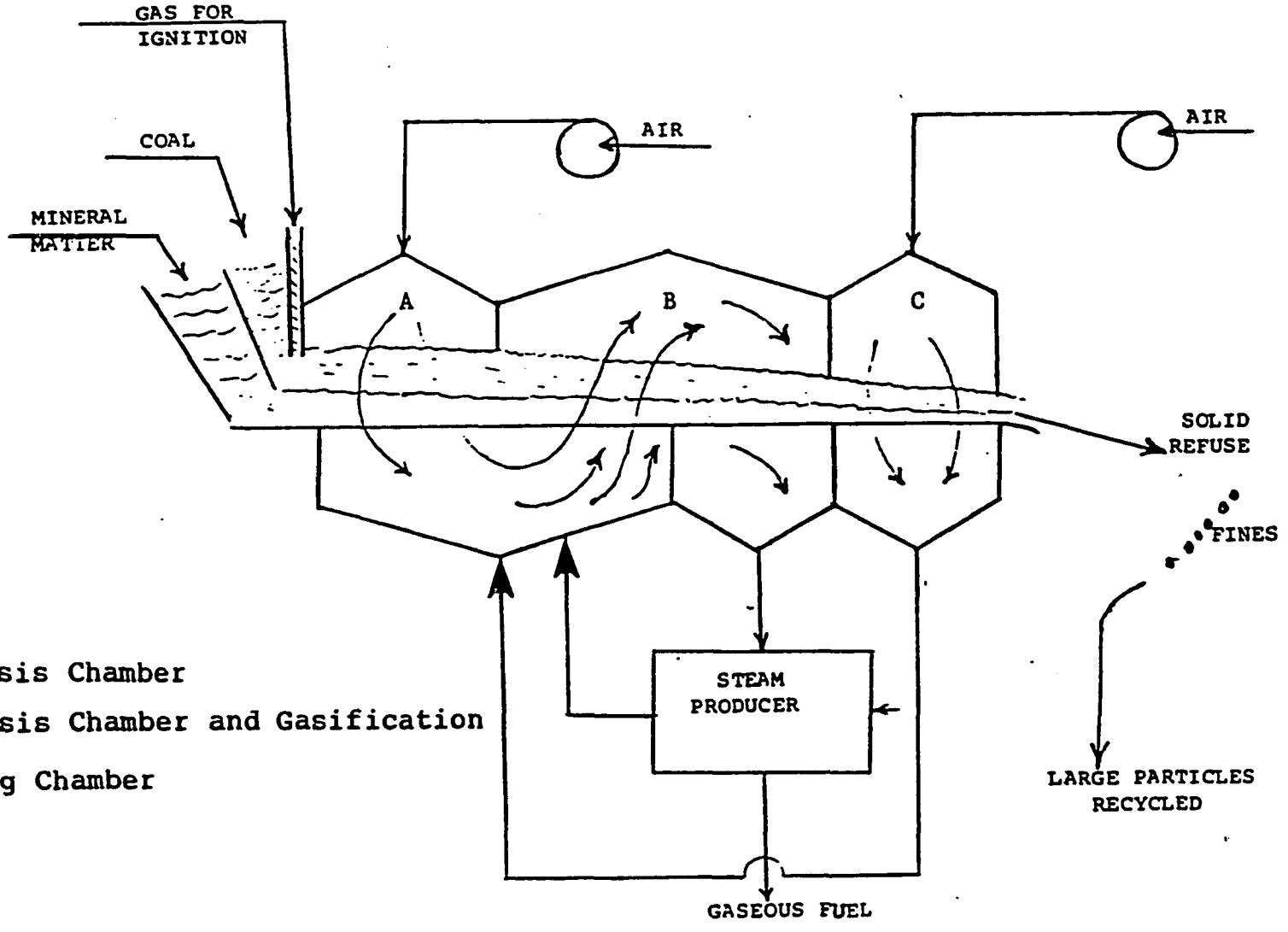

A Pyrolysis Chamber

B Pyrolysis Chamber and Gasification

C Cooling Chamber

Figure 1.2 illustrates a more complex crossflow coal gasification concept. Green pellets are used as fuel instead of regular coal. The green pellets may consist of a wet mixture of ground coal and limestone and a small amount of binder. These green pellets are then dried and sent to a sulfur-fixation chamber where partial pyrolysis occurs. In this chamber, sulfur reacts with the mineral matter within the coal to form relatively stable, sulfur containing, chemical compounds. The pellets can either continue through the pyrolysis chamber, completing the gasification-combustion process or they may enter a steam-char reaction chamber to complete the gasification. The last chamber is the cooling chamber in which the ash, mineral matter, and inert gases are cooled by heat exchange with ambient air. The heated air is recycled back to the drying chamber. The obvious advantage of this complex process is that a large percentage of the coal sulfur remains in the product ash, and is not emitted into the product gas.

1.2 Objectives

The specific objectives of this study were to develop a computer model to simulate the char-gasification process for the combustion pot test and to build and run an experimental system to verify the model.

The objectives of the computer modeling effort were to

FIGURE 1.2: CLEAN GAS CROSSFLOW COAL GASIFICATION CONCEPT

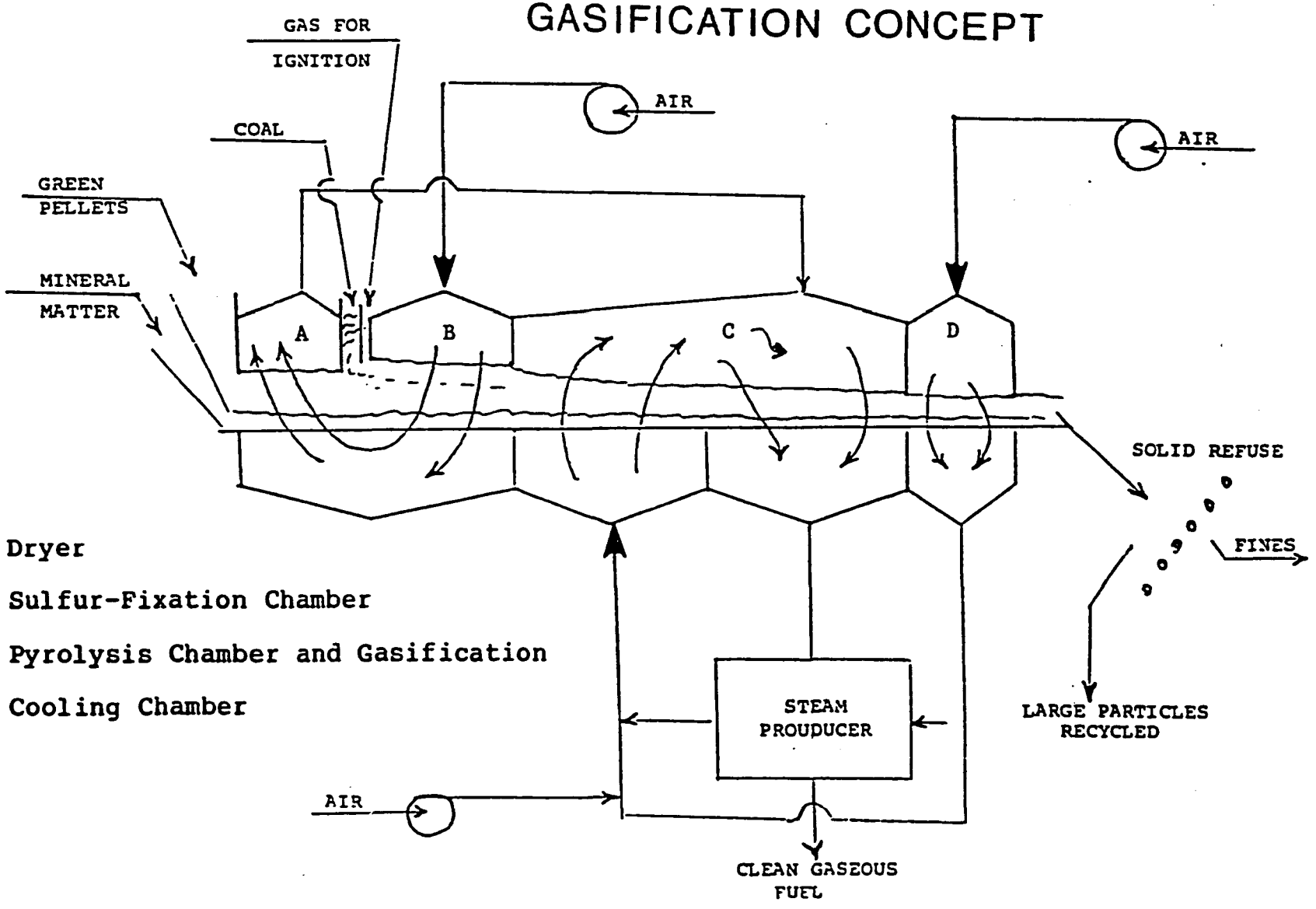

A Dryer

B Sulfur-Fixation Chamber

C Pyrolysis Chamber and Gasification

D Cooling Chamber

determine the output gas composition, the coke conversion, and the solid and gas temperatures of the system.

The objectives of the experimental apparatus effort were to improve and verify the applicability of the computer model by simulating the char-gasification process, using a combustion pot test facility.

The results of this study are to be employed in a subsequent study to determine the potential of the crossflow coal gasification concept.

1.3 Literature Survey

1.3.1 Modeling

While many references are available that provide information on the analysis of various coal gasification processes, the crossflow process has only been of sporadic interest and consequently; essentially no literature is available on this subject. Therefore, the literature survey was directed towards the appropriate references on counterflow, entrained flow, and fluidized-bed gasification process.

The performance of a counterflow coal gasifier was modeled in a series of papers, starting in 1978, by Yoon et al. (2). Their first paper presented a computer model which was based on the conservation of energy and mass and a chemical

kinetics model for simulating the coal gasification process. Because the computer model contained many assumptions, a parameter was employed in the chemical kinetics which allowed the model's results to be adjusted to agree with a predetermined set of experimental data. Their next publication described the transient performance of the system as a series of "patched-together" steady state solutions (3). In a third paper, these authors established the operating characteristics of a counterflow gasifier based on thermodynamic principles (4). Thus, a knowledge of the chemical kinetics was not necessary to determine the temperature and composition of the product gases. But this information is required to determine the temperature and composition profiles as well as the overall production rate of the counterflow system.

The model, developed by Yoon et al. (2) is basically simple, yet appropriate. The main assumptions of this model are as follows:

1. At each location in the system, the gas and solid temperatures are equal.
2. Plug flow for the solid phase and the gas phase.
3. The chemical kinetics model employs a shell progressive model. In shell progressive model, the core of the shell is a lumped system in which the reactions between solid and gas take place.
4. The water-gas shift reaction is so rapid that the gases in the bed are in thermodynamic equilibrium with respect to the local temperature.

5. The reactor was divided conceptually into two regions,an adiabatic core occupying most of the reactor volume and a colder boundary layer which occupies an annular portion of the coal bed that surrounds the adiabatic core.

The results produced by their model were compared with the available plant data for one large reactor. The results seemed to be in good agreement; however, an unspecified parameter was employed to adjust the model results. The most important conclusions listed in the report were as follows (2):

1. The maximum temperature in the bed is determined largely by the steam to oxygen ratio into the bed.
2. The thermal efficiency (defined as a heat value of the product gas) of a given steam to oxygen ratio is determined by the carbon-oxygen feed ratio.

Cho et al. (5) extended the chemical kinetics model of Yoon (2) to the unreacted core concept and introduced a CO/CO correction which is function of temperature for the combustion zone. Also, they considered the local gas and solid temperature to be different.

The results produced by their model were compared with the available plant data. The results seemed to be in good agreement; however, the CO_2 concentration showed almost a 100 % increase for small changes in operating conditions. The most important conclusions listed in the report were as follows (5):

1. The optimum thermal efficiency appears to be at the point where the conversion of char is nearly complete and the ash layer thickness is small. This optimum operation also favors a lower maximum solid temperature in the gasifier.

2. The model shows that significant differences between the gas and solid stream may exist in the combustion zone where considerable heat is generated on the solid surface and is then transfered to the gas stream by different mechanisms.

A mathematical model by Desai and Wen (6) was developed to describe the performance of the Morgantown Energy Technology Center (METC) fixed-bed gasifier. Like many others, this model is only useful for a limited range of operating conditions. The main assumptions of this model are as follows:

1. Plug flow in the solid phase and the gas phase;

2. Steady State;

3. Drying and devolatilization reactions are instantaneous and devolatilization reactions are thermally neutral;

4. Carbon-steam and carbon-carbon dioxide reactions are volume reactions while the carbon-oxygen reaction is a surface reaction;

5. Temperature of the bed at the bottom of the gasifier is within the range defined by the feed gas temperature and the ash temperature 500 ^{o}K to 650 ^{o}K;

6. Heat loss, which includes the heat recovered by cooling water and unaccountable heat, is proportional to the heat of generation.

7. At each location in the system, the gas and solid temperatures are equal.

The comparison of results of their model with METC's fixed-bed gasifier data show that METC's bed gasifier has been modeled successfully. The following conclusions were made from their study:

1. Pressure, (higher than 5 atms. and less than 17 atms.) does not have a significant effect on the gasifier performance except that more coal can be gasified per unit area.
2. Large amounts of air have to be supplied to the gasifier because of the high heat loss.
3. The use of excess air reduces the heating value of the product gases.

Amundsen and Arri (7) published two papers dealing with counterflow coal gasification. The first paper was an in-depth study of a single char-particle gasification with steam and oxygen as reactants. The chemical kinetics were based on the progressive model and were in a very complex form. This study illustrated the relationship of the process complexity relative to the reaction zone phenomena.

The application of this single particle model to a counterflow reactor was described in their second paper (8). The chemical kinetics were simplified and a finite difference technique was successful in generating a solution.

The phenomena involved in crossflow gasification are similar to those occurring in other gasification processes. Thus, the literature on modeling counterflow gasification,

fluidized-bed gasification and entrained flow gasification was used as a source for data for rate processes and chemical kinetics. This data is described as it is incorporated into Chapter 3, which describes each reaction in detail, and Chapter 4, which describes the development of the energy and mass transport equations used in this study.

1.4.2 Experimental Studies

In the experimental studies, notable work has been done in the area of coal gasification. The experiment of Eapen et al. (9) utilized a rectangular combustion pot with inside dimensions of 6.5" by 15.5" and a height of 19.5". They studied the gasification of fuel in this device under carefully controlled conditions and the gas composition, O_2, CO_2 and CO, was measured down through the bed. Their work was largely confined to gasification in deep fuel beds of the under-fire type. Therefore, this study is not directly applicable to our study which combusts thin fuel beds of the over-fire type on a traveling grate.

Karzhavina (10) studied the gasification of wood charcoal in a reaction tube which was 40 mm in diameter. The spherical particles, 5 to 6 mm in diameter, in a layer 10 mm deep and weighing approximately 2.67 gm were used in his experimental studies. The gas formed during the burning of a

layer of charcoal was completely removed in a series of from 15 to 30 consecutive aspiration steps. The primary purpose of his experiment was to determine accurately the magnitude of the combustion zone as a function of the blast speed. In order to avoid changes in reaction product compositions, the reaction products were immediately cooled. Karzhavina (10) concluded that:

1. The formation of CO_2 is accompanied by independent formation of CO.
2. With wood charcoal of 5 mm in diameter, the oxygen is consumed with a zone about 7-10 mm long. The length of the zone is almost independent of the blast velocity (within the limits of 0.1 to 2.5 m/sec).

Lewis (11) studied the combustion of coke in a coal-fired furnace, and reached the following conclusions by analysis of his results;

1. Carbon dioxide is formed by a primary reaction of carbon and oxygen by $C + O_2 = CO_2$.
2. The reaction velocity is determined by diffusion of oxygen through the superficial gas film on the coke particle.
3. The rate of formation of carbon monoxide was approximately proportional to the concentration of carbon dioxide.

2. PHYSICAL AND CHEMICAL EVENTS.

2.1 Introduction

The purpose of this chapter is to desribe how the various processes have been modeled in counterflow gasification and how this approach is utilized in this study.

For modeling purposes the common approach to a counterflow reactor is to divide the reactor into zones where distinct physical and chemical processes take place Figure (2.1). The first zone is the drying zone where the coal is heated and dried, removing all the free moisture. The second zone is a devolatilization zone, where the volatile matter and tar are expelled from the solids. The gasification is the third zone where product gases (CO, H_2, CO_2, etc...) are formed by gasification reactions. The final zone is the combustion zone where the combustion reactions between char and oxygen take place and provides the energy needed for the endothermic gasification and drying processes. In reality some or all of these zones may be indistinguishable.

2.2 Drying

In the drying zone, the coal particles are heated by the gaseous products generated by the combustion and gasification reactions. During this process most of the free moisture in the coal is driven out.

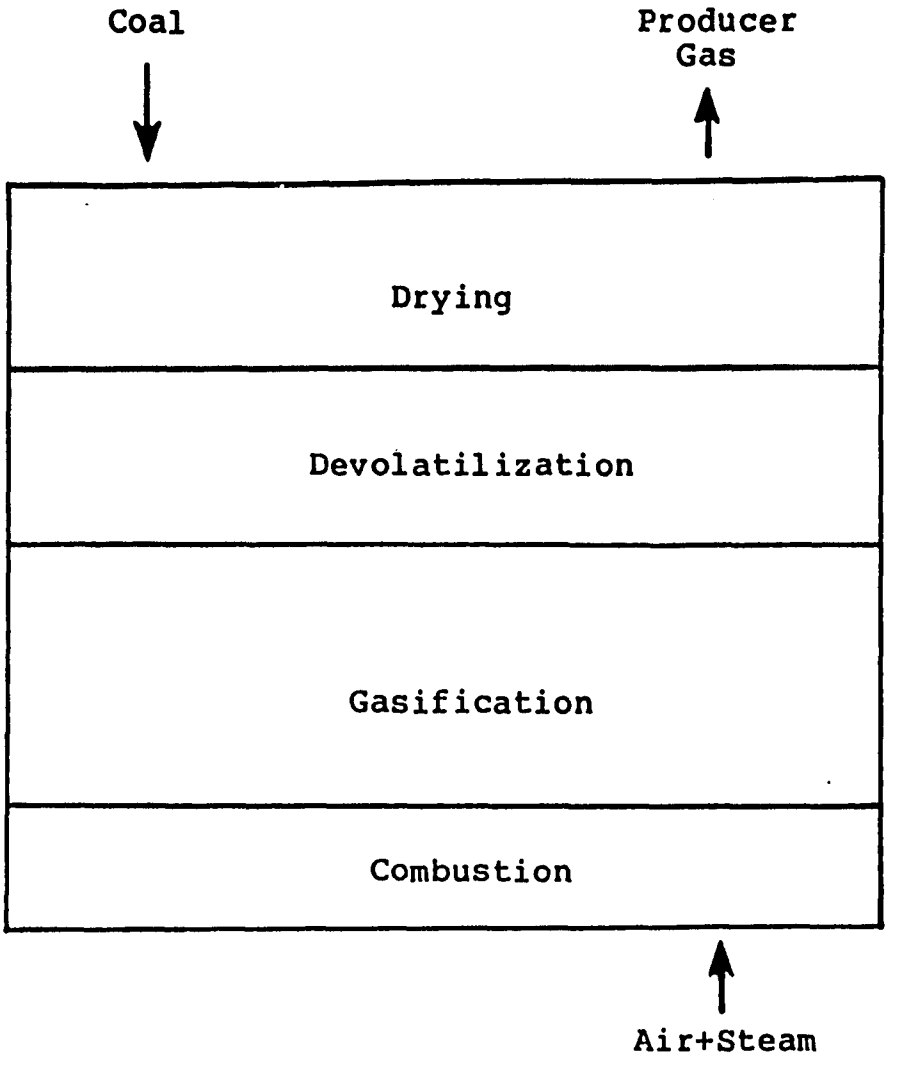

Figure 2.1 Typical Zones in Counterflow Gasifier

2.3 Devolatilization

In the devolatilization zone, the temperature of the coal particles is increased to release volatile gaseous products and tars from the coal, leaving only char. The mechanisms of this phenomenon are still not completely understood. The mechanisms involved in devolatilization seem to depend on operating conditions such as temperature, pressure, particle size, the type of coal, and the heating rate, as well as the mineral content of coal (13). There are even uncertainties about classifying the net process (devolatilization) as endothermic or exothermic (5).

2.4 Gasification and Combustion

The reactions of char with steam, carbon dioxide, and hydrogen, along with the water-gas shift reaction, are considered to be the major reactions taking place in the gasifier. The remaining char is burned in the combustion zone consuming oxygen in the feed gas, leaving only an ash residue.

The main objective of this dissertation was to study only the gasification and combustion zones of the crossflow coal gasification process.

3. COAL GASIFICATION REACTION KINETICS.

3.1 Introduction

Major solid-gas reactions involved in coal gasification are char-steam, char-carbon dioxide, char-oxygen, and char-hydrogen reactions. The kinetics of each individual reaction are discussed in the following sections.

3.2 Char-Gas Reaction

The char-gas reactions are heterogenous reactions and the process can be idealized as one of two distinct models, i.e, volumetric reaction and surface reaction model. In the volumetric reaction model, the gaseous reactants diffuse throughout the interior of the particle and react. The chemical reaction rate for a volumetric reaction is considered to be much slower than the diffusion rate and it is consequently the rate controlling step of the process (14). In the case of surface reaction model, the chemical reaction rate is considered greater than the diffusion rate; consequently, reacting gases are assumed not to penetrate into the interior of the solid particles. Thus, the reactant gas is confined to the exterior of the surface of the "shrinking core of unreacted solid" (15). In the literature, one can find many investigations on the coal gasification

reactions. Several reviews are available: Johnson (16), Walker et al. (17), Dutta et al. (18), and Wen et al. (19). Unfortunately, because of the complexity of these reactions, a model for the overall gasification reactions is first hypothesized. Experimental data are then obtained and reduced according to the assumptions of the model. Thus the resulting chemical kinetics data may then only be used, at a later date, in conjunction with that specific model. Consequently, one can not compare the chemical kinetics data from several studies with any degree of confidence. Also, the various assumptions employed in these models are difficult to reconcile, and consequently, it is difficult to "rework" the original information. Thus, a basic study of the detailed mechanisms for a more advanced model appears to be in order.

In the crossflow coal gasification model, the char gasification is classified as an irreversible gas-solid reaction, and operates at high temperature. It is therefore reasonable to use, as a first attempt of interpretation, the surface reaction (shrinking core) model described by Levenspiel (20) and Wen (15). At the beginning, the reaction will occur at the external surface of the particle and then the reaction front will gradually move inward leaving an ash layer between the original surface and the reaction front. At the intermediate conversion of the solid, there is essentially a shrinking core of unreacted solid which

diminishes as the reaction proceeds. There are three resistances for the reactant gas to pass through to form the product gas; 1) diffusion through the boundary layer around the particle; 2) diffusion through the ash layer; 3) chemical reaction at the surface. The overall rate, according to this model can be expressed for each reaction, i, as follows:

$$\dot{R}''_i = \frac{(P_j - P_j^*)}{\frac{1}{K_g} + \frac{1}{K_{ash}}\left(\frac{1}{\xi} - 1\right) + \frac{1}{K_s \xi^2}} \qquad (3.1)$$

where:

K_g is the gas film constant

K_s is the surface reaction constant

K_{ash} is the ash diffusion constant

$$\xi = \frac{r_c}{R}$$

r_c is the radius of unreacted-core

R is the radius of whole particle including the ash, and is assumed constant.

P_j is partial pressure of j-component gas

$P_j - P_j^*$ is effective partial pressure of j-component taking into account of the reverse reaction effect.

The ash diffusion rate constant, K_{ash} depends both on the gas diffusivity and the voidage of the ash layer. Here, K_{ash} is roughly estimated by the following correlation (30).

$$K_{ash} = K_g \epsilon^n \qquad 2 < n < 3 \qquad (3.2)$$

where ϵ is the voidage of the ash layer. The values of ϵ, and n are assumed (14) to be 0.75 and 2.5, respectively for this study. It should be noted that the value of K_g in equation (3.2) is different for each reaction (see Appendix II).

In this model it is assumed that the relative motion between particles is insignificant and therefore that the ash layer formed remains intact on the fuel particle during the reaction.

Detailed descriptions of the kinetics for each individual solid-gas reaction are given in the following sections. A summary of the rate expression used in the model development is given in Appendix II.

3.2.1 Char-Oxygen Reactions

The burning of char is the fastest among the char-gas reactions taking place in the gasifier. Both carbon monoxide and carbon dioxide are formed as primary products of the

surface reaction, as shown in the following equation (14):

$$C^* + \frac{1}{\phi} O_2 \longrightarrow 2(1 - \frac{1}{\phi})CO + (\frac{2}{\phi} - 1)CO_2 \quad , \quad (3.3)$$

where C* represents the carbon in the char and ϕ is the mechanism factor of the combustion reaction (moles of carbon consumed per mole of oxygen).

A main difficulty in this reaction rate model is the estimation of the product ratio of CO/CO_2. This product ratio seems to depend on the amount of carbon converted, surface conditions (24), and gasification rate (16). Arthur (26) presented an empirical correlation for the CO to CO_2 ratio as follows:

$$\frac{CO}{CO_2} = K^o \exp(-E/\bar{R}T_m) \quad , \quad (3.4)$$

where CO/CO_2 represents the molar ratio of carbon monoxide to carbon dioxide, K^o is equal to 2.512×10^3, E is equal to 0.124×10^5 cal/mole, $\bar{R}$ is the universal gas constant, and T_m is the mean temperature of gas and solid. It is apparent that CO is the dominant product at high temperatures.

The burning mechanisms of char, and the subsequent product gas composition around the burning char, are very complex, and many researchers have proposed different models (27).

Essenhigh (21) presents a physical model of char combustion as shown in Figure 3.1 (14). Gases diffuse through the boundary layer and penetrate into the porous solid. The reaction $C-CO_2$ occurs heterogeneously at all available exterior and interior surfaces of the solid. In his model the CO/CO_2 ratio rises with temperature, and CO becomes the principle product at 1000 ^{o}C. The CO also reacts in the gas phase with oxygen to produce CO_2.

Avedesian and Davidson (22) suggested that O_2 and CO burn rapidly in a very thin reaction zone surrounding the particle. Carbon monoxide produced at the surface diffuses out toward the reaction zone while O_2 from the main stream diffuses in and burns in a diffusion flame to produce CO_2 as shown in Figure 3.1 (14).

Caram and Amundson (23) suggested that large particles (>2mm) burn according to the double film theory (28), shown in Figure 3.1 (14), whereas small particles (<100 microns) burn according to the single film model. In analyzing the reaction of carbon with oxygen and with carbon dioxide according to double film models, they conclude that large particles (5 mm) tend to reach an upper steady state in which the particle is surrounded by a CO flame. For very small particles (<50 microns) such a flame does not develop. Thus, it is evident that the char-oxygen reaction occurs in the interior surface of small particles at low temperatures

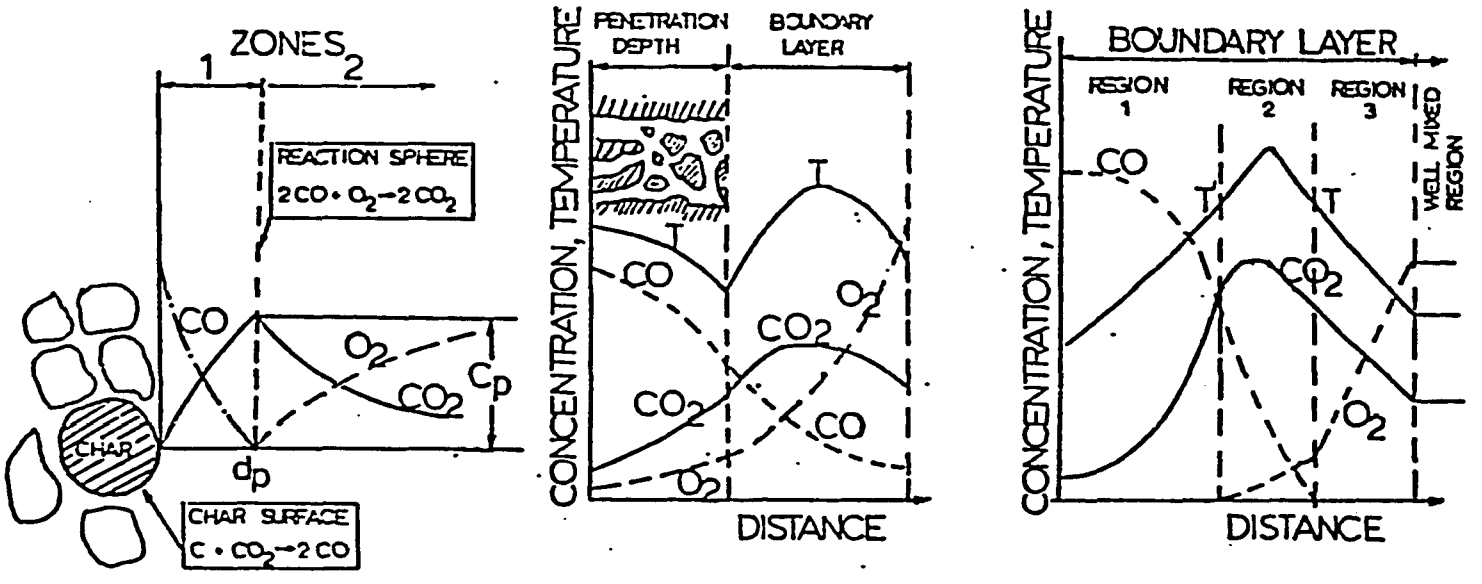

d_p : diameter of char or coke particle

C_p : oxygen concentration

T : temperature

MODEL 1	MODEL 2	MODEL 3
(Avedesian & Davidson 22)	(Essenhigh 21)	(Caram & Amundson 23)

FIGURE 3.1 TYPICAL PHYSICAL MODELS OF COAL-CHAR COMBUSTION (27)

because oxygen does not get consumed near the external surface while enough is supplied to the interior by the pore diffusion from the bulk phase.

The mechanism factor, ϕ, is also a function of the coal rank, particle size and temperature. For large paticle sizes, according to the double film model (23), CO_2 might be the only product gas in the char-oxygen reaction. Arthur's correlation (26) is applicable only for small particle sizes. Wen and Dutta (25) proposed a correlation for a rough estimation of the mechanism factor, ϕ, by a linear interpolation between small particle sizes and large particle sizes. This correlation is shown below:

$$\phi = \frac{(2Z + 2)}{(Z + 2)} \qquad \text{for } d_p < .005 \text{ cm}$$

$$\phi = ((2Z + 2) - Z(d_p - .005)/.095)/(Z + 2) \qquad \text{for } .005 < d_p < 0.1 \text{ cm}$$

and

$$\phi = 1.0 \qquad \text{for } d_p > 0.1 \text{ cm}$$

where

$$Z = 2500 \exp(-6249/T_m) \tag{3.5}$$

$$T_m = (T_s + T_g)/2. \qquad [^\circ K]$$

Thus, Arthur's formula, Eq. (3.4), does not apply to large particles and CO_2 appears to be the only direct product.

A surface reaction rate coefficient K_s has been developed by Field et al. (29) for char-O_2 reaction. The universal use of such an expression implies no effect of fuel type, and the internal structure of the fuel is of no importance, since the rate is expressed in terms of external surface area (29). The reaction rate of Field (29) is

$$K_s = A \exp(-E/\bar{R} T_s) \qquad (3.6)$$

where

$A = 8710.$ (gm/cm^2 sec atm)

$E = 35700.$ (cal/mol)

$R = 1.986$ (cal/mol $^\circ$K)

T_s = surface temperature ($^\circ$K)

The diffusional reaction rate coefficient K_g is given by Field et al. (29) and depends on the particle diameter, the mechanism factor and mean temperature, but is completely independent of fuel type (29).

$$K_g = 24. \phi D/R d_p T_m \qquad (3.7)$$

where

ϕ = mechanism factor

$\bar{R} = 82.06$ (atm cm^3/mol ^oK)

d_p = particle diameter (cm)

T_m = mean temperature (^oK)

The diffusivity D of oxygen, in the gas film, is given by (29).

$$D = D_o (T_g/T_o)^{1.75} (P_o/P_t) \quad cm^2/sec \qquad (3.8)$$

where D_o is the diffusion coefficient at a reference temperature and pressure, which may be chosen arbitrarily, and P_t is total pressure in atm. By using a reference temperature T_o of 1800 ^oK, and P_o of 1 atm, the value of D_o is 4.26 cm^2/sec (29).

There are many papers available on coal combustion; however, the phenomena is still not completely understood. Even for small particles, the available combustion rate data is very confusing. Thus the selection of this model has been an arbitrary decision.

3.2.2 Char-Steam Reaction

The char-steam reaction is

$$C + H_2O \rightleftharpoons CO + H_2 \qquad (3.9)$$

This reaction is one of the most important reactions for the production of CO and H_2. There are two basic reaction rate models for the char-steam reaction. The volumetric reaction rate was proposed by Wen (30) and applied to the analysis of METC's pilot plant by Deasi (6). This model appears to be acceptable within a moderate temperature range (700 - 900 ^{o}C). Reid and Hanesian (32) found that the carbon-steam reaction is surface-reaction controlling between (500 - 900 ^{o}C) and the gas film diffusion becomes gradually important above 700 ^{o}C. The data obtained by Gray and Kimber (33) represents the only set of kinetic measurements made on the gasification of pulverized char at flame temperature. They estimated the surface reaction constant at 2300 ^{o}K and 2800 ^{o}K, from which the activation energy is calculated to be 42 Kcal/g mole. Based on the data of Gray and Kimber (33), Dobner (34) proposed the same surface reaction rate expression for both carbon-steam and carbon-carbon dioxide reactions. This expression,

$$K_s = 247 \exp(-21060/T_s) \quad gm/cm^2 \text{ sec atm} \quad (3.10),$$

was also used by Chaung (14).

At the low temperature range, the apparent energy has been reported to vary from 35-45 Kcal/mol (30) to 60-80 Kcal/mol (54). Depending on the type of coal, the volumetric reaction rate constant, K_V, can vary almost three orders of magnitude

at temperature below 1200 ^{o}C (14). Since adequate data were not available to estimate the reaction rate constant for the char-steam and char-CO_2 reactions at temperatures higher than 1200 ^{o}C, it is difficult to postulate the accuracy and proposed rate expression used in this model.

3.2.3 Char-Carbon Dioxide Reaction

The char-carbon dioxide reaction is

$$C + CO_2 \rightleftharpoons 2CO \qquad (3.11)$$

The rate of the char-CO_2 reaction is relatively slow and is comparable with that of the char-steam reaction, as already mentioned by Dobner (34). Yang and Steinberg (35) measured the rates of reaction beteween nuclear graphite and carbon dioxide at temperature between 1200 ^{o}C and 1600 ^{o}C, and concluded that the rates are controlled by both surface reaction and the ash diffusion in this temperature range. Dutta et. al. (31) measured the rate of char-CO_2 reaction and concluded that for particles smaller than 0.3 cm and temperatures lower than 1000 ^{o}C., the reaction is controlled by the chemical reaction rate, which appears to take place nearly uniformly throughout the interior of the char particles. Gray and Kimber (33) estimated the surface reaction rate constant at 2300 ^{o}K and 2800 ^{o}K for both char-steam and char-carbon dioxide reaction. However, Dobner (34) proposed the same rate expression as equation (3.10) for both

char-steam and char-carbon dioxide reactions based on Gray and Kimber's (33) data. This expression,

$$K_s = 247 \exp(-21060/T_s) \quad gm/cm^2 \text{ sec atm} \qquad (3.12),$$

was also used by Chaung (14).

This expression appears to be independant of particle size. In the low temperature range the reported volumetric reaction rate constant for char-carbon dioxide reaction also scatters widely as shown in Figure 3.2 (25).

3.2.4 Char-Hydrogen Reaction

The char-hydrogen reaction is

$$C + 2H_2 \rightleftharpoons CH_4 \qquad (3.13)$$

The reaction of char and hydrogen is quite exothermic and produces methane. The model predictions of methane produced are usually lower than actual plant data (5). There is even an interesting finding that the methane concentration can be larger than the equilibrium value in the product gas stream (36). To overcome these uncertainties, Gumz (37) has suggested an approach factor for an hypothetical equilibrium constant which depends on the coal type. Wen and Huebler (38) proposed the following empirical equation for the rate of hydrogasification (char-hydrogen reaction).

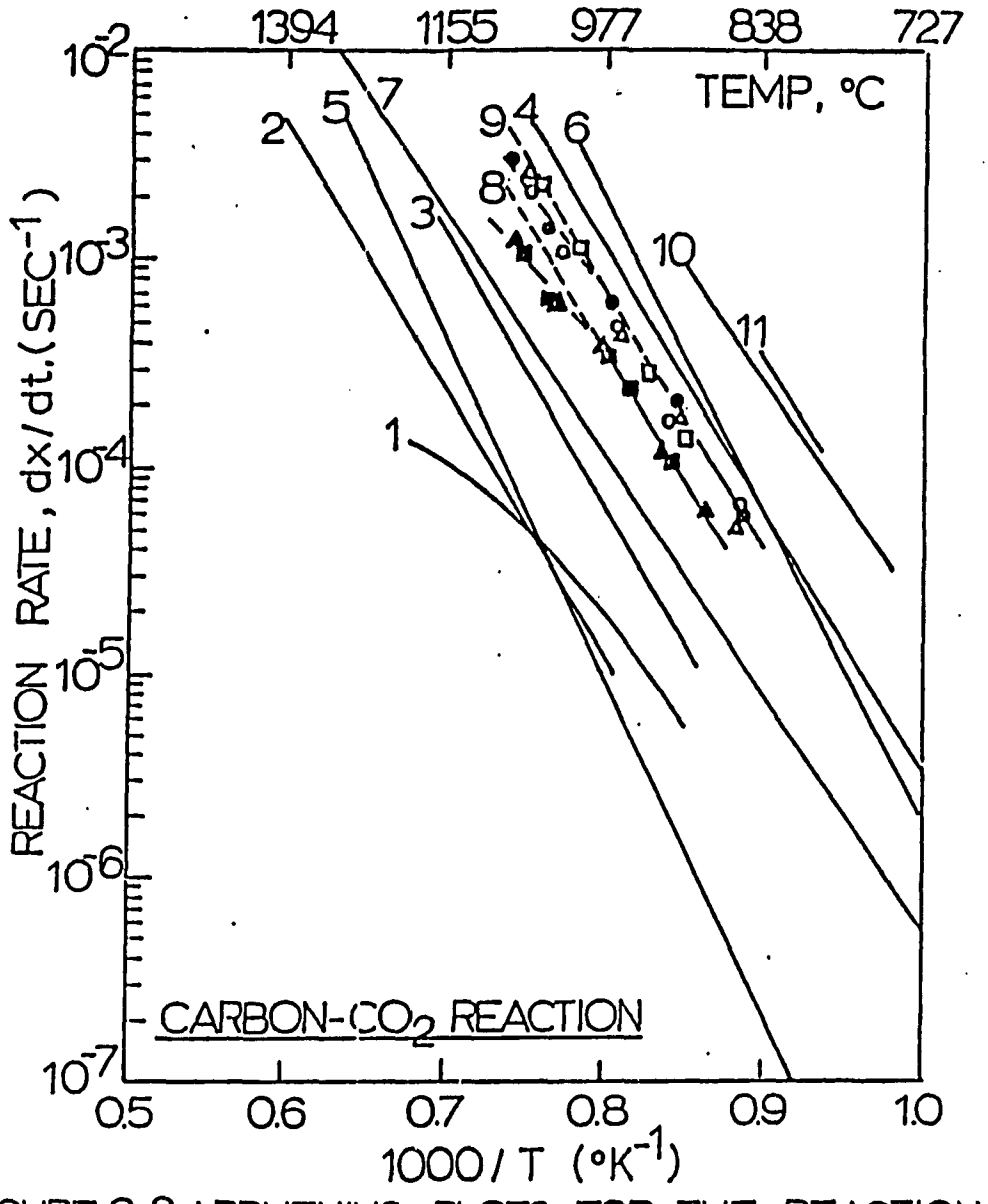

FIGURE 3.2 ARRHENIUS PLOTS FOR THE REACTION BETWEEN CO_2 AND VARIOUS FORMS OF CARBON (SEE THE LEGEND IN TABLE 3.1) (25)

Table 3.1 Legend to Figure 3.2

Line No.	Investigators	Year	Type, Size and Shape of Carbon	Remarks
1	Yoshida and Kunii(39)	(1969)	Graphite Sphere, 1.5 Cm. Dia.	Initial Rates
2	Ergun(40)	(1956)	Ceylon Graphite, -10 +200 mesh	Initial Rate in a fluidized bed.
3	-do-		Activated Graphite, -10 +200 mesh	-do-
4	-do-		Activated Carbon, -10 +200 mesh	-do-
5	Turkdogan and Vinters (41)	(1969)	Electrode Graphite Particles, -10+200 mesh	Initial Rates
6	-do-		Coconut Charcoal Particles, -10+40 mesh	Initial Rates
7	Austin and Walker (42)	(1963)	Graphitized Carbon cylinder, 5.1 cm. long and 1.27 cm. dia.	Calculated Initial Rates
8 & 9	Dutta et al.(31)	(1977)	○ - Illinois Coal #6 ● - Synthane Char #122 △ - Hydrane Char #49 □ - IGT Char #HT155 ▲ - Hydrane Char #150 × - Pittsburgh HVab Coal all of size -35 +60 mesh	Rates at 20% conversion level
10	Fuchs and Yovorsky (43)	(1975)	Hydrane Char from Pittsburgh Coal, -60 +100 mesh	Average Rate in a fluidized bed at 16-32 atm. partial pressure of CO_2 with He as diluent
11	-do-		Synthane Char from Illinois Coal #6, -60 +100 mesh	Average Rate in a fluidized bed at 32 atm. partial pressure of CO_2 with He as diluent

$$\frac{dX_c}{dt} = K_v \left(P_{H_2} - \left(\frac{P_{CH_4}}{K_{eq}}\right)^{1/2}\right)(1-X_c) \qquad (3.14)$$

where X_C is carbon conversion and K_V is volumetric reaction rate constant. Figure 3.3 (25,14) shows the reported volumetric reaction rate constant based on this expression.

In order to simplify the calculation procedure, an approximate conversion from K_V to K_S is made so that the overall rate can be calculated by unreacted-core shrinking model (14). Since the char-hydrogen reaction is mostly in the chemical kinetics controlling regime ($K_S << K_g, K_{ash}$), based on the unreacted-core shrinking model, the rate can be expressed as follows:

$$\text{Rate} = K_{over} \left(\frac{6}{\rho_s . d_p}\right) P_{eff} \qquad (3.15)$$

$$K_{over} = \frac{1}{\frac{1}{K_g} + \frac{1}{K_{ash}}\left(\frac{1}{\xi} - 1\right) + \frac{1}{K_s \xi^2}} \qquad (3.16)$$

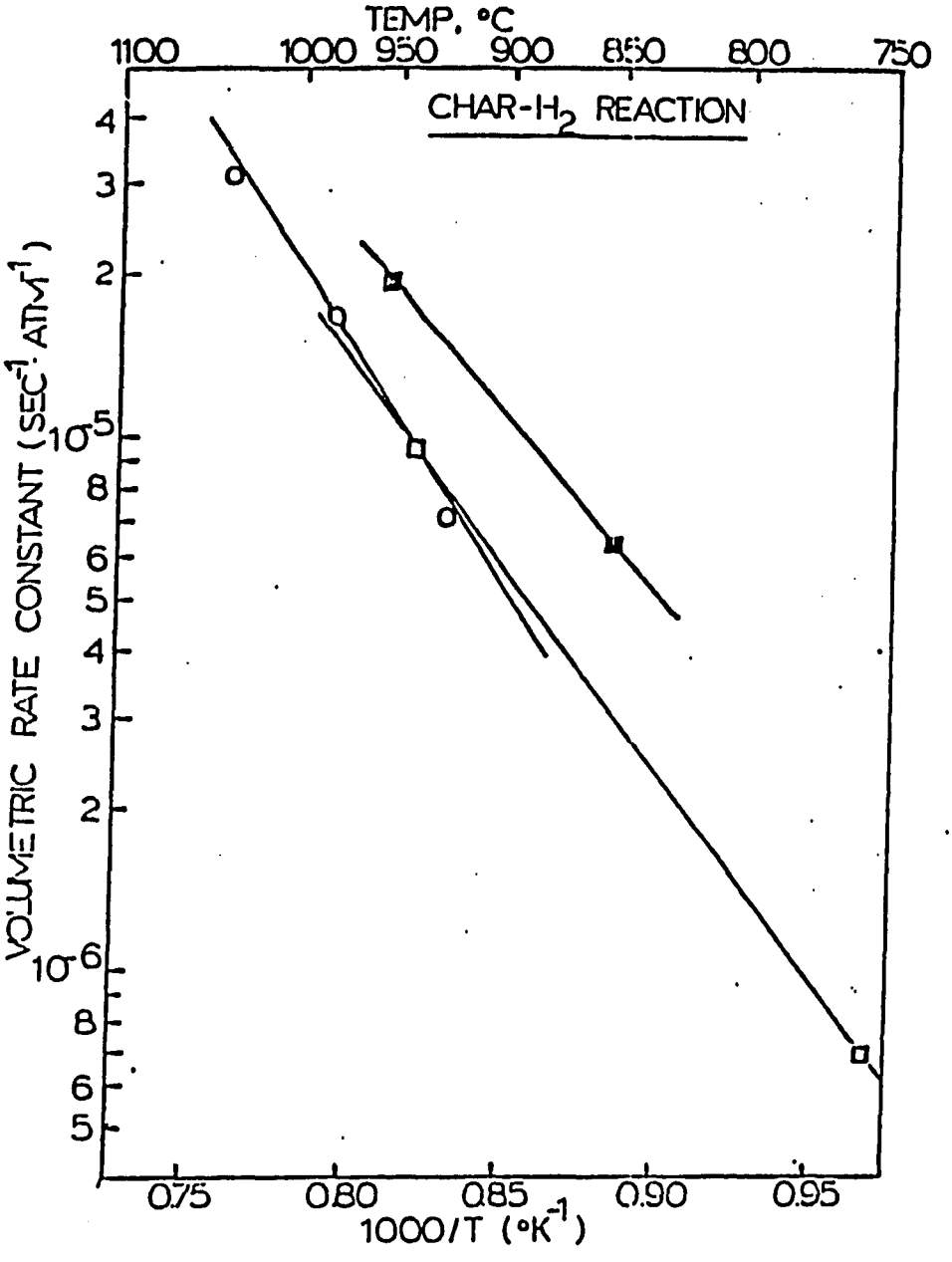

FIGURE 3.3 ARRHENIUS PLOTS FOR CHAR HYDROGASIFICATION

- ▪ Australian Yallourn coal char Birch et al. (44) pressure : 42 atm
- ▫ Concoal Montour No.10 Bitu. Coal Char, Pyrocloch and Linden (45); pressure 104 atm
- o Air-pretreated Pittsburgh No 8 coal char. Johnson (16) pressure : 35 atm.

$$= K_s \xi^2 = K_s (1-X_c)^{2/3} \qquad (3.17)$$

$$P_{eff} = P_{H_2} - (P_{CH_4}/K_{eq})^{1/2} \qquad (3.18)$$

However, based on the volumetric rate expression;

$$\text{Rate} = K_v (1-X_c) P_{eff} \qquad (3.19)$$

From equations (3.15), (3.16), and (3.19), K_s can be approximated from K_v by:

$$K_s = K_v (1-X_c)^{1/3} \frac{\rho_s R_p}{3} \qquad (3.20)$$

Thus the rate constant can be calculated from the experimental data (25), which leads to the equation:

$$K_s = 0.12 \exp(-17921/T_s) \qquad (3.21)$$

3.2.5 Water-Gas Shift Reaction

The water-gas shift reaction is:

$$CO + H_2O \rightleftharpoons CO_2 + H_2 \qquad (3.22)$$

The water-gas shift reaction is one of the most important reactions which determines the composition of the product distribution of a gasifier. The rate of this reaction has not been well established because of the strong effect of

local catalyst. This reaction is very fast and could proceed to a finite equilibrium. Therefore, this reaction was assumed to be in equilibrium at every location within the gas filled voids in the bed, with K_{eq} (12):

$$K_{eq} = K^{o} \exp(-\Delta H_5 / \bar{R}\, T) \qquad (3.23)$$

In this study K_{eq} was taken as (12);

$$K_{eq} = \exp(-3.6893 + 4020/T_m) \qquad (3.24)$$

An error in this assumption would introduce only a small error in the energy balance, because of the slight exothermicity of the reaction (2) and the gasification rate will not be affected (2). It should be noted that if one assumes that the water-gas shift reaction is very fast and always at equilibrium, the concentration of hydrogen, carbon monoxide, carbon dioxide, and water are related throughout the gasification zone by the equilibrium relationship.

For the purpose of being rigorous, a reaction rate $\dot{R}''_5$ is used for this reaction in developing the conservation equations. However, in order to obtain the numerical solutions to this model, a local equilibrium equation will be established in Chapter five.

3.2.6 Char Reactivity

The surface reaction rate expression K_S for different gas-solid reactions (which has been explained in sections 3.2.1 through 3.2.4) have been taken from the literature. These expressions were substituted in the model as a part of overall chemical reaction rates. For the reactions of carbonaceous materials the values of the coefficient for their surface reaction rates vary in a wide range. The values determined by experiments for these coefficients cited in the literature, are strictly dependant on the form of the carbonaceous material being examined, on the specific surface area, and on the corresponding value of fuel (char/coke) reactivity. It is, therefore, necessary to consider in the application of these literature data, a wide range of admissible values for these coefficients for the fuel (char/coke) which will be used in the model.

Therefore, a reactivity factor coefficient has been chosen to account for the reactivity of fuel (char/coke) used. This reactivity factor coefficient is used for char-carbon dioxide and char-steam reactions only. The surface reaction rate for the char-oxygen reaction does not vary with fuel type (29). It is assumed that the K_S for char-hydrogen reaction does not vary with fuel type in this study because of the source of calculation (25). The reactivity factor coefficient is an

adjustable parameter for the surface reaction rate constant K_S , because K_S is strongly dependant on the solid temperature. The reactivity factor coefficient can be varied for each reaction, for different types of fuel (char/coke) used.

4. DEVELOPMENT OF THE MODEL

In this chapter, a mathematical model has been developed for the batch gasification of char in a combustion pot is presented. The model is based on the chemical reaction kinetics and mass and energy balances.

4.1 Reaction Kinetics

The number of chemical components present within the reactor is very large. Some of these components are present in trace amounts and do not have a significant effect on the gasification process. In this work, the following compounds are considered in the solid stream:

Carbon, Ash

The following compounds are considered to be present in the gas stream.

$$H_2O,\ H_2,\ O_2,\ CO_2,\ CO,\ CH_4$$

With the preceding considerations, the major reactions in the gasifier can be expressed as shown in Table 4-1. It is also possible for the following reactions to occur:

Table 4.1 Major Reactions in the Gasifier

Reactions	Rate Notation
$C + \frac{1}{\phi} O_2 \rightarrow 2(1 - \frac{1}{\phi})CO + (\frac{2}{\phi} - 1)CO_2$	$\dot{R}''_1$
$C + H_2O \rightleftarrows CO + H_2$	$\dot{R}''_2$
$C + CO_2 \rightleftarrows 2CO$	$\dot{R}''_3$
$C + 2H_2 \rightleftarrows CH_4$	$\dot{R}''_4$
$CO + H_2O \rightleftarrows CO_2 + H_2$	$\dot{R}''_5$

$$CO + 3H_2 \longrightarrow CH_4 + H_2O \qquad (\dot{R}''_6)$$

$$S + H_2 \longrightarrow H_2S \qquad (\dot{R}''_7)$$

It is assumed that reactions $\dot{R}''_6$ and $\dot{R}''_7$ are negligible since the effect of these reactions rates are insignificant and they do not affect the gasifier performance (5,2).

In developing the mathematical model, it was assumed that there is no radial gradients for mass and energy (53). In fact, the dominant transport mechanism in the gasifier is turbulent mixing due to the high axial flux of the gaseous stream.

Char-oxygen, char-steam, char-carbon dioxide and char-hydrogen reactions are all heterogeneous. In this work, the shrinking core model is chosen to describe the kinetics of these reactions.

4.2 Material and Energy Balance Equations

The basic conditions and assumptions used in the model development are summarized below:

1. Solid phase is stationary throughout the system.
2. The conduction resistance of the solid core is small in comparison to the convection resistance of the surface. Therefore, the conduction resistance is neglected (the lumped-system analysis).

3. Negligible heat-lost through the reactor wall to the ambient.

4. Positive direction is downwards.

5. The exchange of energy between the gas and solid phase through conduction, convection, and radiation is represented by a gas-solid heat transfer coefficient.

Based on the above assumptions, the mass and heat balance equations were set up as follows:

4.2.1 Material Balance (Gas Phase)

The differential equation for the mass balance in the gas phase was derived for the system shown in Figure 4.2.1.

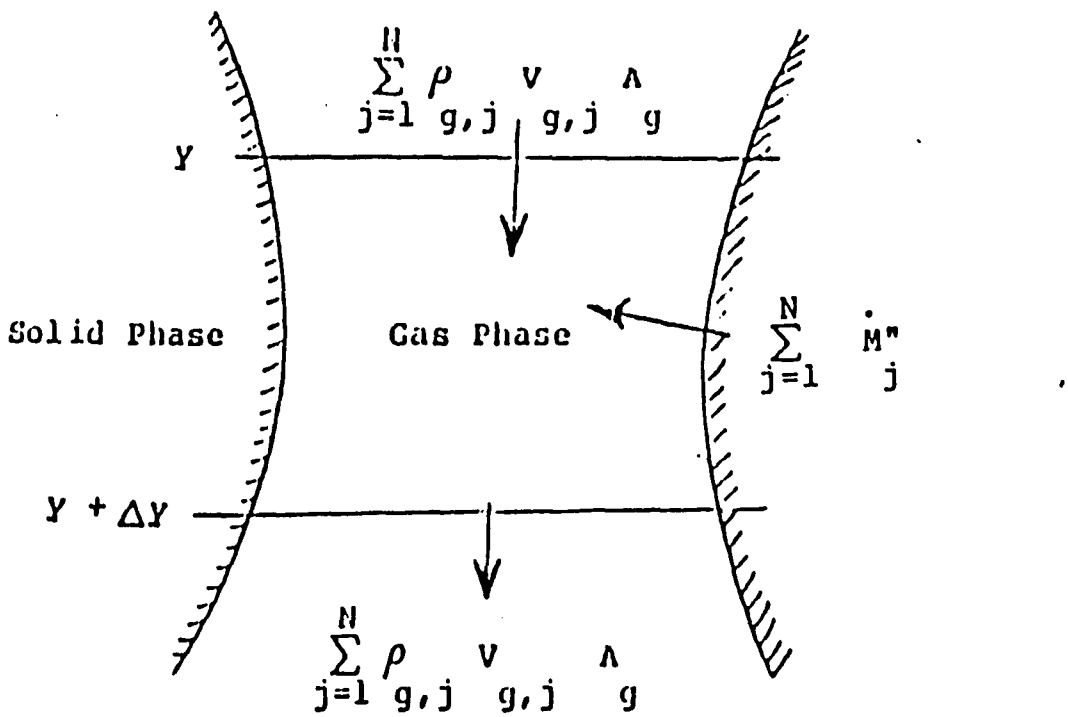

Figure 4.2.1 System for Gas Phase Analysis (Material Balance)

$$A_g \Delta y \frac{\partial \sum_{j=1}^{N} \rho_{g,j}}{\partial t} = A_g \sum_{j=1}^{N} \rho_{g,j} V_{g,j} \Big|_{y} - A_g \sum_{j=1}^{N} \rho_{g,j} V_{g,j} \Big|_{y+\Delta y}$$

$$+ \sum_{j=1}^{N} \dot{M}''_j A'_t \Delta y \qquad (4.1)$$

Dividing the equation (4.1) by $A_g \Delta y$ and letting $\Delta y \rightarrow 0$, then in the limit;

$$\frac{\partial \sum_{j=1}^{N} \rho_{g,j}}{\partial t} = - \frac{\partial \sum_{j=1}^{N} \rho_{g,j} V_{g,j}}{\partial y} + \sum_{j=1}^{N} \dot{M}''_j \frac{A'_t}{A_g} \qquad (4.2)$$

Defining

$$\frac{A'_t}{A_g} = \frac{(A'_t \Delta y / A_b \Delta y)}{(A_g \Delta y / A_b \Delta y)} \qquad \frac{\left(\frac{\text{transfer area}}{\text{bed volume}}\right)}{\left(\frac{\text{void volume}}{\text{bed volume}}\right)}$$

$$= \frac{a}{\epsilon} \qquad (4.3)$$

and

$$\sum_{j=1}^{N} \rho_{g,j} V_{g,j} = \sum_{j=1}^{N} \dot{m}''_{g,j} \qquad (4.4)$$

and also,

$$\sum_{j=1}^{N} \dot{M}''_j = \sum_{i=1}^{4} \dot{R}''_i \qquad \text{mass flux of net gas source due to the reaction of solids} \qquad (4.5)$$

For example, for carbon-steam reaction, the equation (4.5) yield;

$$\dot{M}''_{CO} = \dot{R}''_2 \, \nu_{2CO}$$

$$\dot{M}''_{H_2} = \dot{R}''_2 \, \nu_{2H_2}$$

$$\dot{M}''_{H_2O} = -\dot{R}''_2 \, \gamma_{2H_2O}$$

and

$$\sum_{j=1}^{3} \dot{M}''_j = \dot{M}''_{CO} + \dot{M}''_{H_2} - \dot{M}''_{H_2O} = \dot{R}''_2 \left(\nu_{2CO} + \nu_{2H_2} - \gamma_{2H_2O} \right)$$

$$= \dot{R}''_2 \, x(1.0) = \dot{R}''_2$$

By substituting the equations (4.3), (4.4), and (4.5) into the equation (4.2), and yield;

$$\frac{\partial \sum_{j=1}^{N} \rho_{g,j}}{\partial t} = - \frac{\partial \sum_{j=1}^{N} \dot{m}''_{g,j}}{\partial y} + \frac{a}{\epsilon} \sum_{i=1}^{4} \dot{R}''_i \qquad (4.6)$$

The local component mass balances yield:

$$\frac{\partial \rho_{g,j}}{\partial t} = -\frac{\partial \dot{m}''_{g,j}}{\partial Y} + \frac{a}{\epsilon}\left[\sum_{i=1}^{4} \dot{R}''_i \sum_{j=1}^{N} (\nu_{ij} - \gamma_{ij}) + \widetilde{MW}_j \dot{R}''_5 \sum_{j=1}^{N} (b_{ij} - a_{ij})\right] \qquad (4.7)$$

Where ν_{ij} and γ_{ij} are mass stoichiometric cofficients of the product and reactant gas species j, in reaction i, b_{ij} and a_{ij} are molar stoichiometric coefficient of the product gas and reactant gas species j, in reaction 5. It should be noted that the j does not include carbon as this term only applies to gaseous species.

4.2.2 Energy Balance (Gas Phase)

The differential equation for the energy balance in the gas phase was derived for the system shown in Figure 4.2.2.

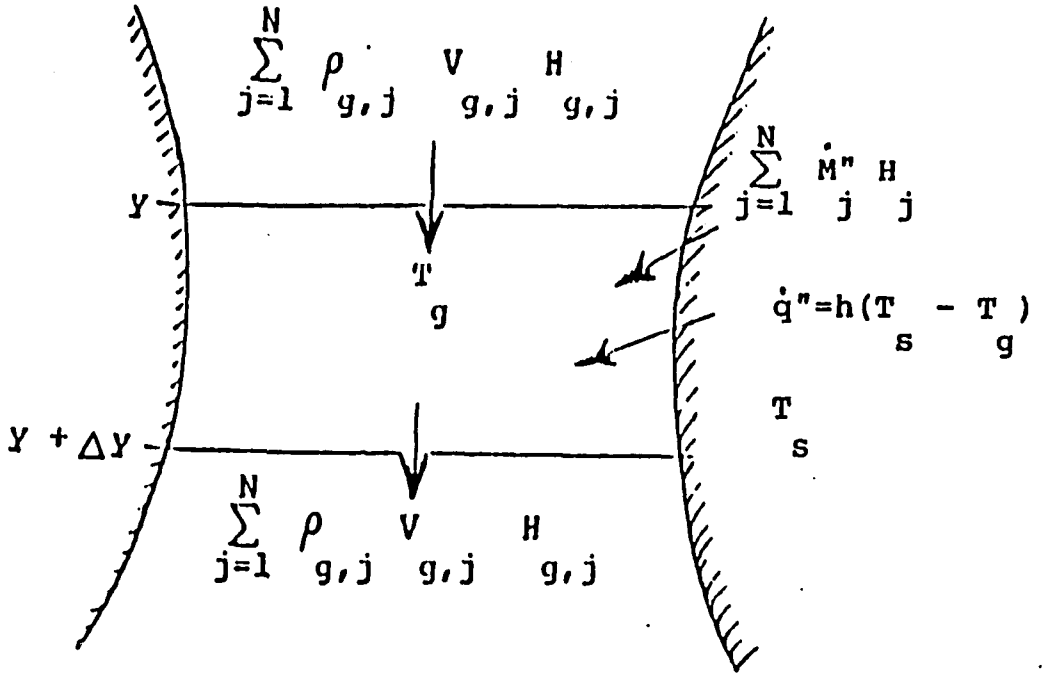

Figure 4.2.2 System for Gas Phase Analysis (Energy Balance)

$$A_g \Delta y \sum_{j=1}^{N} \frac{\partial \rho_{g,j} U_{g,j}}{\partial t} = A_g \sum_{j=1}^{N} \left(\rho_{g,j} V_{g,j} H_{g,j} \right|_{y} -$$

$$\rho_{g,j} V_{g,j} H_{g,j} \Big|_{y+\Delta y}) + hA' \Delta y (T_t - T_s)_g + \sum_{j=1}^{N} \dot{M}''_j H_j (T_s) A' \Delta y_t +$$

$$(\dot{R}''_5 \hat{H}_5 - \lambda \dot{R}''_5 \hat{H}_5 (T_s)) A' \Delta y_t \qquad (4.8)$$

Dividing the equation (4.8) by $A_g \Delta y$ and letting $\Delta y \rightarrow 0$, then in the limit;

$$\sum_{j=1}^{N} \frac{\partial \rho_{g,j} U_{g,j}}{\partial t} = - \frac{\partial}{\partial y} \sum_{j=1}^{N} (\rho_{g,j} V_{g,j} H_{g,j}) + \frac{a}{\epsilon} (h(T_s - T_g) +$$

$$\sum_{j=1}^{N} \dot{M}''_j H_j (T_s) + \dot{R}''_5 \hat{H}_5 - \dot{R}''_5 \hat{H}_5 (T_s)) \qquad (4.9)$$

and $\frac{\partial}{\partial y} \sum_{j=1}^{N} (\rho_{g,j} V_{g,j} H_{g,j})$ can be written explicitly as;

$$\frac{\partial}{\partial y} \sum_{j=1}^{N} (\rho_{g,j} V_{g,j} H_{g,j}) = \sum_{j=1}^{N} \frac{\rho_{g,j} V_{g,j} C_{pg,j}}{\tilde{M}W_j} \frac{\partial T_g}{\partial y} +$$

$$\sum_{j=1}^{N} H_{g,j} \frac{\partial \rho_{g,j} V_{g,j}}{\partial y} \qquad (4.10)$$

where

$$\sum_{j=1}^{N} H_{g,j} \frac{\partial \rho_{g,j} V_{g,j}}{\partial Y} = \sum_{j=1}^{N} H_{g,j} \left(\frac{a}{\epsilon} \sum_{i=1}^{4} \dot{R}''_{i} (\nu_{ij} - \gamma_{ij}) - \frac{\partial \rho_{g,j}}{\partial t} \right) \quad (4.11)$$

and

$$\sum_{j=1}^{N} \dot{M}''_{j} H_{j}(T_{s}) = \sum_{i=1}^{4} \dot{R}_{i} \sum_{j=1}^{N} H_{g,j}(T_{s}) (\nu_{ij} - \gamma_{ij}) \quad (4.12)$$

and also,

$\sum_{j=1}^{N} \frac{\partial \rho_{g,j} U_{g,j}}{\partial t}$ can be written explicitly as;

$$\sum_{j=1}^{N} \frac{\partial \rho_{g,j} U_{g,j}}{\partial t} = \sum_{j=1}^{N} \left(\rho_{g,j} \frac{\partial U_{g,j}}{\partial t} + U_{g,j} \frac{\partial \rho_{g,j}}{\partial t} \right) \quad (4.13)$$

Substituting the equations (4.10), (4.11), (4.12), and (4.13) into the equation (4.9), and yield:

$$\sum_{j=1}^{N} \left(\rho_{g,j} \frac{\partial U_{g,j}}{\partial t} \right) = \sum_{j=1}^{N} \frac{\dot{m}''_{g,j} C_{pg,j}}{\tilde{MW}_j} \frac{\partial T_g}{\partial Y} +$$

$$\frac{a}{\epsilon} \left(h_s (T_s - T_g) + \sum_{i=1}^{4} \dot{R}''_i \sum_{j=1}^{N} (H_j(T_s) - H_j(T_g)) (\nu_{ij} - \gamma_{ij}) + \right.$$

$$\left. \dot{R}''_5 \left(\hat{H}_5 - \lambda \hat{H}_5 (T_s) \right) \right) \qquad (4.14)$$

or

$$\sum_{j=1}^{N} \left(\rho_{g,j} \frac{\partial U_{g,j}}{\partial t} \right) = \sum_{j=1}^{N} \frac{\dot{m}''_{g,j} C_{pg,j}}{\tilde{MW}_j} \frac{\partial T_g}{\partial Y} +$$

$$\frac{a}{\epsilon} \left(h_s (T_s - T_g) + \frac{1}{\tilde{M}_c} \sum_{i=1}^{4} \dot{R}''_i \sum_{j=1}^{N} (\hat{H}_j(T_s) - \hat{H}_j(T_g)) (b_{ij} - a_{ij}) + \right.$$

$$\left. \dot{R}''_5 \left(\hat{H}_5 - \lambda \hat{H}_5 (T_s) \right) \right) \qquad (4.15)$$

Where $\dot{m}''_{g,j}$ is the local mass flux of gas species, $H_j(T_s)$ and $H_j(T_g)$ are the total molar enthalpies of gas species at local solid and gas phase temperature, a_{ij} is the stoichiometric coefficient of reactant gas species j in reaction i, b_{ij} is the stoichiometric coefficient of product gas species j in reaction i, N is the total number of gas species. The effective contact area of the solid particle per

unit volume of the bed, a, is given by (30)

$$a = \frac{6(1-\epsilon)}{d_p}$$

The water-gas shift reaction is exothermic, and the λ is the fraction of this energy released which is absorbed by the ash products around the solid particles. In this study the λ was assumed to be zero (5). In reality, λ could be a function of the mineral contents in the coal (53).

4.2.3 Material Balance (Solid Phase)

The differential equation for the mass balance in the solid phase was derived for the system shown in Figure 4.2.3.

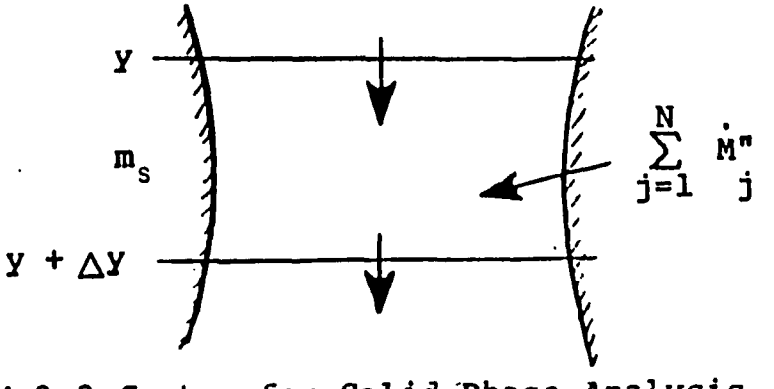

Figure 4.2.3 System for Solid Phase Analysis (Material Balance)

$$A_s \Delta y \frac{1}{\forall} \frac{dm_s}{dt} = - \sum_{j=1}^{N} \dot{M}''_j A'_t \Delta y \qquad (4.16)$$

Dividing the equation (4.16) by $A_s \Delta y$, and yield;

$$\frac{1}{\forall} \frac{dm_s}{dt} = - \sum_{j=1}^{N} \dot{M}''_j \frac{A'_t}{A_s} \qquad (4.17)$$

where

$$\frac{A'_t}{A_s} = \frac{a}{(1-\epsilon)} \qquad (4.18)$$

and

$$m_s = \forall_s \rho_s = 4 \pi r_s^3 \rho_s /3 \qquad (4.19)$$

and also,

$$\forall = \text{Volume of particle} = 4 \pi R_p^3 /3 \qquad (4.20)$$

By substituting the equations (4.18), (4.19), and (4.20) into the equation (4.17), and yield;

$$\frac{d\xi}{dt} = - \frac{a}{3(1-\epsilon)\rho_s \xi^2} \sum_{j=1}^{N} \dot{M}''_j \qquad (4.21)$$

or

$$\frac{d\xi}{dt} = - \frac{a}{3(1-\epsilon)\rho_s \xi^2} \sum_{i=1}^{4} \dot{R}''_i \qquad (4.22)$$

where

$$\xi = \frac{r_s}{R_p} \qquad (4.23)$$

4.2.4 Energy Balance (Solid Phase)

The differential equation for the energy balance in the solid phase was derived for the system in Figure 4.2.4.

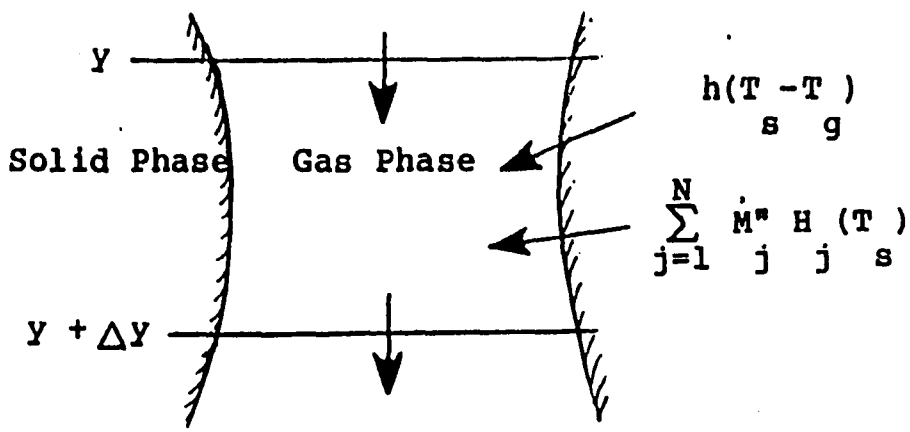

Figure 4.2.4 System for Solid Phase Analysis (Energy Balance)

$$A_s \Delta y \frac{\partial \rho_s U_s}{\partial t} = - hA'_t \Delta y (T_s - T_g) - \sum_{j=1}^{N} \dot{M}''_j H_j (T_s) A'_t \Delta y \qquad (4.24)$$

Dividing the equation (4.24) by $A_s \Delta y$, and yield;

$$\frac{\partial \rho_s U_s}{\partial t} = - \frac{a}{(1-\epsilon)} (h(T_s - T_g) + \sum_{j=1}^{N} \dot{M}''_j H_j (T_s)) \qquad (4.25)$$

or

$$\rho_s C_s \frac{\partial T_s}{\partial t} = - \frac{a}{(1-\epsilon)} (h(T_s - T_g) + \frac{1}{\tilde{M}_c} \sum_{i=1}^{4} \dot{R}''_i$$

$$\sum_{j=1}^{N} \hat{H}_j (T_s) (b_{ij} - a_{ij})) \qquad (4.26)$$

where ρ_s is solid density, and C_s is solid specific heat, and their values (6) are given as follow:

$\rho_s = 1.4$ gm/cm^3

$C_s = 0.25$ (cal/g $^\circ$K) $\quad T_s \geq 1200^\circ$K

$C_s = 0.27 \quad 1100 < T_s < 1200^\circ$K

$C_s = 0.30 \quad 1000 < T_s < 1100^\circ$K

$C_s = 0.32 \quad T_s \leq 1000^\circ$K

4.2.5 Boundary and Initial Conditions

The boundary and initial conditions are as follows:

$$\left.\begin{aligned}
\dot{m}''_{H_2O} &= (\dot{m}''_{H_2O})_f \\
\dot{m}''_{O_2} &= (\dot{m}''_{O_2})_f \\
\dot{m}''_{CO_2} &= 0 \\
\dot{m}''_{CO} &= 0 \\
\dot{m}''_{H_2} &= 0 \\
\dot{m}''_{CH_4} &= 0 \\
T_g &= T_{gf}
\end{aligned}\right\} \quad \text{at } y=0 \quad \text{(air entry point)}$$

and

$$\left.\begin{aligned}
T_s &= T_{si}(y) \\
\xi &= 1.0 \ (y)
\end{aligned}\right\} \quad \begin{aligned} &0 \leqslant y \leqslant L \\ &\text{at } t= 0 \text{ and is given at the} \\ &\text{end of ignition process.} \end{aligned}$$

where T_{gf} is the feed temperature of the gas, and T_{si} is the temperature of solid after ignition. This solid temperature can be found either experimentally or numerically.

If an experimental apparatus was available, the following approach is used to find the initial conditions for solid temperture:

> At the onset of combustion, or when the local temperature at the top of the bed is about 2000 ^{o}F, the temperature of the bed is taken at different bed height, i.e 2" intervals, by means of thermocouples. This temperature distribution is now the initial solid temperture, T_{si}.

If an experimental apparatus is not available, the numerical approach (an option of the computer model) is to be used which is:

> The char is ignited in the presence of the combustion of methane and air with a product temperature at 1200 ^{o}F. After about five minutes of combustion, the methane is removed. Then the temperature of the solid in the bed is obtained numerically at every 1/2" interval. This temperature distribution is now the initial solid temperature T_{si}. Combustion and gasification then continues in the presence of air and the specified relative humidity.

A numerical solution procedure for the above system of partial differential equations will be described in the next Chapter.

4.3 Gas-Solid Heat Transfer Coefficient

No data was available for estimating the local gas-solid heat coefficient for the coal bed in which complicated chemical reactions take place. An empirical expression to

calculate the gas-solid heat transfer coefficient for nonreactive systems is obtained from a j-factor correlation given by Gupta and Thodos (46). For the particle Reynolds number, a value of 200 was found to be a value characteristic of the fixed-bed gasifier in this study for char diameters up to 1 cm (2). The correlation can be rearranged to the form,

$$h_n = \frac{2.06}{\epsilon}\left(\frac{\mu}{d_p \dot{m}''_g}\right)^{.575}\left(\frac{k_e}{C_p \mu}\right)^{2/3} C_p \dot{m}''_g \qquad 90 < Re \leq 4000$$

where, μ is the local viscosity of the gas. Because of the difficulty involved in calculating the local viscosities of each gas, they were assumed to be the same as the viscosity of the inlet air at the inlet temperature. The error caused by this assumption can be neglected because its overall value is to the power 0.09. The specific heat, C_p, of each gas is given by;

$$C_p = a + b\,T_g + c\,T_g^2$$

The a, b, and c are constants specific for each gas.

The local effective heat conductivity of the gas, k_e, is (53,47);

$$k_e = 0.376 \times 10^{-3}\,\dot{m}''_g \qquad 100 < Re < 1000$$

This suggested relationship, by Cho, Y. S. (53), for k_e accounts for turbulent diffusion which is a result of turbulent mixing of portions of the gas stream. However, one can argue that the Reynolds number in the empirical expression for the heat transfer coefficient h_n, already accounts for turbulent diffusion. Therefore, it appears that Cho (53) accounted for the effect of turbulent diffusion in both the heat transfer coefficient and thermal conductivity. However, in this study the effective thermal conductivity was used because it generally accounts for the radiation, thermal diffusion, and molecular thermal conductivity between the gas and solid.

In this work the actual heat transfer coeficient h is taken as a function of h_n, the empirical heat transfer coefficient for the nonreactive system. A proportionality factor was suggested by Cho Y. S. (12) and is defined as;

$$\zeta = \frac{h}{h_n}$$

The value of ζ could depend on several parameters such as coke type, reactivity of coke, rate of reactions, and radiation (5). Therefore, its value will be left as an adjustable parameter. It should be noted that the value of ζ is assumed constant throughout the bed.

5. COMPUTER SIMULATION

5.1 Numerical Difficulties

The mass and energy balance equations are transient boundary value problems which may be solved in closed form or approximated by numerical methods. The numerical methods used in the papers described in the literature survey are as follows; The simplest approach , utilized by Yoon, et al. (2), is a shooting marching type integration method. This method integrates from the initial state to the final state of their homogeneous (gas temperature = solid temperature) model (2). While this method worked well for the homogeneous case, it was inadequate for analyzing the heterogeneous (gas temperature $\neq$ solid temperature) model (2). Amundson and Arri (7) also applied the shooting marching type integration method to their heterogenous model, which yielded inaccurate results (2). Therefore, they employed an implicit method (a finite - difference approximation) to solve the sets of ordinary differential equations in their model. Cho, et al. (5) also solved their ordinary differential equations by using a shooting method for modeling and simulating a Lurgi-type gasifier. A fourth order explicit Runge-Kutta scheme was used for the integration. In attempting to solve the mass and energy equations which involve chemical kinetics, a

condition known as stiffness may have introduced difficulties (5). Stiffness refers to a system of ordinary differential equations having drastically different time constants that often impose severe " Δt limitation" upon numerical integration routines in order to insure stability. Such systems are known as time constant limited, or "stiff," systems.

The finite-difference method was one of many methods applied to solve the mass and energy equations associated with the model developed in this dissertation. Since almost all of the heat is generated on the surface of the solid (by combustion) and transferred through the gas film, integration over extremely small time intervals did not yield a stable solution. The difficulty of stiffness in the model can be avoided by assuming that no endothermic reactions take place in the combustion zone (7). However, this assumption was not employed in this study.

These stiff systems can be solved by applying pseudo-steady-state assumptions which allow the extremely fast modes of the differential equations to go to zero. In this case, one could effectively neglect the accumulation of mass in the gas stream, with respect to time, by setting the left hand side of equation (4.6), equal to zero. Therefore, the mass accumulation in the gas stream was negligible in relation to the mass generated by chemical reaction and the convective

mass flux. For similar reasons, one can neglect the energy accumulaton in the gas stream in relation to the heat generated by chemical reaction and the convective heat flux.

Employing this additional assumption, the mass and energy equations (gas phase) 4.6, 4.7, and 4.15 can be reformulated. Equation (4.6) may now be written as;

$$\frac{d \sum_{j=1}^{n} \dot{m}''_{g,j}}{dy} = \frac{a}{\epsilon} \sum_{i=1}^{4} \dot{R}''_i \qquad (5.1)$$

and for the local component mass balance, equation (4.7) yields.

$$\frac{d\dot{m}''_{g,j}}{dy} = \frac{a}{\epsilon} \left(\sum_{i=1}^{4} \dot{R}''_i \sum_{j=1}^{N} (\nu_{ij} - \gamma_{ij}) + \widetilde{MW}_j \dot{R}''_5 \right.$$

$$\left. \sum_{j=1}^{N} (b_{ij} - a_{ij}) \right) \qquad (5.2)$$

And for the gas phase, the energy equation (4.15) reduces to

$$\sum_{j=1}^{N} \frac{\dot{m}''_{g,j} C_{pg,j}}{\widetilde{MW}_j} \frac{dT_g}{dy} = \frac{a}{\epsilon} h (T_s - T_g) + \frac{a}{\epsilon} \frac{1}{\widetilde{M}_c}$$

$$\sum_{i=1}^{4} \dot{R}''_i \sum_{j=1}^{N} (\hat{H}_j (T_s) - \hat{H}_j (T_g)) (b_{ij} - a_{ij}) + \frac{a}{\epsilon} \dot{R}''_5 \Delta H_5 \qquad (5.3)$$

5.2 Solution Procedure

A total of seven ordinary differential equations (ODE's) for the local component mass balances yield:

$$\frac{d\dot{m}''_{O_2}}{dy} = -\frac{a}{\epsilon}\frac{\widetilde{MW}_{O_2}}{\widetilde{M}_c}\frac{1}{\phi}\dot{R}''_1 \qquad (5.4)$$

$$\frac{d\dot{m}''_{H_2O}}{dy} = -\frac{a}{\epsilon}\frac{\widetilde{MW}_{H_2O}}{\widetilde{M}_c}\dot{R}''_2 \qquad (5.5)$$

$$\frac{d\dot{m}''_{CO_2}}{dy} = \frac{a}{\epsilon}\frac{\widetilde{MW}_{CO_2}}{\widetilde{M}_c}\left(\left(\frac{2}{\phi} - 1\right)\dot{R}''_1 - \dot{R}''_3\right) \qquad (5.6)$$

$$\frac{d\dot{m}''_{CO}}{dy} = \frac{a}{\epsilon}\frac{\widetilde{MW}_{CO}}{\widetilde{M}_c}\left(\left(2 - \frac{2}{\phi}\right)\dot{R}''_1 + \dot{R}''_2 + 2\dot{R}''_3\right) \qquad (5.7)$$

$$\frac{d\dot{m}''_{H_2}}{dy} = \frac{a}{\epsilon}\frac{\widetilde{MW}_{H_2}}{\widetilde{M}_c}\left(\dot{R}''_2 - 2\dot{R}''_4\right) \qquad (5.8)$$

$$\frac{d\dot{m}''_{CH_4}}{dy} = \frac{a}{\epsilon}\frac{\widetilde{MW}_{CH_4}}{\widetilde{M}_c}\dot{R}''_4 \qquad (5.9)$$

$$C \qquad \frac{d\xi}{dt} = - \frac{a}{3(1-\epsilon)\rho_s \xi^2} \sum_{i=1}^{4} \dot{R}''_i \qquad (5.10)$$

and two ordinary differential equations for the energy balance are:

$$\sum_{j=1}^{N} \frac{\dot{m}''_{g,j} C_{pg,j}}{\widetilde{MW}_{,j}} \frac{dT_g}{dy} = \frac{a}{\epsilon} h (T_s - T_g) + \frac{a}{\epsilon} \frac{1}{\widetilde{M}_c} \sum_{i=1}^{4} \dot{R}''_i \sum_{j=1}^{N} (\hat{H}_j (T_s) - \hat{H}_j (T_g)) (b_{ij} - a_{ij}) \qquad (5.11)$$

and

$$\rho_s C_s \frac{dT_s}{dt} = - \frac{a}{(1-\epsilon)} h (T_s - T_g) - \frac{a}{(1-\epsilon)} \sum_{i=1}^{4} \dot{R}''_i \sum_{j=1}^{N} \hat{H}_j (T_s) (b_{ij} - a_{ij}) \frac{1}{\widetilde{M}_c} \qquad (5.12)$$

These set of nine ODE's must be solved simultaneously.

The water-gas shift reaction, $\dot{R}''_5$, is not included in the rate process given by the above equations, because of the assumption of equilibrium at every point in the system. From the point of view of the computer solution this deletion is unimportant, since for each step in numerical integration, the physical and chemical processes can be considered as having two steps. The first is rate controlled by the above

equations and the second is instantaneous and is given by the equilibrium condition (12):

$$\frac{P_{H_2} P_{CO_2}}{P_{CO} P_{H_2O}} = \exp(-3.6893 + 4020/T_m) \qquad (5.13)$$

Because of the difficulty involved in solving these nine ordinary differential equations analytically, a numerical integration method is used to approximate the solution. For this purpose, the method of Runge-Kutta (48) is employed as follows:

To calculate an integral curve of the equation $dy/dx=f(x,y)$ through the point (x_o, y_o) to the point $(x+\Delta x, y+\Delta y)$, let:

$$K_1 = f(x_i, y_i)$$

$$K_2 = f(x_i + \frac{h_o}{4}, y_i + \frac{h_o}{4} K_1)$$

$$K_3 = f(x_i + \frac{3h_o}{8}, y_i + h_o(\frac{3}{32} K_1 + \frac{9}{32} K_2)$$

$$K_4 = f(x_i + \frac{12h_o}{13}, y_i + h_o(\frac{1932}{2197} K_1 - \frac{7200}{2197} K_2 + \frac{7296}{2197} K_3))$$

$$K_5 = f\left(x_i + h_o,\ y_i + h_o\left(\frac{439}{216}K_1 - 8K_2 + \frac{3680}{513}K_3 - \frac{845}{4104}K_4\right)\right)$$

$$K_6 = f\left(x_i + \frac{h_o}{2},\ y_i + h_o\left(-\frac{8}{27}K_1 + 2K_2 - \frac{3544}{2565}K_3 + \frac{1859}{4104}K_4 - \frac{11}{40}K_5\right)\right) \qquad (5.14)$$

Then

$$y_{i+1} = y_i + h_o\left(\frac{25}{216}K_1 + \frac{1408}{2565}K_3 + \frac{2197}{4104}K_4 - \frac{1}{5}K_5\right) \qquad (5.15)$$

where h_o is the initial guess value for the step size, and will be changed to meet the required tolerance.

In the SUBROUTINE RFK in Appendix III, the code is to integrate from y to y + Δy or t + Δt. On input, the y contains the initial values of the dependent variables; on output it contains the solution values at the output value of y. The parmeters ABSERR and RELERR are absolute and relative accuracy requests respectively. The code estimates the local error in the computation of each component, relative to the step size being used and test whether this estimate EST satisfies;

$$|EST| < RELERR \times |y| + ABSERR$$

for each component. If RELLER = 0, this is pure absolute error test; if ABSERR = 0, it is a pure relative error test; otherwise, it is mixed test. The step size is adjusted so as to meet the accuracy request. The quantity HMX is the maximum

step size to be permitted. It should be taken small enough so that no interesting behavior of the solution will be "jumped over." Values larger than $|\Delta y|$ are, of course, limited to $|\Delta y|$ internally. An input h_o is the nominal step size to be tried. On output it is set to the step size the code believes for continuing the integration. Because a user guess for h_o is often unrealistic, a forgiving approach is taken in the code; an input h_o is changed until it has a reasonable size.

Figure 5.2.1 shows the computational sequence schematically. The computation of the nine ODE's begins by guessing average values for the gas temperature, and mass flow rate of the gas species, (CO_2, O_2, CH_4, H_2, H_2O) between y and $y + \Delta y$. The solid temperature, and ξ were also guessed values between t, $t + \Delta t$. The values of the gas temperature, mass flow rate of the gas species (CO, CO_2, O_2, CH_4, H_2, H_2O) were calculated by performing numerical integration at $y + \Delta y$. Also the values of the solid temperature and ξ were found at $t + \Delta t$. By knowing these values and the initial conditions, average values can be found. At this point, these known average values were compared by guessing average values. If these values were not within 0.1 % agreement, then new guess values were chosen. Since these nine ODE's involved chemical reactions, the direct substitution of known average values for guessed average values failed to converge. Therefore, the new guess

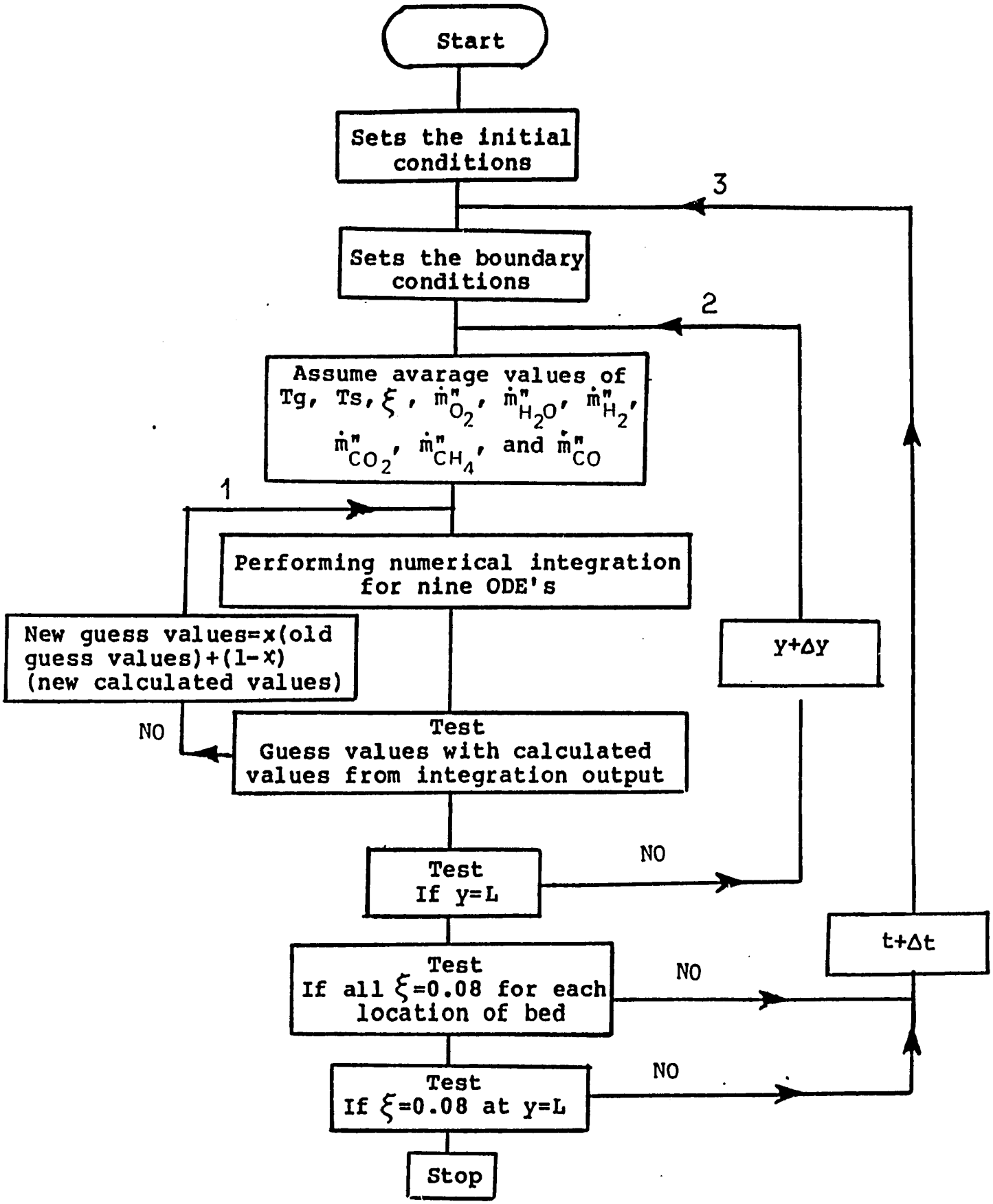

Figure 5.2.1 Computational Sequence

values were found by,

$$\text{New guess values} = x(\text{old guess values}) + (1-x)(\text{new calculated values})$$

where x is defined as the damping coefficient. This substitution of a low damping coefficient (loop 1 in Figure 5.2.1) seems to be the best for convergence. By trial and error, the numerical value of 0.1 for x was found to be the best for this model. The average number of iterations of the loop 1 in Figure 5.2.1 is about ten and the maximum number of iterations is close to forty.

The numerical integration continues for the whole height of the reactor (loop 2 in Figure 5.2.1). When the numerical integration has reached the known value of the reactor height, it is necessary to check the value of ξ to be about 0.08. This corresponds to 1% of actual carbon remaining in the solid. If the value of ξ goes below 0.08, it causes an instability in the computational sequence, because the value of $1/\xi$ is used in the chemical reation rates [Eq. (3.1)]. If the value of ξ is still greater than 0.08, the numerical integration is continued to the next time step ($t + \Delta t$) (loop 3 Figure 5.2.1). This procedure continues until the value of ξ is within the range of 0.08 at the bottom of the reactor.

In this study the values of Δy, and Δt were arbitrarily chosen to be 0.5" and 10 sec., respectively.

6. EXPERIMENTAL SIMULATION OF CROSSFLOW COAL GASIFICATION

6.1 Introduction

Initial gasification studies frequently utilize small scale equipment to reduce the expense and difficulties associated with large scale gasification units. Simulation of this type can be very useful for modeling and predicting critical responses for newly developed gasification processes.

In the combustion of coal on a traveling grate stoker , the top surface of the coal is ignited by radiation from an ignition source. The combustion of coal continues until only ash remains, which is removed at the end of the furnace. In the WVU experimental pot-furnace (49), a fuel can be burned under similar conditions. If the burnout time for the pot-furnace test is correlated with the time the fuel spends on the traveling grate, a close approximation of the fuel bed conditions (e.g compositions of the gases, and the temperature profiles) can be obtained for any part of the bed on a traveling grate. Figure 6.1 shows the relationship between the fuel burned on a traveling grate and the fuel burned in a combustion pot test.

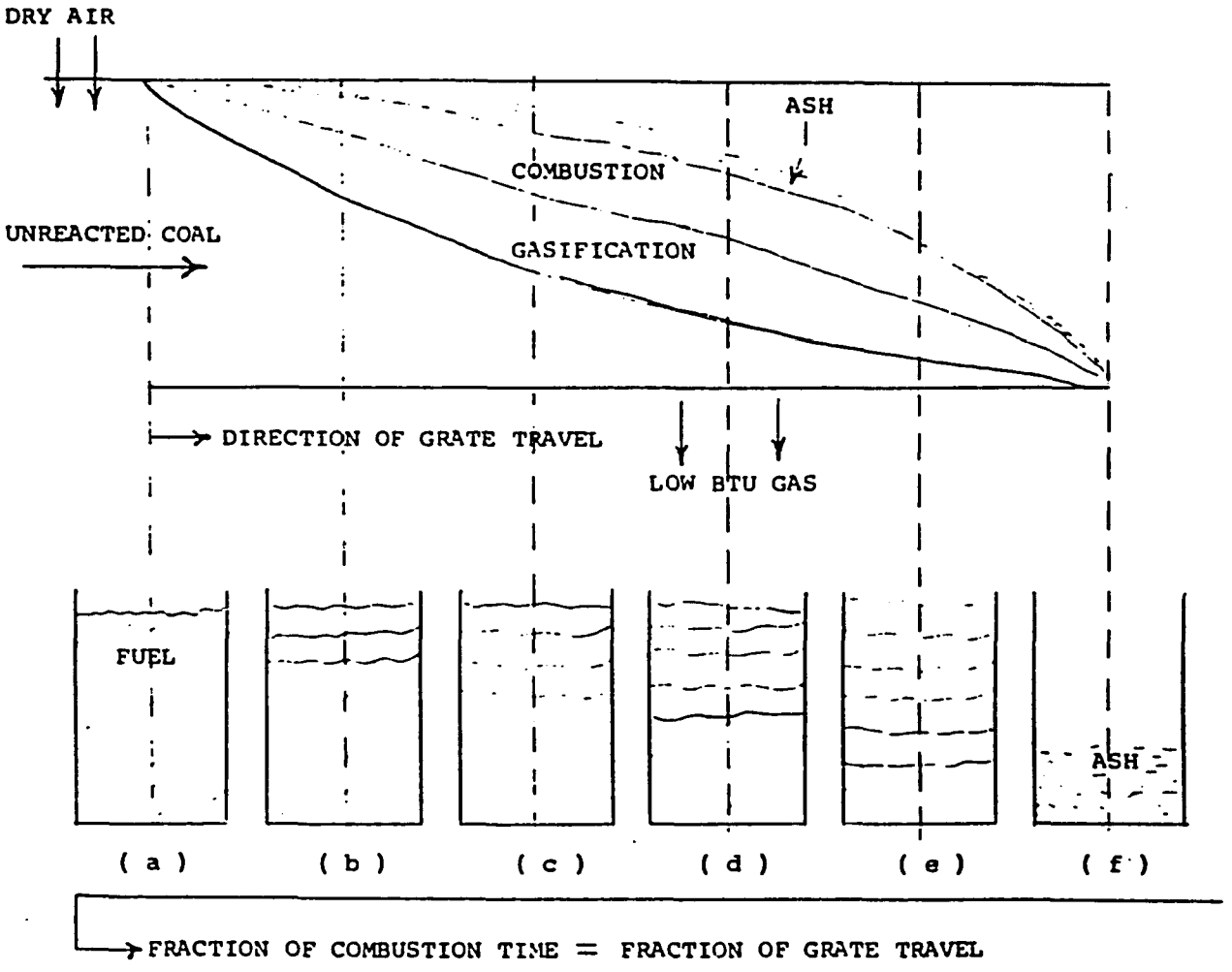

Figure 6.1 Correlation Between Pot Furnace and Crossflow Gasification

The goal of the experimental effort in this study was to furnish data in order to evaluate and improve the computer model. Flow in the experimental system has been simplified to be only downflow. Note that Figure 1.1 shows that flows may be both upflow and downflow in the proposed commercial gasifier.

6.2 Apparatus and Method of Operation of Experiment

6.2.1 Apparatus

The apparatus employed in this study is shown in Figure 6.2. The furnace consists of a cylindrical pot (Figure 6.3), which has a 23" outside diameter and a height of 24" with a stainless steel grate bottom. The pot is lined with 5" of insulating refractory brick to reduce the inside diameter to 13". In addition the bottom of the pot is filled with 6" of inert crushed refractory bricks which allows for possible bed depths of 18". The grate is a 1/8" thick stainless - steel plate with 256 (3/8" diameter) holes. The fuel bed is formed in the pot to a predetermined depth (e.g 13"). The air necessary for combustion was supplied by a Spencer Vortex Blower (serial No. V8-004-E) with maximum volume rate at 75 CFM. This air was preheated as it passed through the steam heater. Supply steam was regulated at 30 psig, using a Kaye MacDonald regulator, to obtain the desired heated air

FIGURE 6.2: CROSSFLOW COAL GASIFICATION EXPERIMENTAL RESEARCH FACILITY

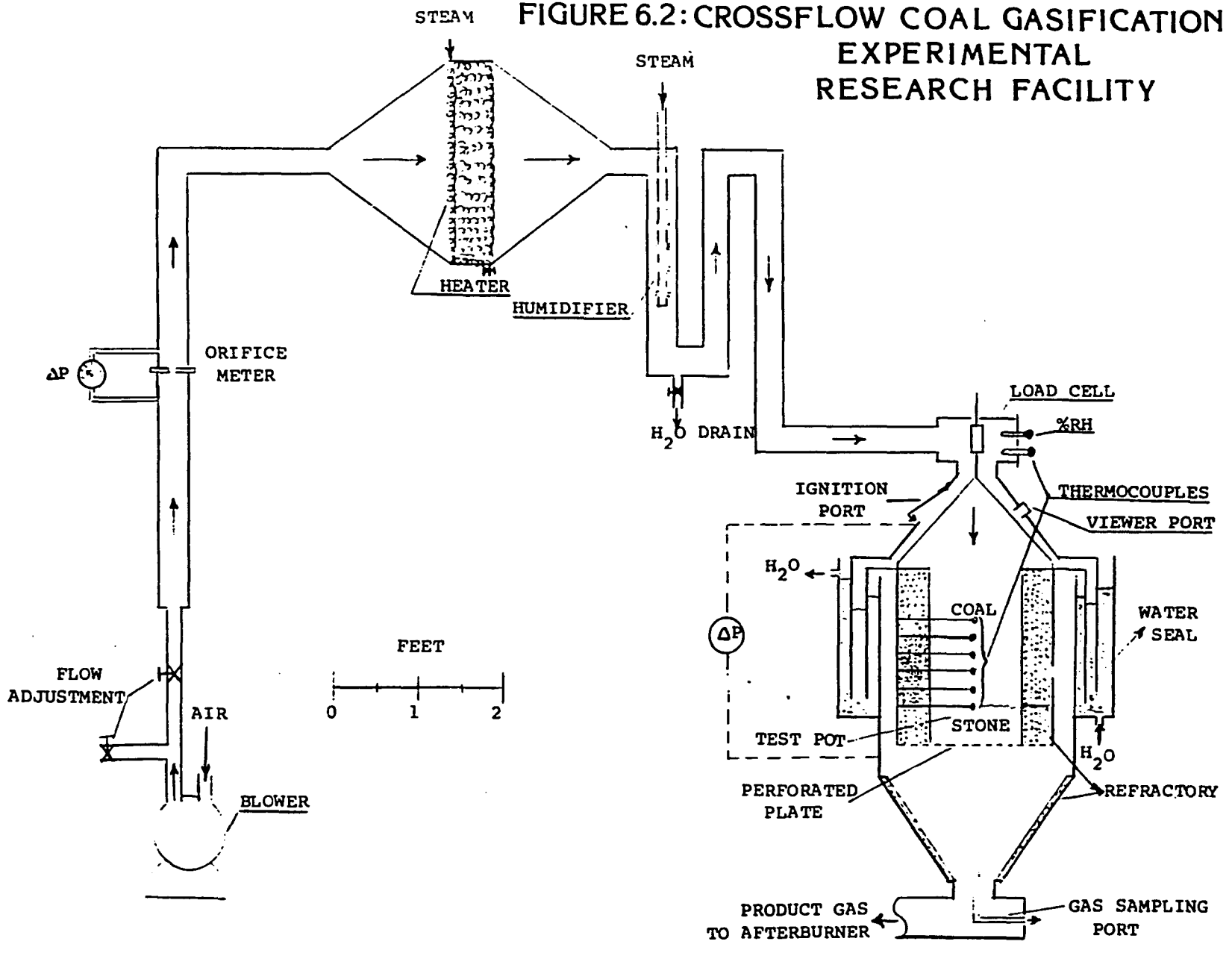

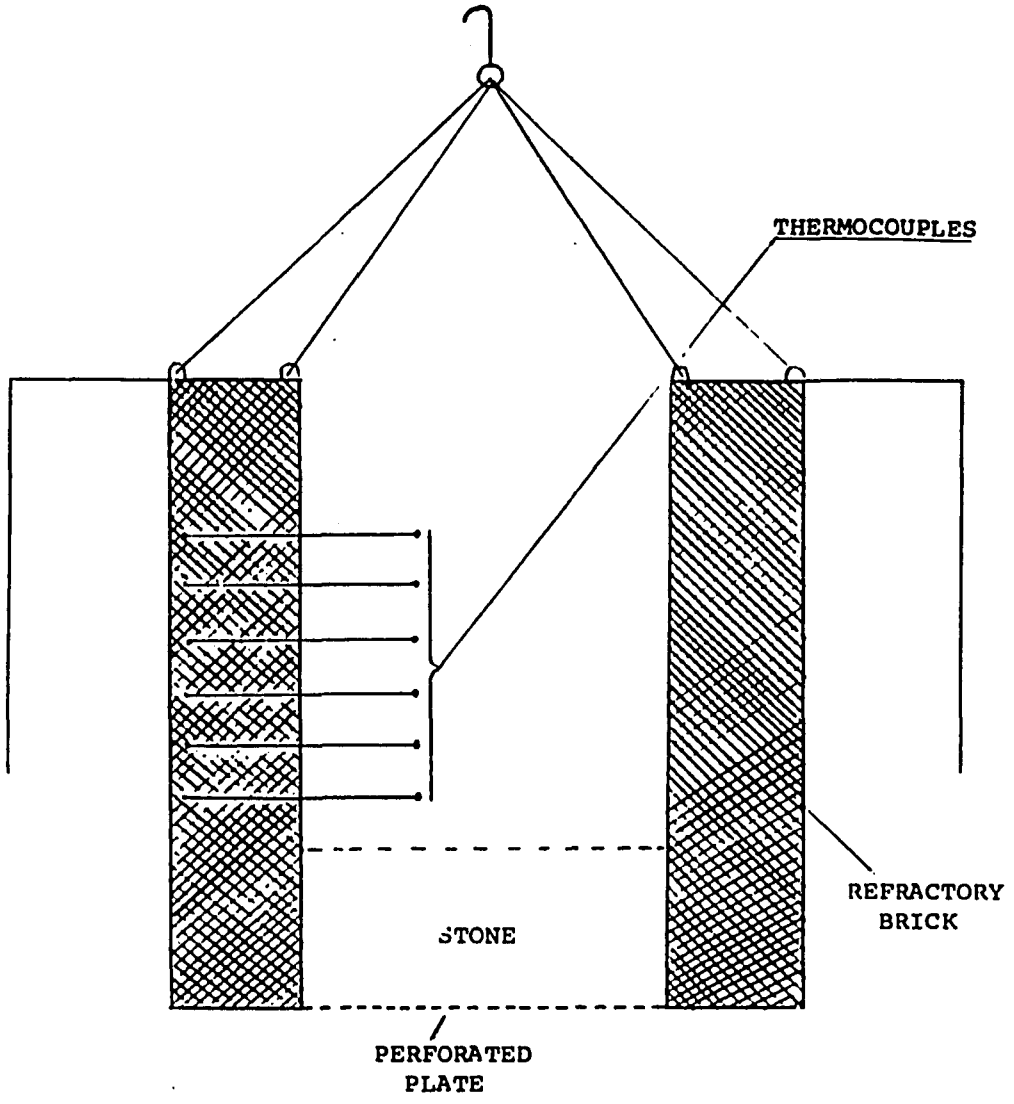

FIGURE 6.3: COMBUSTION POT

temperature. The rate of airflow was measured by an orifice plate. This orifice plate was designed to measure an air flow rate of 50 CFM at a differential pressure of 2" of water. The air was humidified by injecting saturated steam through a 12" long closed end copper tube (3/8" dia.) with six pairs of 1/8" holes, spaced 2" apart in a vertical plane, (Figure 6.2). The air temperature was measured by an Omega RH-20F hydrometer. This instrument is capable of reading temperatures up to 175 ^{o}F, with an error of $\pm$ 1 ^{c}F. The air's relative humidity was measured by a Hydrodynamics L4-4822W sensor and a L15-3050 universal indicator. This instrument is capable of reading relative humidities up to 98 %. with an error of $\pm$1 %.

The fuel bed temperatures were obtained by six platinum/platinum-rhodium thermocouples spaced 2" apart in a vertical plane. These thermocouples are contained in a single, highly refractive (Omegatite 300) sheath and are connected to an Omega jack panel with a rotory selector switch and readout (Serial No. 3530044).

The pressure drop across the combustion pot was measured by connecting two 1/4" copper tubes from the top and bottom of the pot to the Dwyer pressure gage (Cat. No. 2003C). This pressure gage measures pressures ranging from 0" to 3" of water, with an error of $\pm$ 0.06" of water.

The combustion pot was suspended from a lever arm. This lever arm was equipped with a load cell that enabled the weight of the pot and its contents to be measured independently from the experimental apparatus. This was accomplished by a liquid seal which allowed the test pot to hang freely and maintain a division between the inlet and outlet gas streams (Figure 6.2). The load cell was a Sensotec model RM - 1K, hermetically sealed to withstand humid and corrosive environments and provided for a temperature compensation from 60 to 160 ^{o}F. This load cell was capable of reading weights from 0 to 1000 lbs. with an accuracy of $\pm$2 lbs. A radiation shield was installed to prevent the load cell from exposure to the radiation from the gasification and combustion in the pot. A Sensotec 450 D digital readout with 0 to 5 volts recorder output was used in conjunction with the load cell. For continuous reading, this readout was connected to a strip - chart recorder (Fisher Recordall Series 5000).

When the coke was gasified, the gasification products entered an insulated pipe that prevented the tars and other heavier products from being condensed out. The majority of these products were sent to the afterburner where the product gases were burned. Gas samples were also taken from these products at ten minute intervals, and analyzed with a gas chromatograph.

The gas chromatograph was a thermal conductivity type, Gow -Mac Series 550, equipped with a gas sampling valve, purge and inject positions, series by-pass column swithching valve, one molecular sieve 5 A column and one porapak Q column. When the gas sampling valve was set on the inject position, the samples were introduced into the porapak column where CO_2, CH_4 are retained. By setting the by - pass valve in the series position, the components H_2, N_2, O_2, and CO pass through the porapak column and into the molecular sieve column. At this point, the switching valve was changed to the by - pass position and the components retained in the porapak column were purged with the helium carrier gas to the detector. Meanwhile, the components in the molecular sieve column were being stored. Then the switching valve was returned to the series position, allowing the stored components in the molecular sieve column to be carried to the detector. A Hewlett Packard 3300 integrator was used to analyze the gas chromatograph output. Before the gas sample reached the gas - chromatograph, it passed through a cold trap where the tars and H_2O were condensed. The volumetric flow rate of each gas sample was also monitored using a gas buret. A flow sheet of the gas sampling train is shown in Figure 6.4.

The afterburner (Figure 6.5), is essentially a furnace in which the product gas is burned. The vessel was lined with 2" of insulating refractory block and 1" of ceramic fiber

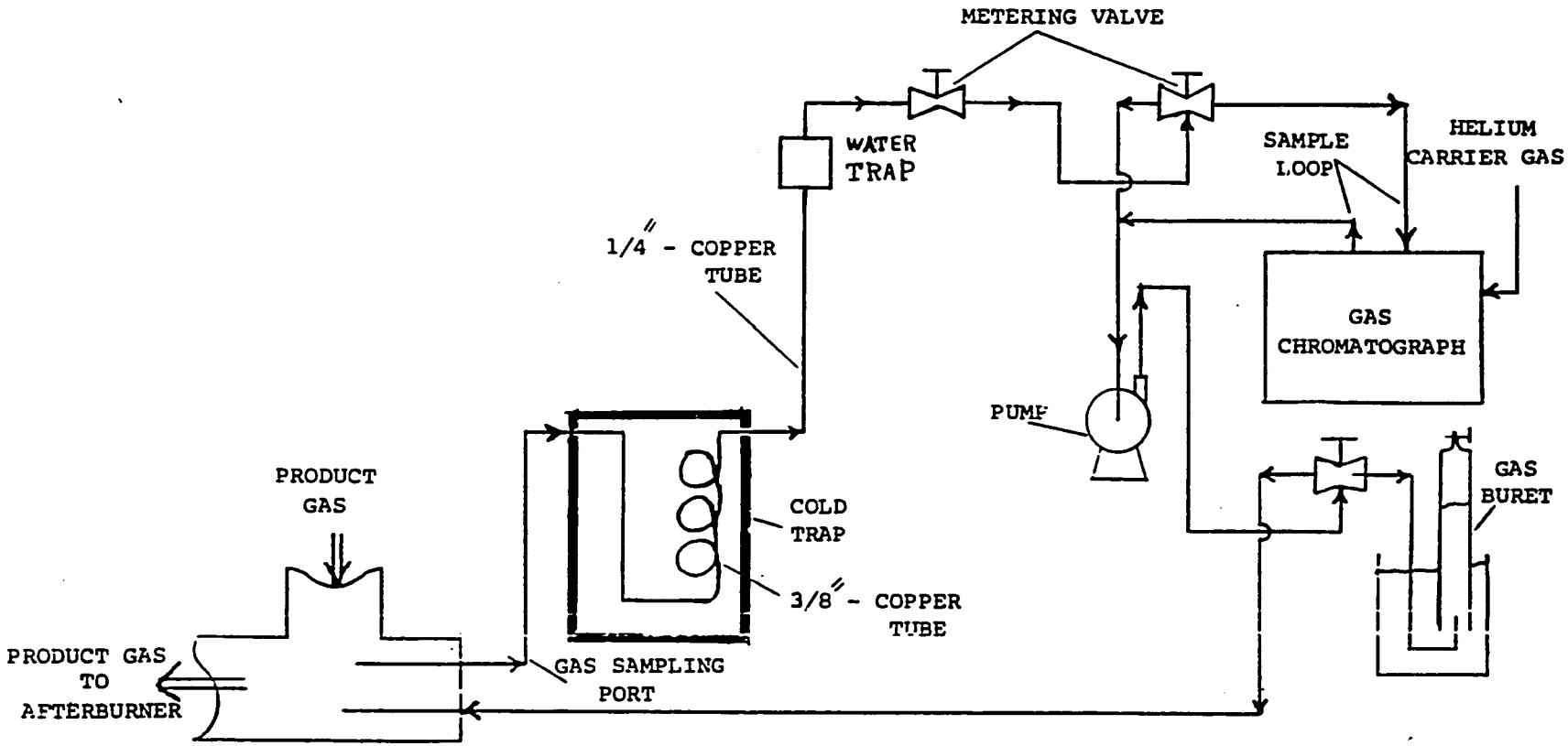

FIGURE 6.4: GAS SAMPLING TRAIN

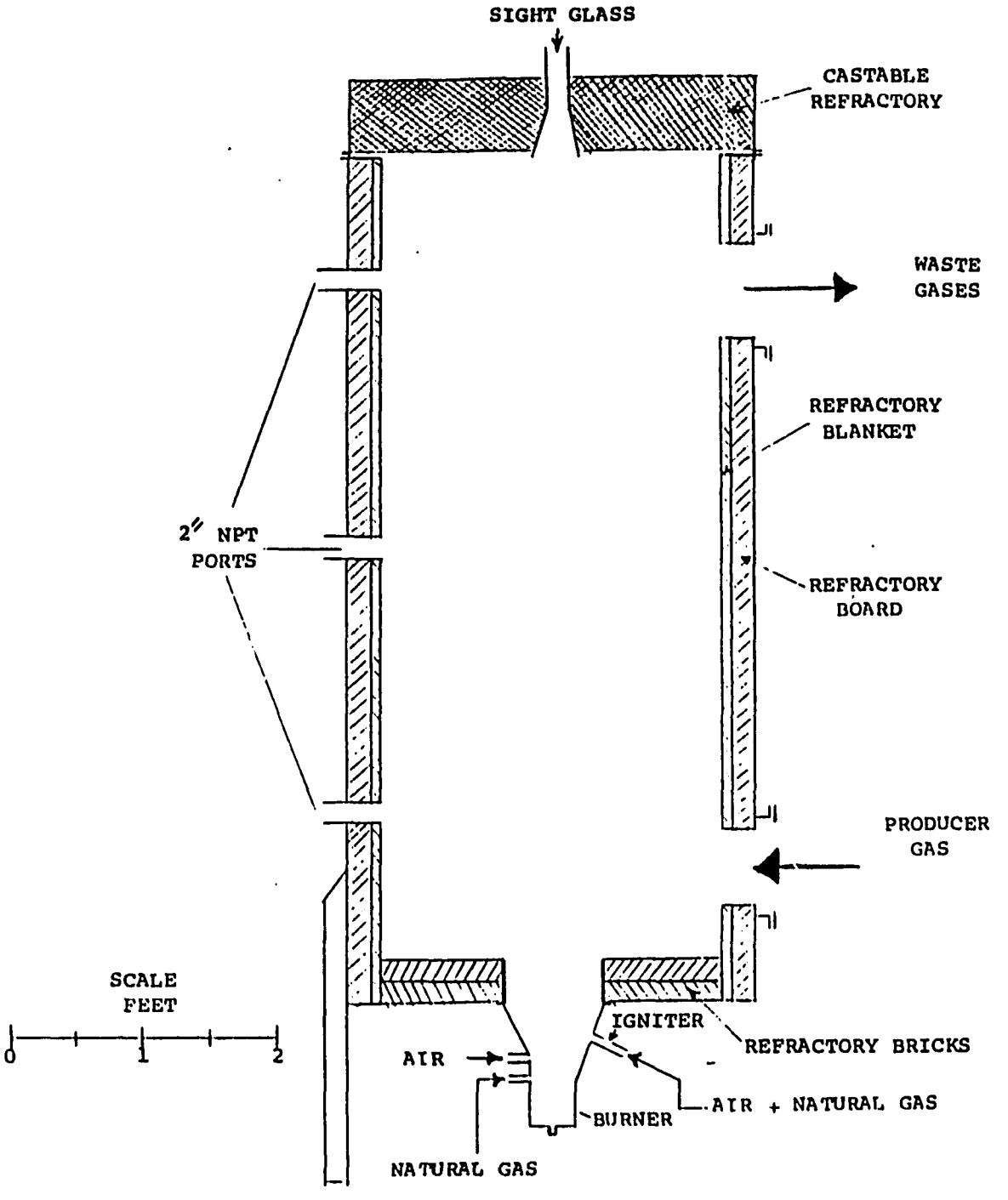

FIGURE 6.5: AFTERBURNER CROSS SECTION

blanket and was fired by a North American Manufacturing natural gas burner which is capable of delivering 160,000 BTU/hr. This burner was equipped with a flame safety system and an electronic pilot system. To assure complete ignition of the product gases, the gases entered at the bottom of the vessel perpendicular to the burner flame. Excess air was also fed to the afterburner to provide for complete combustion of the product gases and to limit the maximum temperature to 2000 ^{o}F. Additional air was supplied to the exhaust gas to cool it to 1,000^{o}F so that it could be safely vented into the atmosphere. A more detailed description of this test facility may be found in (49).

For safety purposes a CO monitor was mounted in the building to detect gas leakage from the system into the environment.

6.2.2 Fuel Preparation

Metallurgical quality crushed coke was gasified in these experiments. These pieces were crushed by a mechanical crusher in West Virginia University's, mineral science building, White Hall. The pieces were then sized by hand, using standard twelve inch square mesh sieves with openings of 1/4" x 3/16", and 3/16" x 1/8" to yield nominal particle sizes, 7/32" ($\pm$ 1/32") and 5/32" ($\pm$ 1/32"). Approximately 35

lbs. of the sized coke was gasified in each experimental run.

6.2.3 Method Of Operation

After the fuel sample was prepared and weighed, it was charged into the pot to a pre-determined depth (e.g 13"). Then the pot was placed into the system (Figure 6.2). The upperhood was carefully lowered into place so that there was no contact between the upperhood, the lower cone, or the combustion pot. The pot thermocouple leads were then attached to the temperature readout. Water was then allowed to flow into the jacket around the outside of the lower cone to cool the surface of the lower cone and the combustion pot, and also to provide an air - tight seal between the inlet and the outlet of the bed (Figure 6.2). Air was fed into the system by means of a blower, and the flow kept constant through a flow adjustment valve. The air was heated to 140 ^{o}F and humidified to 98% RH before entering the combustion pot. The heated air was blown through the system at 60 CFM while the instrumentation was being prepared, so that the air passage would approach the temperature of the air, achieving steady state. At this point, pre-ignited fuel (charcoal) was spread over the top of the fuel sample through the ignition port (Figure 6.2) to start ignition in the combustion pot.

A standard period of five minutes with an air flow of 60

CFM was established to ignite the upper layer of fuel, then the air flow was adjusted. During the run the temperature profile in the combustion pot, the pressure drop across the pot, the weight of pot, and the temperature of gases leaving the pot were recorded at 1 minute time intervals. Gas samples were also recorded at 10 minute time intervals. Six to eight samples were recorded during each run. The gasification was considered complete when the combustion front reached the bottom of the fuel bed. This was tracked by the thermocouples placed at 2" intervals within the depth of the bed. At this point the air supply and measuring instruments were shut off. Nitrogen gas was blown through the combustion pot to prevent any additional reactions between the gases.

Coke was employed as the fuel in order to avoid any devolatilization or caking problems, as the model only involves the gasification of coke or char. Analysis of this fuel is given in Table 6.2.1. Coke was gasified in a series of only four experimental runs, due to limited resources. One of the four runs was eliminated due to instrumentation failure. Therefore, three runs are considered, and the conditions are given in Table 6.2.2.

Table 6.2.1 Analysis of Used Coke

	Dried Fuel	As Recieved
Calorific value in BTU's per lbs	12,113	12,071
Proximate Analysis (% W)		
Moisture	---	0.8
Volatile matter	1.5	1.5
Fixed Carbon	84.8	84.1
Ash	13.7	13.6
Ultimate Analysis (% W)		
Moisture		0.4
Carbon		83.19
Hydrogen		0.27
Sulphur		0.78
Nitrogen		1.02
Oxygen		1.04
Ash		13.3
Ash Characteristics		
Ash Fusion at reducing atmosphere;		
Initial deformation temperature		2041 ^{o}F
Softening temperature		2160 ^{o}F
Hemispherical temperature		2412 ^{o}F
Fluid temperature		2506 ^{o}F

Table 6.2.2 Experimental Runs

Run No.	Air Flow Rate (CFM)*	Air Relative Humidity (%)	Particles Diameter (in)
1	36	70	7/32
2	17	95	7/32
3	25	90	5/32

* measured at Temp.=75 ($\pm$2) $^{\circ}$F, and Press.=1 ($\pm$0.02) atm.

The depth of the fuel bed was 13" in all cases, and the inlet air temperature was maintained constant at 140 $^{\circ}$F.

7. RESULT AND DISCUSSION

7.1 Introduction

The initial phase of this study consisted of an extensive examination of previous fixed bed gasifier research. The next phase of this study was to develop a mathematical model to simulate the gasification component of the crossflow coal gasification process. Because of the extensive calculations required to solve the nine ordinary differential equations in this model, a numerical integration method was used to simultaneously solve the equations. The arbitrary input parameters for the numerical analysis consisted of the airflow rate, air temperature, air relative humidity, particle diameter, void fraction, gas-solid heat transfer coefficient factor, and the chemical reaction rate constants. Composition of gases (H_2, CO, CO_2, CH_4, H_2O, O_2, N_2), solid temperature, gas temperature, and carbon conversion were the outputs generated by the numerical analysis. The generated data from the computer model was compared to the data found in the litareature survey.

The sensitivity of several parameters (heat transfer coefficient factor, void fraction, particle diameter, and reactivity factor coefficients) was examined for their effect on the products of the gasification process. The data

generated by the computer model were also compared with experimental data measured from the pot-test apparatus. Based on the comparison of these data, modifications were made to the appropriate parameters of the computer model based on the sensitivity analysis. It was found that by modifying these parameters, the outputs generated by the computer model were consistent with the data actually measured from the experimental effort, and that the modifications are within the experimental data scatter for the phenomena modified.

7.2 Comparison of Basic Model Versus Existing Data

The available data on the fixed-bed gasification of coke, are reasonably consistent with the computer model. For the computer model, the inputed values for the gas-solid heat transfer coefficient factor (ζ) was assumed to be one, and the chemical kinetics used are described in Appendix II, with the reactivity factor coefficients of one for both C-CO_2 and C-H_2O reactions. This model is referred to as the basic model. Since the gas-solid heat transfer coefficient and the chemical kinetics are dependent on the reactivity of char/coke (sections 3.2.6 and 4.3), the values of these parameters in the computer model could be changed for a specific char/coke. The computer model for a specific char/coke is called the specific model.

Table 7.2.1 shows the comparison of gas compositions at the outlet of the bed, between the basic model and the available fixed bed gasification data from the literature. This basic model was run at atmospheric pressure, heated air (140 ^{o}F), an air flow rate of 36 CFM, and a relative humidity of 85%. The Wellman Galusha (50) data are based on a fixed bed gasifier which operates with atmospheric pressure, using saturated heated air (140 ^{o}F). The basic model's data are accurate to within 2% of the Wellman Galusha (50) data. Therefore, the simulated char-gasification for the crossflow coal gasifier can be compared to the Wellman Galusha fixed bed gasifier. Also, according to Hoffman (51), the generated data from the basic model compares to any fixed-bed gasifier in general, to accuracy of 2-5%.

Table 7.2.2 shows the comparison of gas compositions between the basic model and the experimental data by Eapen et al. (9), and Karzhavina (10). The inputed data for the basic model were, air flow rate of 5 CFM, particle diameter of 0.375", relative humidity of 20%, and an air temperature of 80 ^{o}F, the same as Eapen's (9) experimental run. Karzhavina's (10) data are based on the burning of a thin layer of char-coal, in a furnace tube. The data generated by the basic model are accurate within 2-8% of Eapen's (9), and Karzhavina's (10) data. Figure 7.2.1 shows the variation of gas compositions with the depth of the bed for the basic

Table 7.2.1 Comparison of Gas Composition at the Outlet of the Bed Between the Basic Model and Commercial Gasifiers

Component (% V)	Basic Model*	Wellman Galusha (50)	Fixed-Bed Gasifier (51)
H_2	9.0	10.0	15.0
CO	28.0	29.0	27.0
CO_2	5.5	3.5	5.0
N_2	56.0	56.8	52.0
CH_4	0.6	0.7	1.0
Other	0.9	----	----

* This data represents the results for 80% of the total burning time.

Table 7.2.2 Comparison of Gas Composition at the Outlet of the Bed Between the Basic Model and Other Experimental Data

Component (% V)	Basic Model*	Eapen (9)	Karzhavina (10)
H_2	---	---	---
CO	26.0	23.0	24.0
CO_2	8.2	7.0	5.0
CH_4	---	---	---
N_2	65.0	70.0	71.0
Other	0.8	---	---

* This data represents the results for 80% of the total burning time.

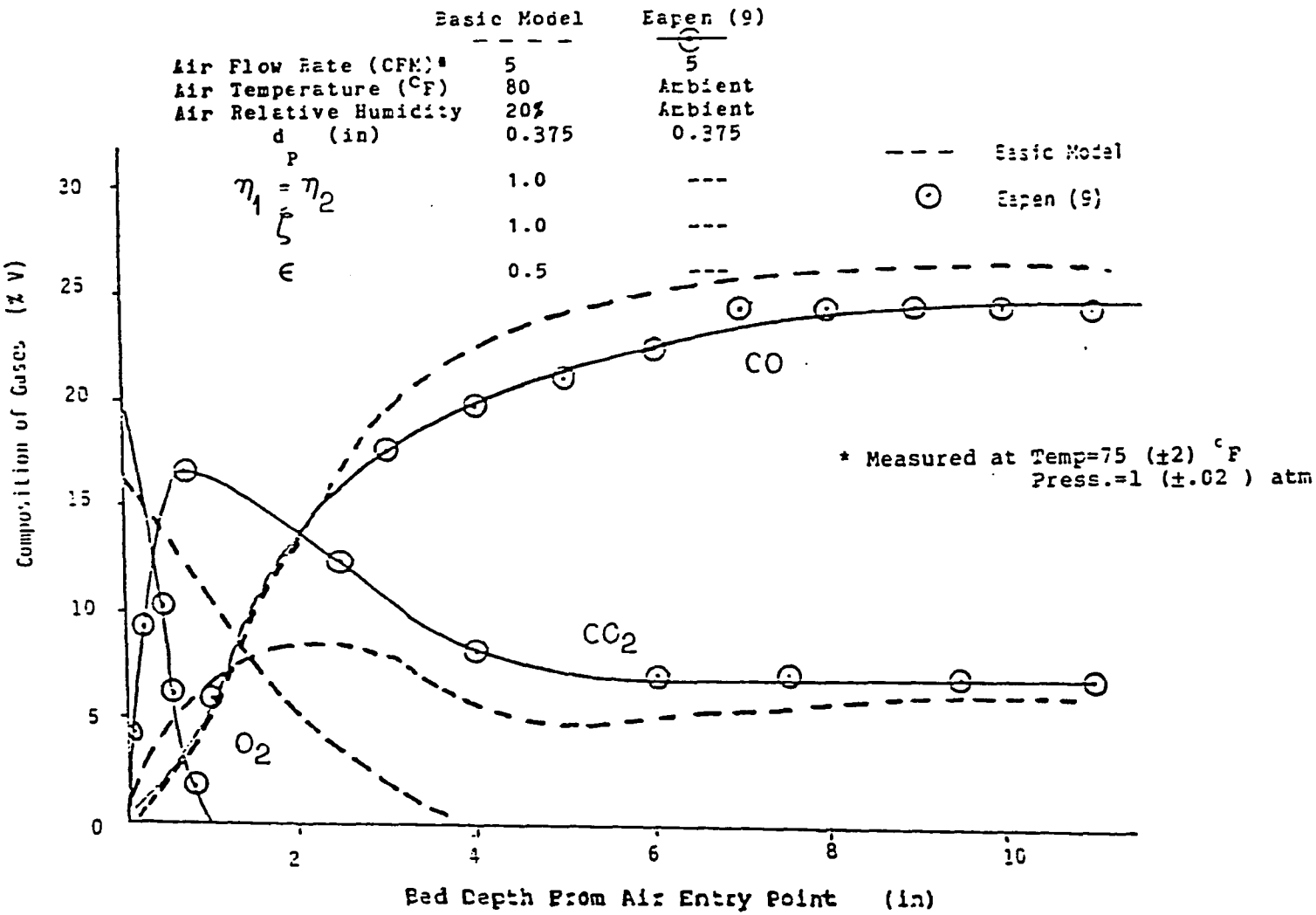

Figure 7.2.1 Comparison of Gas Compositions Between the Basic Model and Eapen's (9) Experimental data within the Bed Depth at Time=30 Min.

model versus Eapen's (9) experimental data. These data are in good agreement, even though Eapen's (9) data are confined to combustion in fuel (coke) beds of the under-fire type, i.e air blown in from the bottom up and combustion started at the bottom of the bed. The basic model uses the over-fire type, where the coke is ignited at the top and air blown from the top down.

Figure 7.2.2 and 7.2.3 show the change in gas composition over the bed depth at different time intervals. Figure 7.2.3 also shows that CO_2 concentration attains a maximum at the height when oxygen has just been consumed.

Figure 7.2.4.A and 7.2.4.B show the effect of variable air flow rate on the gas composition of the outlet bed with time, and time for complete combustion and gasification. The results of these Figures have shown that by changing the air flow rate, there is just a slight difference in the outlet gas composition. This slight difference could be caused by the amount of steam which was carried into the bed by input air, but by decreasing the air flow rate from 36 CFM to 17 CFM, the time for complete combustion increases from 2 hr. to 4 hr. The decrease in air flow rate slows down the reaction between the solid and gases thereby increasing the time for complete combustion.

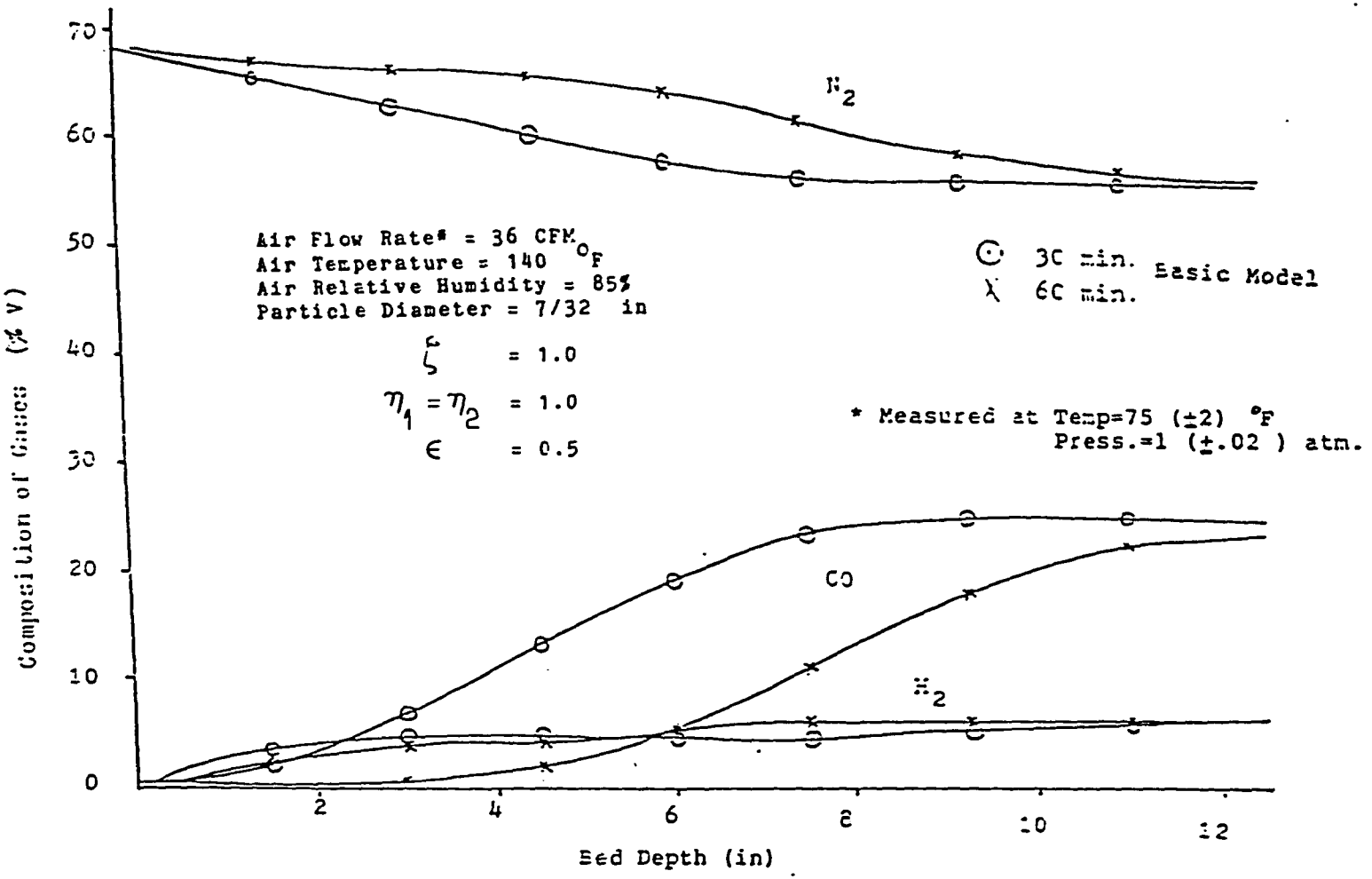

Figure 7.2.2 Effect of Moving Combustion and Gasification Zone Through the Bed on the Gas Compostions, and Location of Air Entery Point for Combustion and Gasification at Different Time Intervals. Air Flow Rate = 36 CFM

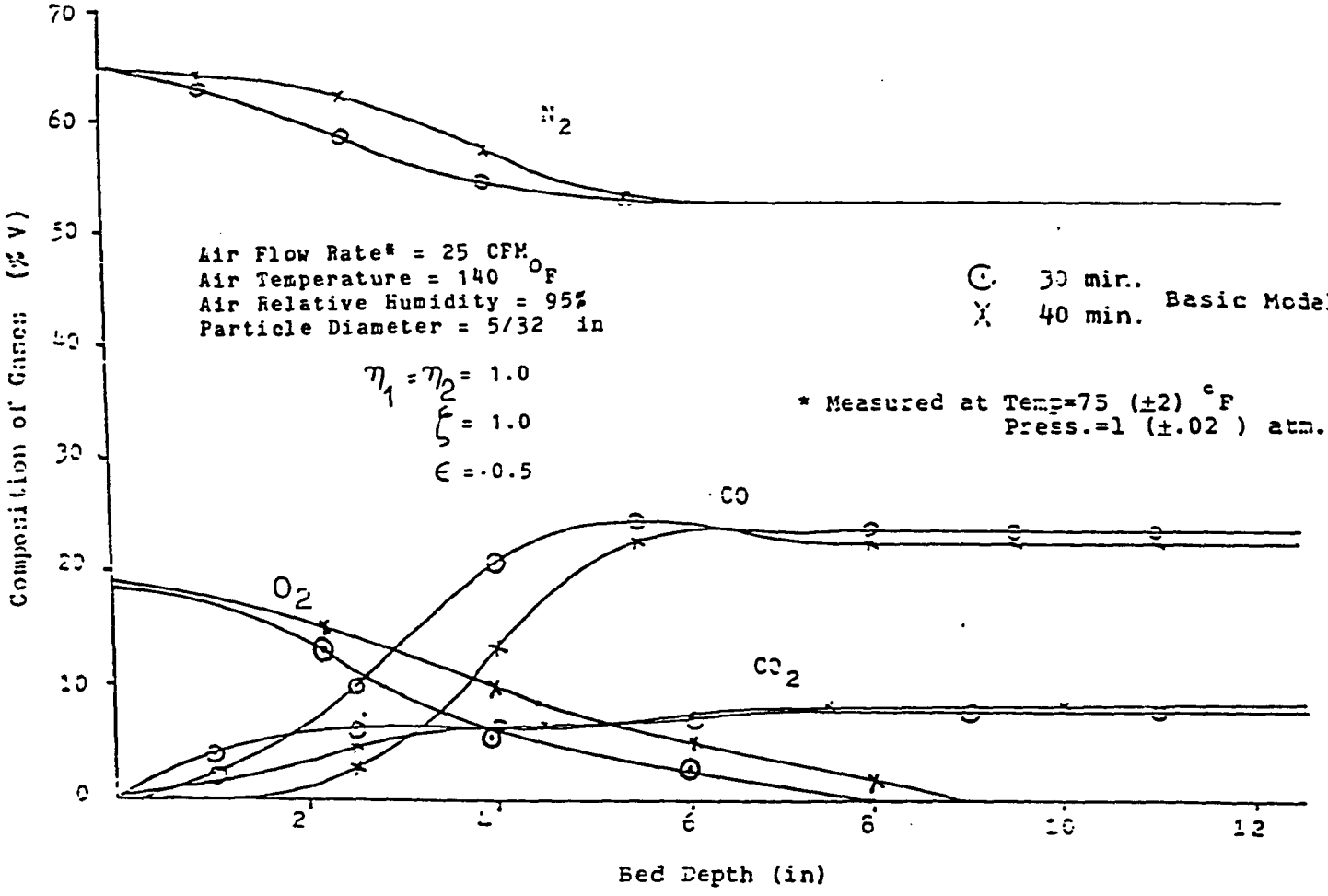

Figure 7.2.3 Effect of Moving Combustion and Gasification Zone Through the Bed on the Gas Compostions, and Location of Air Entery Point for Combustion and Gasification at Different Time Intervals. Air Flow Rate = 25 CFM

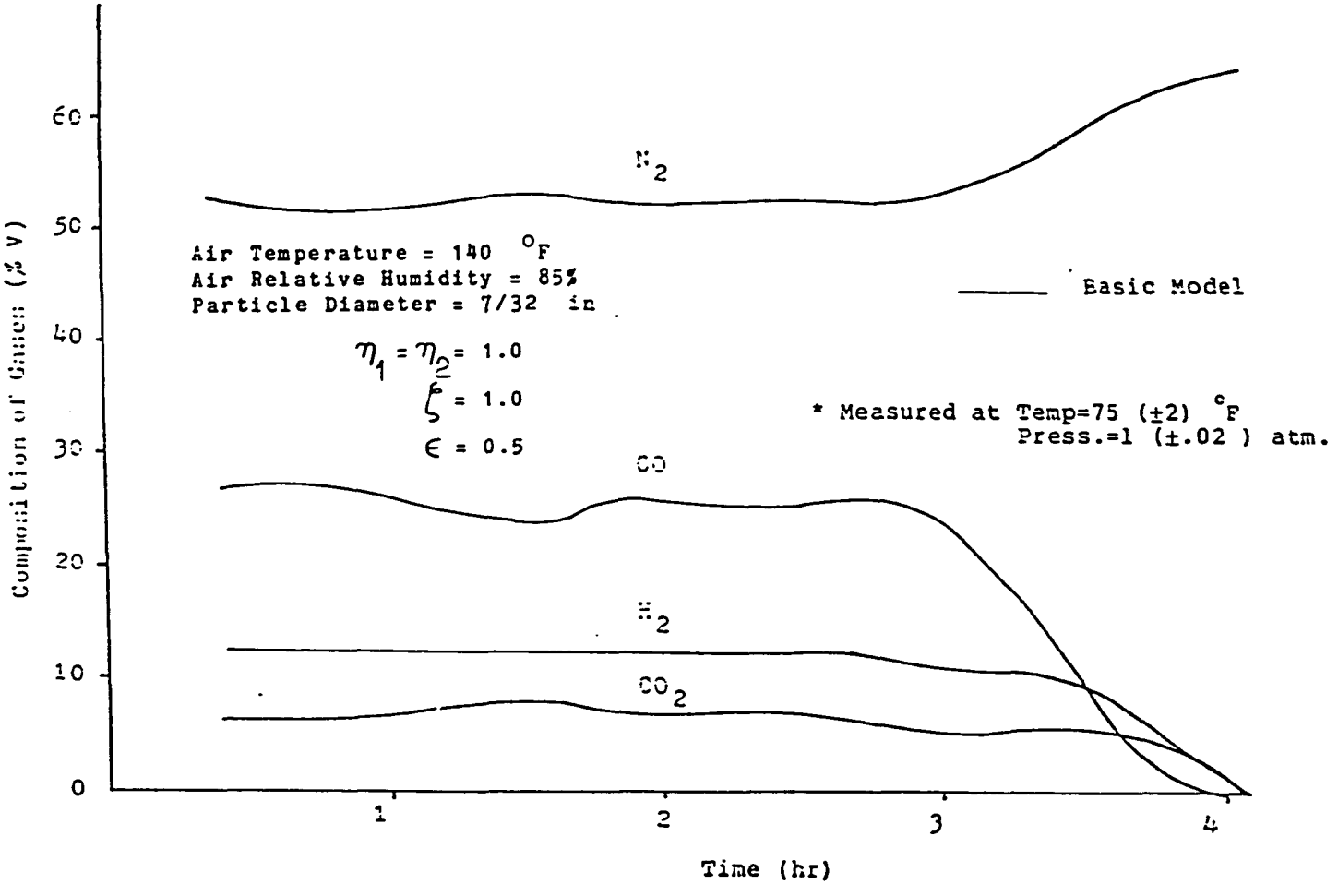

Figure 7.2.4.A Outlet Product Gases as a Function of Time at Air Flow Rate* = 17 CFM

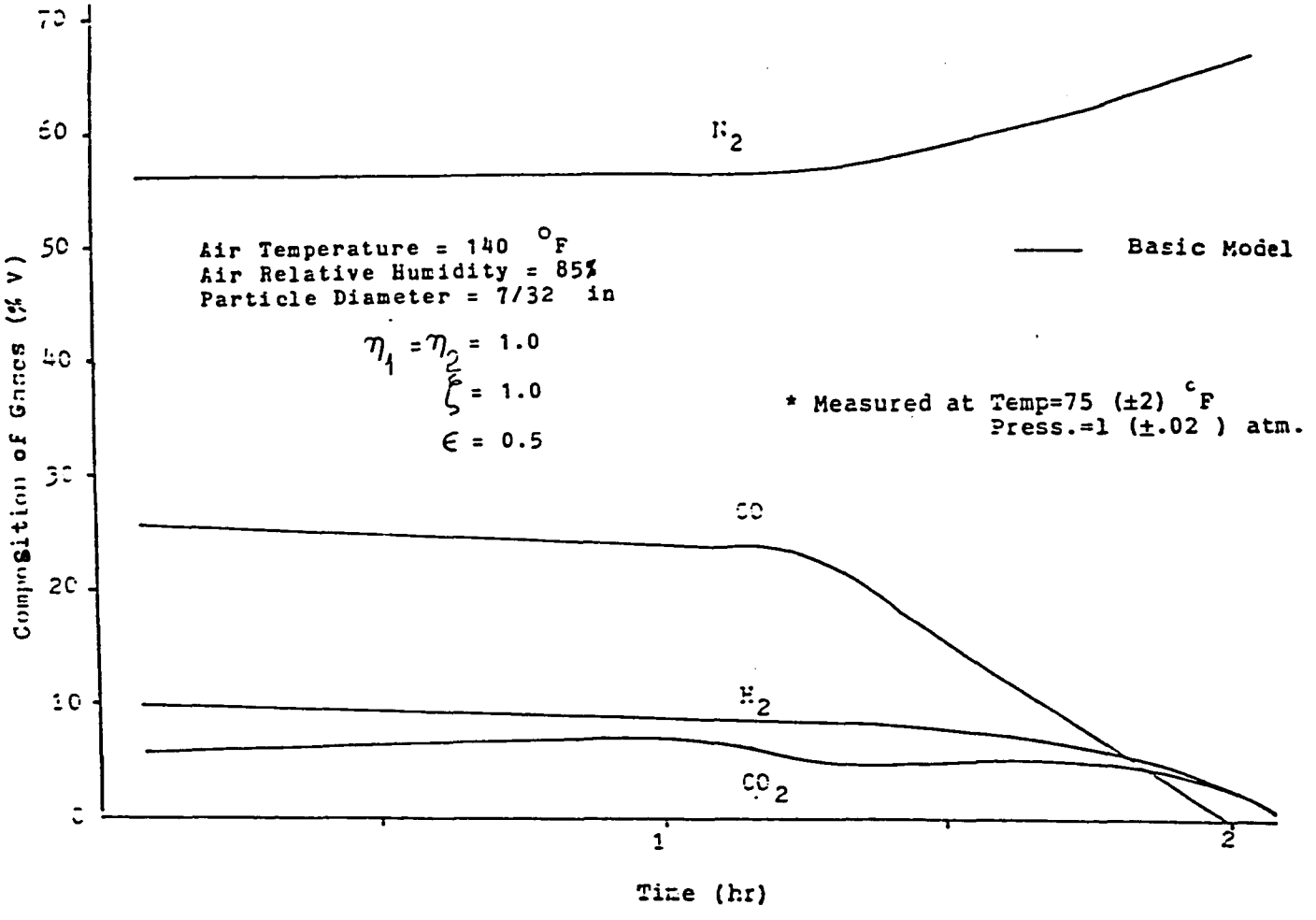

Figure 7.2.4.B Outlet Product Gases as a Function of Time at Air Flow Rate* = 36 CFM

7.3 Sensitivity of the Model Parameters

The simulation model was examined for the sensitivity of certain parameters that were not well established experimentaly and / or in the literature. Parameter sensitivities examined include: 1. the effect of the solid - gas heat transfer coefficient ζ, 2. the effect of bed voidage, 3. the effect of particle size, and 4. the effect of the reactivity factor coefficients (η_1, η_2) on the overall bed performance.

For these parameteric studies, the following conditions were arbitrarily selected; an air flow rate of 36 CFM, an air temperature of 140 ^{o}F., a particle diameter of 7/32", heat transfer coefficient factor ζ of one, a relative humidity of 85%, void fraction of 0.5, and the chemical kinetics as described in Appendix II with the reactivity factor coefficients of one for both C-CO_2 and C-H_2O reactions. The values of these arbitrary parameters were chosen to match the inputed data of the experimental run No.1 as described in section 7.4. The effect of all tested parameters were examined by holding all other parameters constant, while varying the input values of the parameter to be examined.

7.3.1 Effect of the Gas-Solid Heat Transfer Coefficient

Temperature profiles of various values of ζ are shown in Figures 7.3.1 through 7.3.3. The differences between solid and gas temperature continually decrease by increasing the values of ζ, and both temperatures are nearly equal through the bed for the value of ζ greater than 5, as shown in Figure 7.3.3 .

Table 7.3.1 shows the results predicted by the computer model for the ζ of 1, 2, and 5. The compositions of CO, and H_2 decreased with the increasing values of ζ, and the compositions of CO_2 , and N_2 increased by increasing the values of ζ. Table 7.3.1 also shows that the time required for complete combustion and gasification decreases as the ζ increases.

The results of this section show that:

Since the gas-solid heat transfer coefficient factor appears as a coefficient for the gas-solid temperature in the energy conservation equations, by increasing its value; (a) the maximum solid temperature decreases (Figure 7.3.1-7.3.3), decreasing gasification rate, (b) time for complete combustion decreases (Table 7.3.1), and (c) the composition of CO and H_2 decreases while the composition of CO_2 increases.

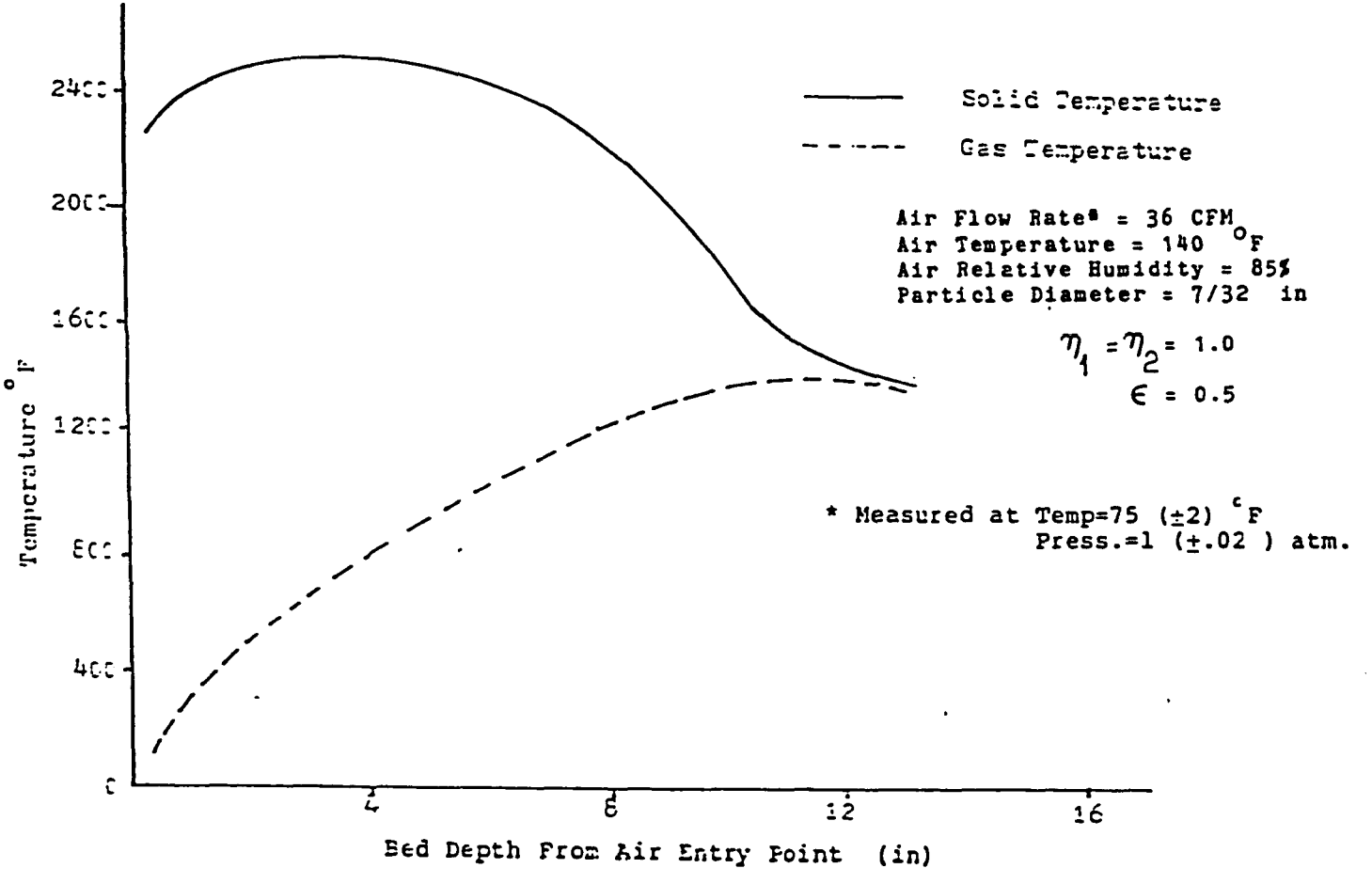

Figure 7.3.1 Variation of Solid and Gas Temperatures within the Bed at Time = 30 Min. for $\zeta = 1.0$

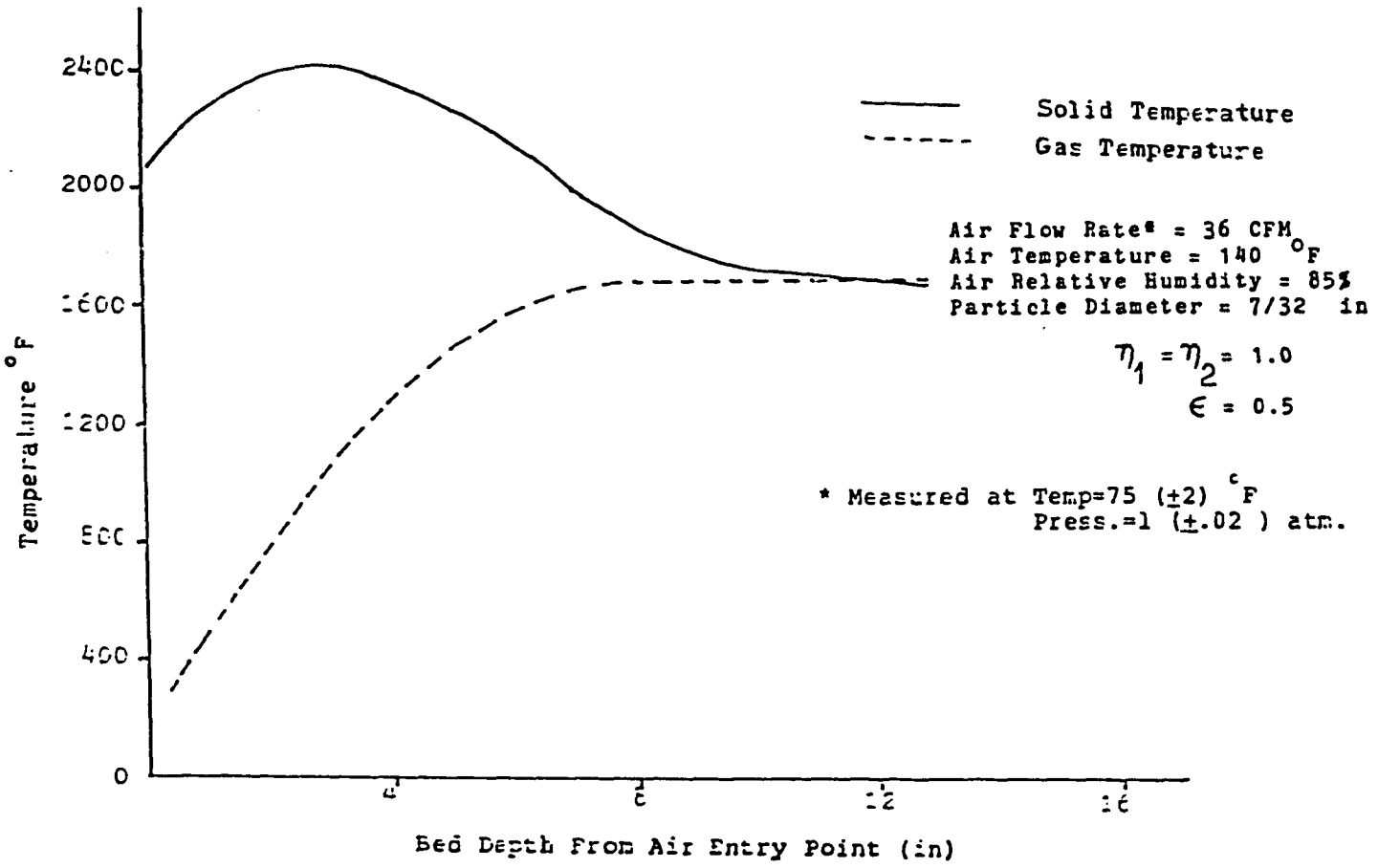

Figure 7.3.2 Variation of Solid and Gas Temperatures within the Bed at Time = 30 Min. for $\zeta = 2.0$

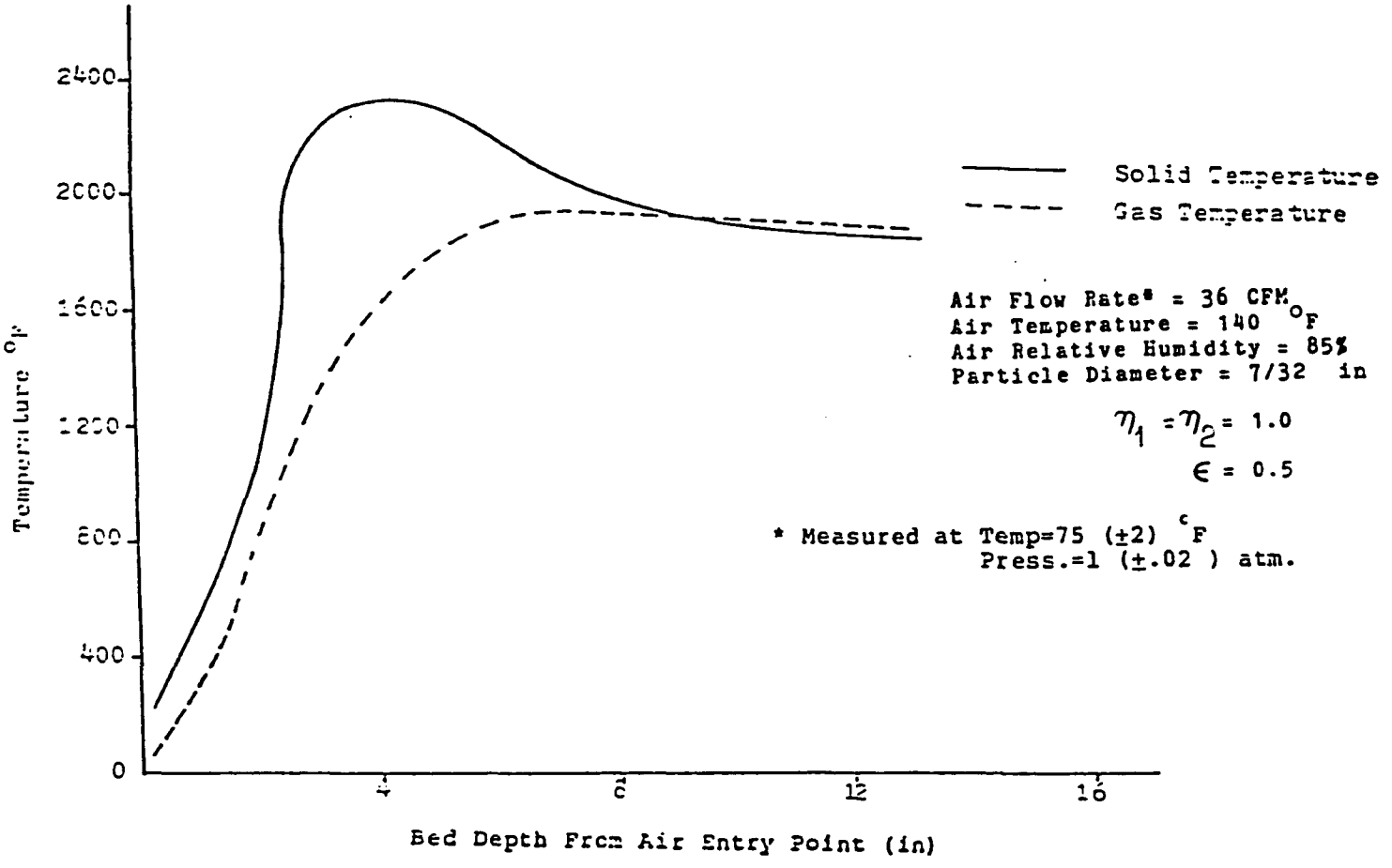

Figure 7.3.3 Variation of Solid and Gas Temperatures within the Bed at Time = 30 Min. for $\zeta = 5.0$

Table 7.3.1 Comparison of Gas Composition at the Outlet of the Bed for Different Value of ζ at Time=30 Min.

Gas Composition (% V)	ζ=1.0	ζ=2.0	ζ=5.0
H_2	9.5	7.5	6.5
CO	26.3	22.5	20.0
CO_2	6.7	8.0	10.0
CH_4	0.5	0.5	0.5
N_2	56.0	60.0	61.5
Other	1.0	1.5	1.5
Total Burning Time (Min)	140.0	125.0	105.0

7.3.2 Effect of Bed Voidage

Temperature profiles of various values of ϵ are shown in Figures 7.3.4 and 7.3.5 . The temperature difference between two phases continually increases with increasing the values of ϵ.

Table 7.3.2 shows the results for ϵ's of 0.3, 0.45, and 0.5 predicted by the model at time=30 minutes. The compositions of CO, and H_2 increase, and the compositions of CO_2, and N_2 decrease with increasing values of ϵ. This table also shows that by increasing the value of ϵ, the time for complete combustion and gasification increase slightly.

The results of this section show that:

1. Since the carbon conversion and solid temperature are inversely proportional to $(1-\epsilon)$, by increasing the value of ϵ; (a) the rate of carbon conversion increases, decreasing the time for complete combustion (as shown in Table 7.3.2), and (b) the maximum solid temperature increases (as shown in Figure 7.3.4, and 7.3.5), increasing the gasification rate.
2. Since the voidage appears as a coefficient for all terms in the right hand side of the conservation equations, if its value is increases; (a) the composition of CO and H_2 increases while the

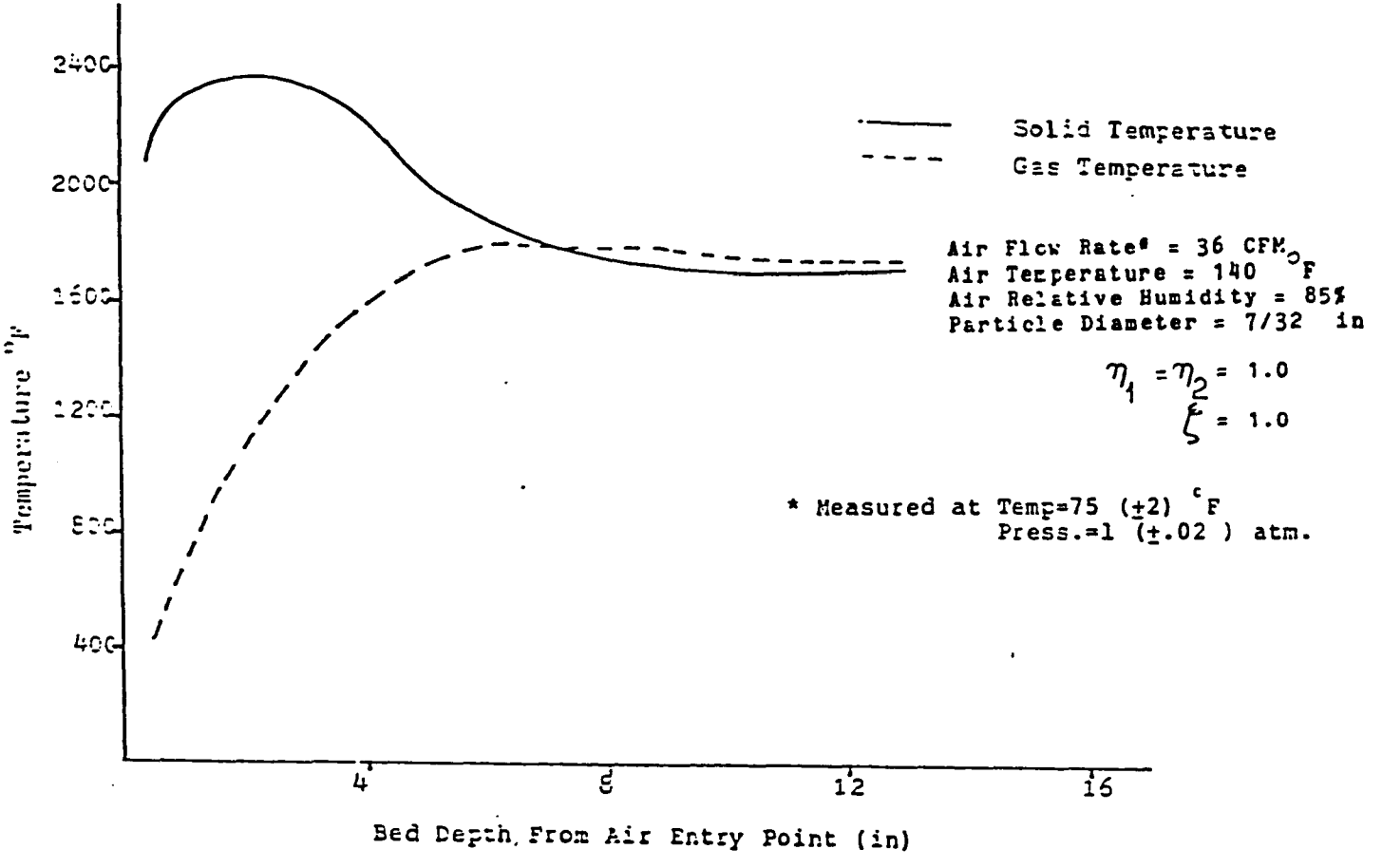

Figure 7.3.4 Variation of Solid and Gas Temperatures within the Bed at Time = 30 Min. for $\epsilon = 0.3$

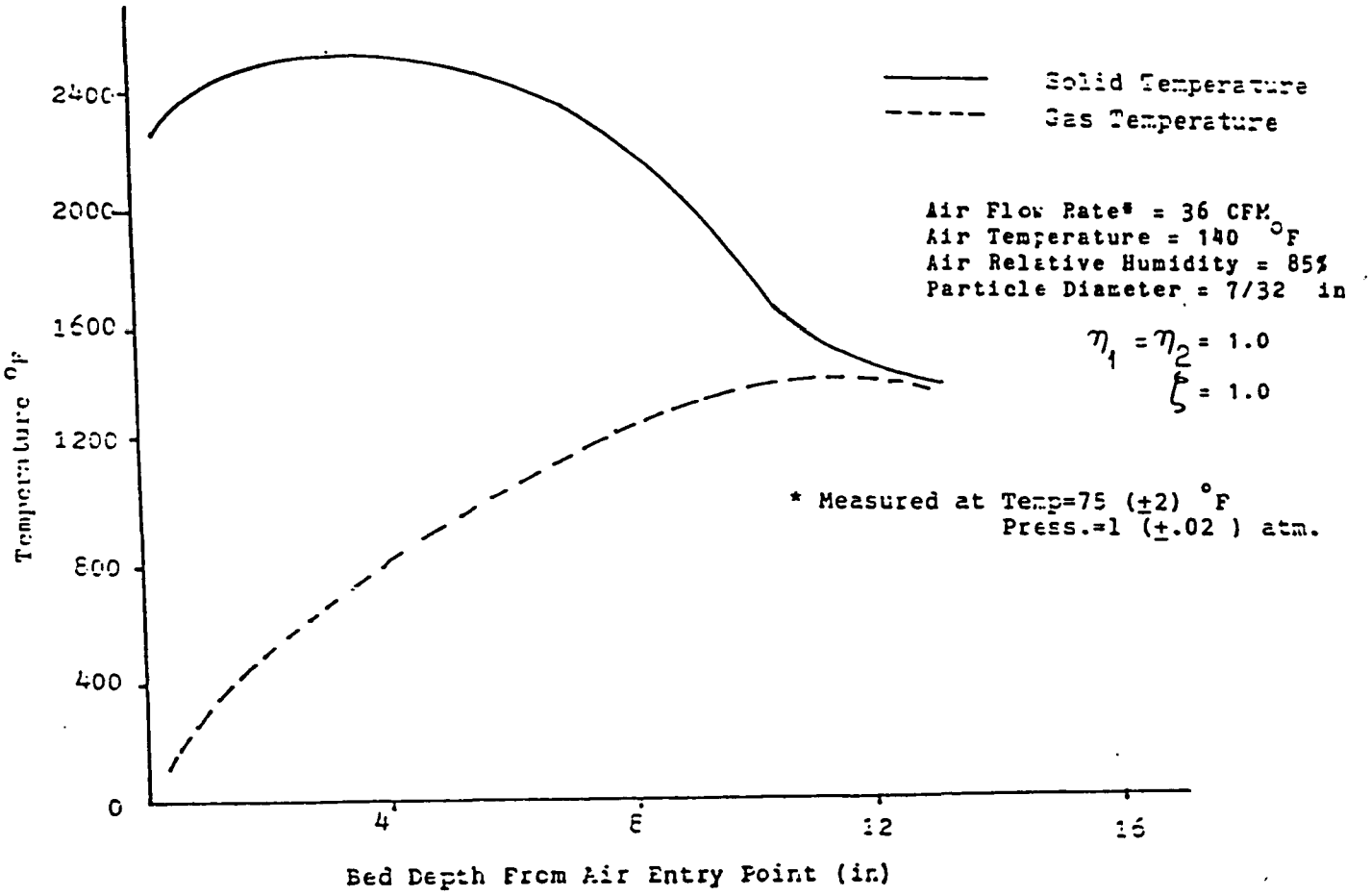

Figure 7.3.5 Variation of Solid and Gas Temperatures within the Bed at Time = 30 Min. for $\epsilon = 0.5$

Table 7.3.2 Comparison of Gas Composition at the Outlet of the Bed for Different Value of ϵ at Time=30 Min.

Gas Composition (%V)	ϵ =0.3	ϵ =0.45	ϵ =0.5
H_2	7.2	9.0	9.5
CO	20.8	25.2	26.3
CO_2	9.5	7.2	6.7
CH_4	0.5	0.5	0.5
N_2	60.0	57.1	56.0
Other	2.0	1.0	1.0
Total Burning Time (Min)	165.0	145.0	140.0

composition of CO_2 and (b) the gas phase temperature decreases.

7.3.3 Effect of Particle Size

Temperature profiles for various particle diameters are shown in Figures 7.3.6 through 7.3.8. The temperature difference between the two phases decreases by increasing the particle diameter.

Table 7.3.3 shows that the results predicted by the model for diameters of 5/32", 7/32", and 10/32" at time=60 minutes. The composition of H_2, CO_2, and CO decrease slightly, and the composition of N_2 increases slightly as the particle diameter increases. Table 7.3.3 shows that at larger particle diameters, some oxygen breaks through the bed when compared to the rapid oxygen consumption with smaller diameters. This is because the particle surface area per unit volume of the bed is not large enough to react with oxygen completely, and therefore some oxygen breaks through. Table 7.3.3 also shows that the time required for complete combustion increases as the particle diameter increases.

The results of this section show that:

1. The fuel particle size has a significant effect on the carbon conversion. This is easily understood

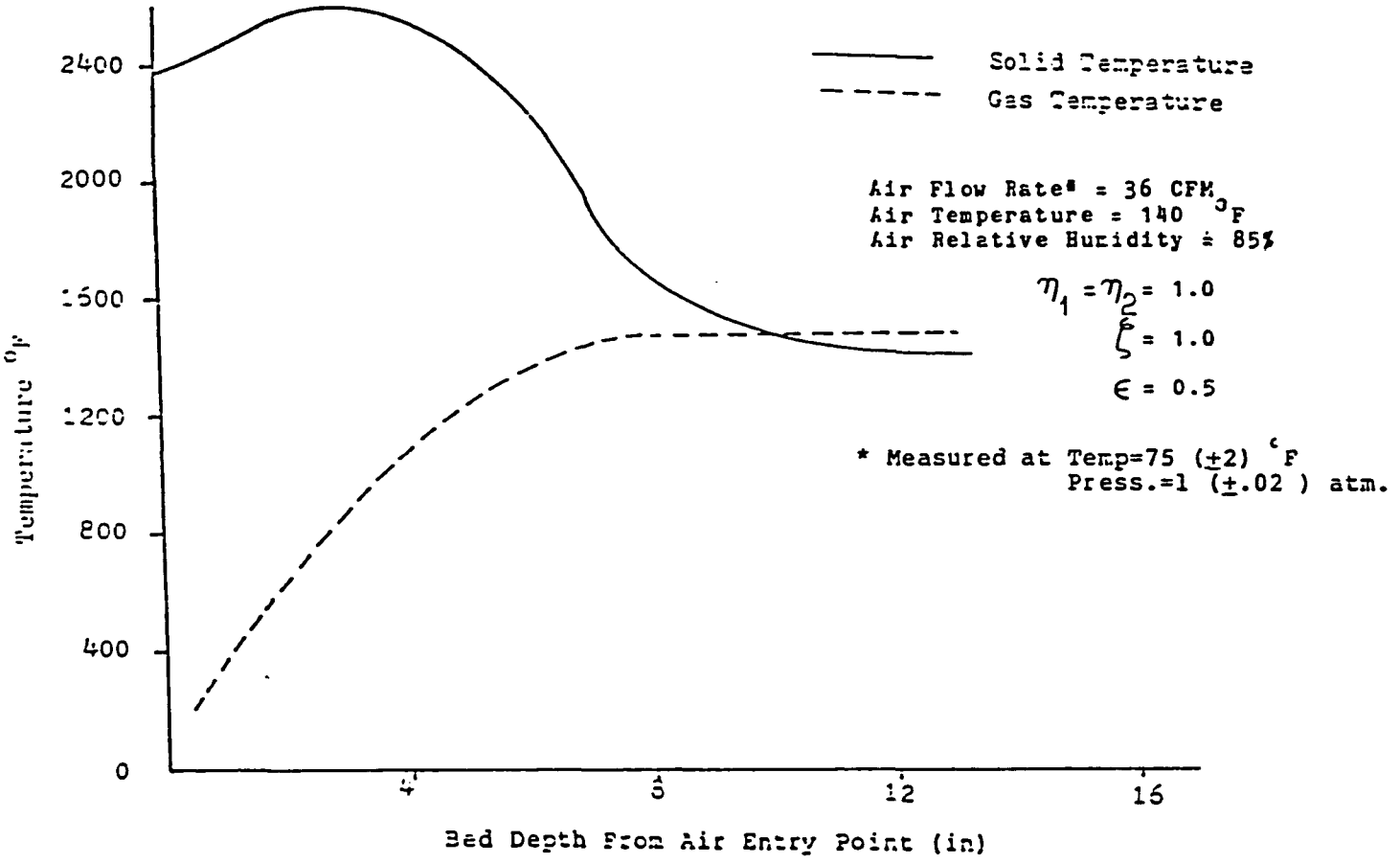

Figure 7.3.6 Variation of Solid and Gas Temperatures within the Bed at Time = 60 Min. for d_p = 5/32 in.

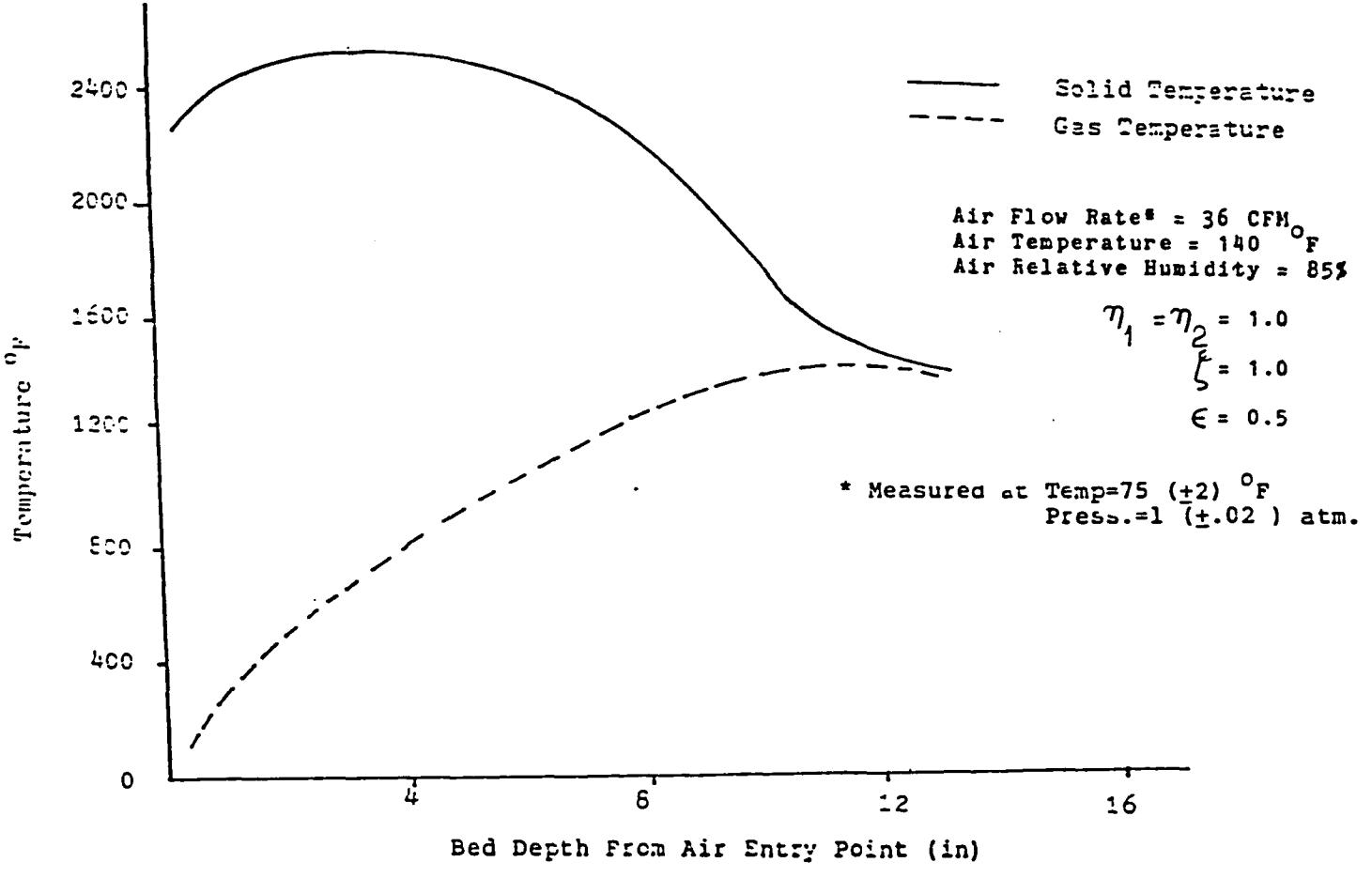

Figure 7.3.7 Variation of Solid and Gas Temperatures within the Bed at Time = 60 Min. for d_p = 7/32 in.

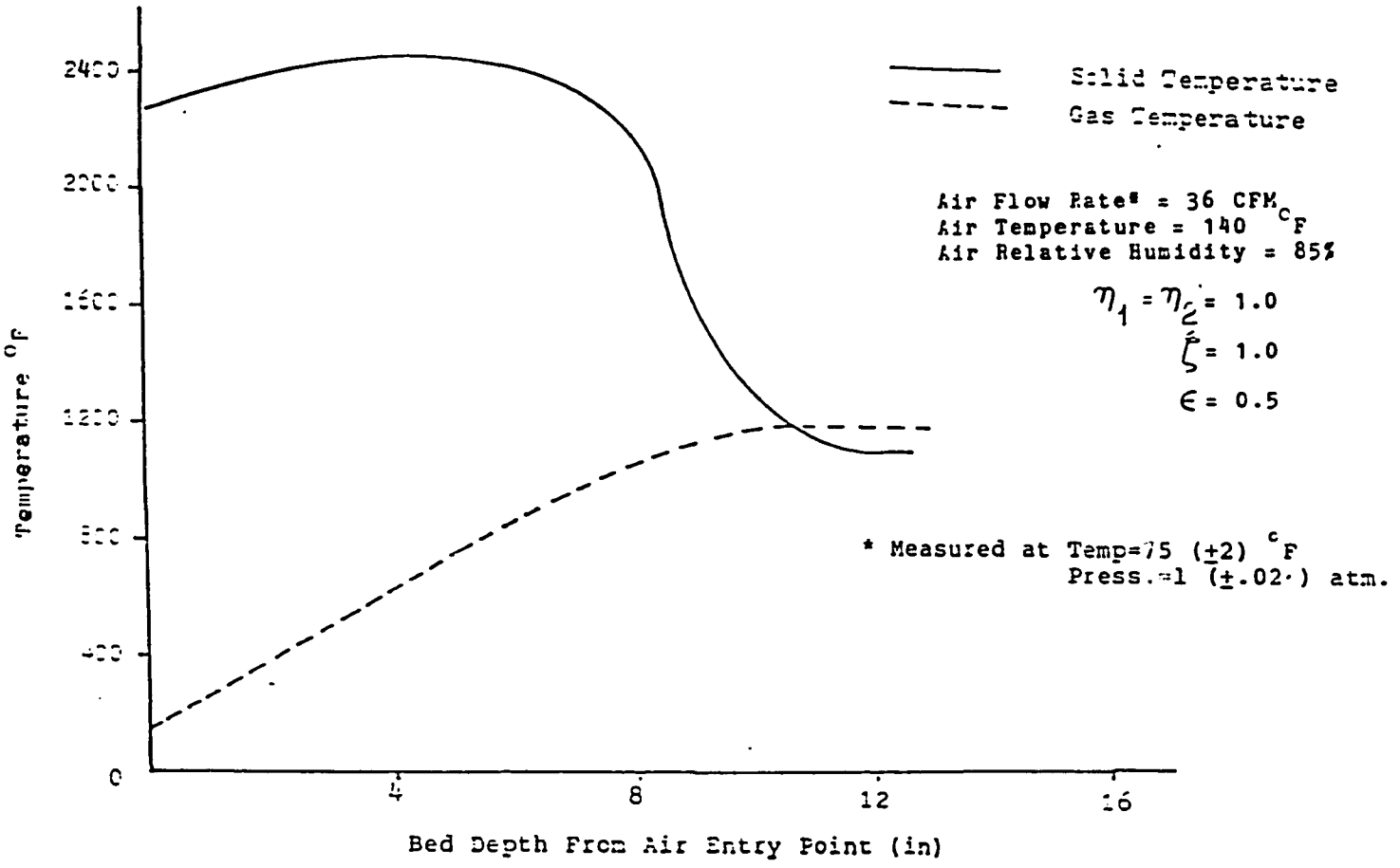

Figure 7.3.8 Variation of Solid and Gas Temperatures within the Bed at Time = 60 Min. for d_p = 10/32 in.

Table 7.3.3 Comparison of Gas Composition at the Outlet of the Bed for Different Value of d_p at Time=60 Min.

Gas Composition (% V)	$d_p = \frac{5"}{32}$	$d_p = \frac{7"}{32}$	$d_p = \frac{10"}{32}$
H_2	9.6	9.5	9.4
CO	26.6	26.3	21.3
CO_2	7.1	6.7	6.4
CH_4	0.5	0.5	0.5
N_2	55.2	56.0	58.9
O_2	----	----	3.5
Other	1.0	1.0	---
Total Burning Time (Min)	120.0	140.0	170.0

since the specific contact area per unit volume of the bed for gas-solid reaction is closely related to the particle size. The specific contact area between reacting gases and the fuel particle is inversely proportional to the particle size. Therefore, by increasing the value of d_p; (a) the rate of carbon conversion decreases, increasing the time for complete combustion (Table 7.3.3), and (b) the maximum solid temperature decreases (Figure 7.3.6-7.3.8), decreasing the gasification rate.

2. The fuel particle size has a slight effect on the composition of gases (Table 7.3.3).

7.3.4 Effect of Reactivity Factor Coefficients on Overall Bed Performance

Figures 7.2.2 and 7.2.3 show the variation of gas compositions within the bed depth and Figure 7.2.4.A and 7.2.4.B show the outlet product gases as a function of time for the chemical kinetics suggested by Dobner (34), with reactivity factor coefficients (η_1, η_2) of one. By varying the reactivity factor coefficients, the computer model yielded some interesting results. By decreasing the reactivity factor coefficients by an order of magnitude, a tremendous drop in CO and H_2 was observed when compared to reactivity factor coefficients of one. Since C-CO_2 and C-H_2O

are endothermic reactions, decreasing the reactivity factor coefficients of their kinetics, the solid temperature increased as much as 4500 ^{o}F for some locations in the bed. Thus, an attempt was made to reduce this high temperature to within a reasonable range. Therefore, as described in section 7.3.1, by increasing the heat transfer coefficient, the solid temperature will decrease to a reasonable temperature. The effect of decreasing the reactivity factor coefficients (η_1, η_2) and increasing the heat transfer coefficient factor ζ on the outlet product gases are shown in Figure 7.3.9.A and 7.3.9.B.

The results of this section show that:

The reactivity factor coefficients have a significant effect on the composition of gases. This effect is easily understood because the reactivity factor coefficients are coefficients of the surface reaction rate (K_s) for C-CO_2 and C-H_2O reactions. By decreasing its value by an order of magnitude; (a) the gas composition of CO and H_2 decrease 50 to 60%, and CO_2 increase 40 to 50% (Figure 7.3.9.A and 7.3.9.B), and (b) the gas-solid heat transfer coefficient factor ζ has to be varied simultaneously in order to keep the solid and gas temperatures within the observed values.

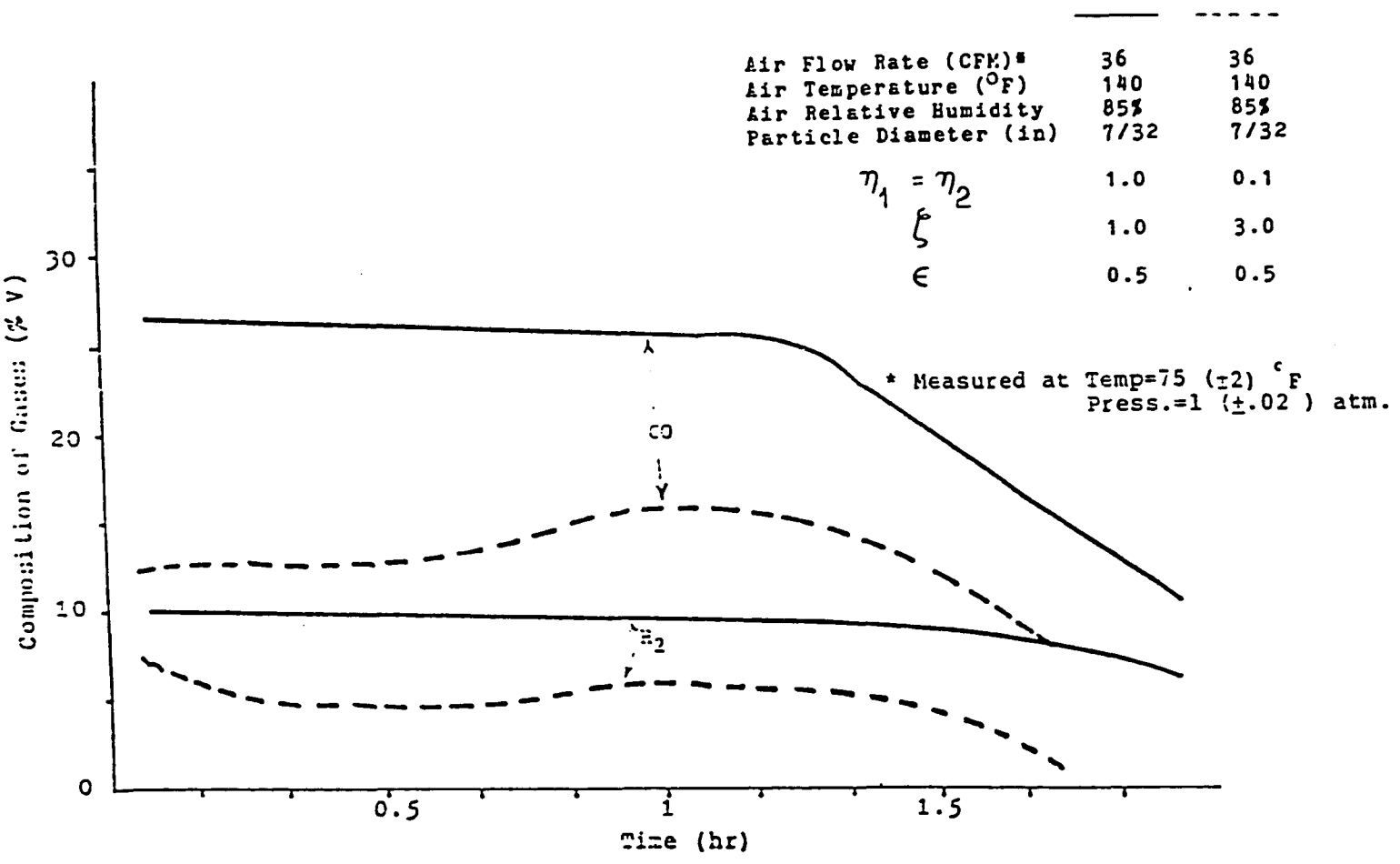

Figure 7.3.9.A Outlet Product Gases as a Function of Time for different η

	———	- - - -
Air Flow Rate (CFM)*	36	36
Air Temperature (°F)	140	140
Air Relative Humidity	85%	85%
Particle Diameter (in)	7/32	7/32
$\eta_1 = \eta_2$	1.0	0.1
ζ	1.0	3.0
ϵ	0.5	0.5

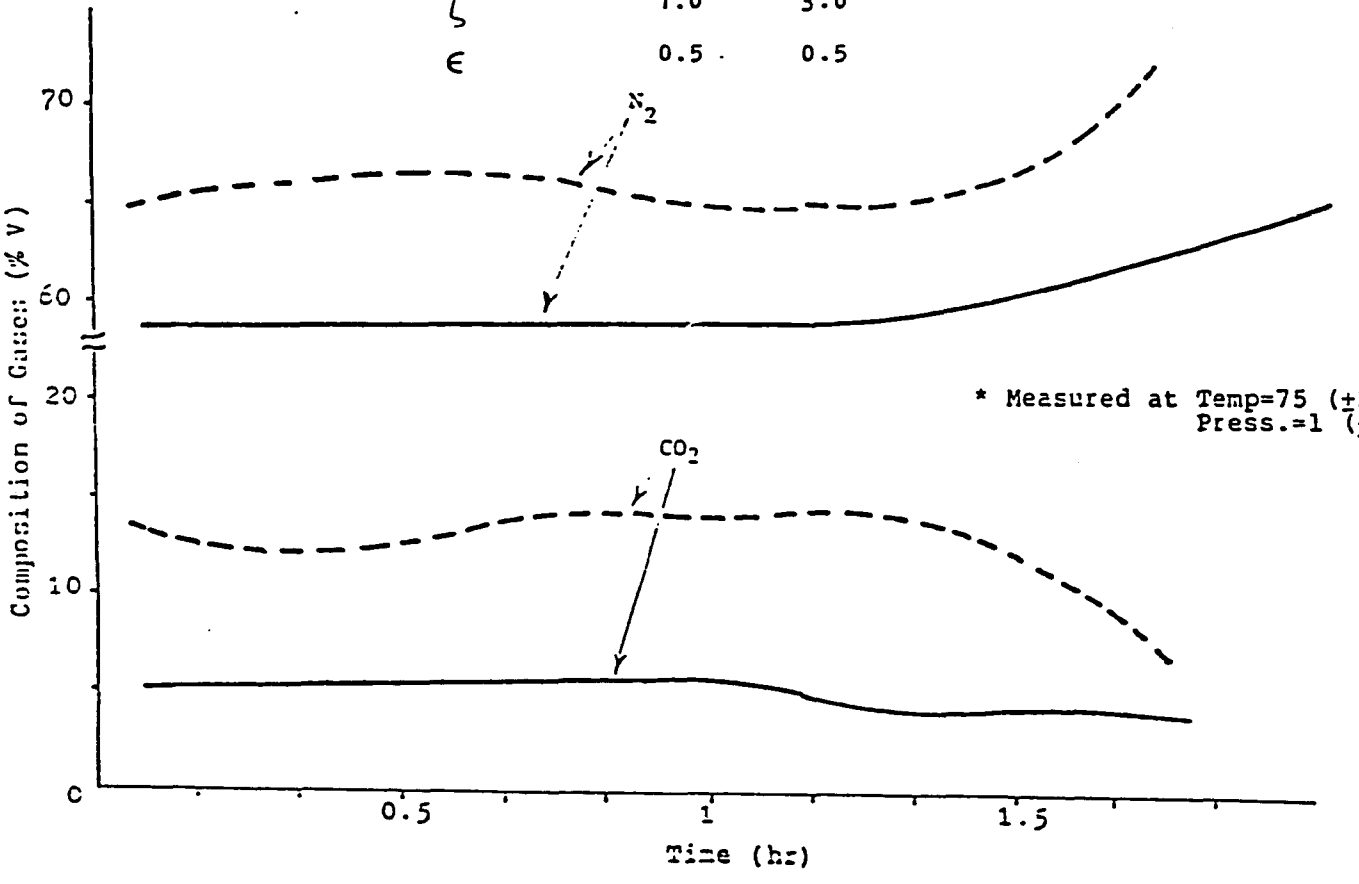

* Measured at Temp=75 (±2) °F
Press.=1 (±.02) atm.

Figure 7.3.9.B Outlet Product Gases as a Function of Time for different η

7.3.5 Summary of the Effect of Input Parameters on the Model Results

A detailed model of a combustion pot can provide temperature and composition profiles throughout the reactor, as well as effluent gas composition and temperature. Temperature and composition profiles are sensitive to certain model input parameters, which are not well established in the literature. These parameters are: 1. gas-solid heat transfer coefficient, 2. void fraction, 3. particle size, and 4. reactivity factor coefficients. Through a sensitive analysis, it was found that detailed temperature and composition profiles in the reactor are sensitive to the parameter values. The relative sensitivity of effluent properties (gas composition of H_2, CO, and CO_2) and total gasification time to these parameters with the assumption of ($\eta = \eta_1 = \eta_2$) are summarized as follows;

7.3.5.A Gas composition (H_2, CO, and CO_2)

7.3.5.A.1 Hydrogen

The gas composition of hydrogen at the outlet of the reactor is sensitive to changes in the parameter values. This functional relationship can be written mathematically as;

$$\%H_2 = f(\zeta, \epsilon, d_p, \eta) \qquad (7.3.1)$$

where $\%H_2$ represent percent by volume of hydrogen.

By applying the chain rule of differentiation to the equation (7.3.1), it can be shown that:

$$\delta \%H_2 = \left.\frac{\partial \%H_2}{\partial \zeta}\right|_{\epsilon, d_p, \eta} \delta\zeta + \left.\frac{\partial \%H_2}{\partial \epsilon}\right|_{\zeta, d_p, \eta} \delta\epsilon + \left.\frac{\partial \%H_2}{\partial d_p}\right|_{\zeta, \epsilon, \eta} \delta d_p + \left.\frac{\partial \%H_2}{\partial \eta}\right|_{\zeta, d_p, \epsilon} \delta\eta \qquad (7.3.2)$$

From the results of sections 7.3.1 through 7.3.4, the values of

$\frac{\partial \%H_2}{\partial \zeta}$, $\frac{\partial \%H_2}{\partial d_p}$, and $\frac{\partial \%H_2}{\partial \eta}$ can be found as;

from Table 7.3.1

$$\frac{\partial \%H_2}{\partial \zeta} = \frac{(9.5-7.5)}{(1.0-2.0)} = -2.0$$

from Table 7.3.2

$$\frac{\partial \%H_2}{\partial \epsilon} = \frac{(9.5-7.2)}{(0.5-0.3)} = 11.5$$

from Table 7.3.3

$$\frac{\partial \%H_2}{\partial d_p} = \frac{(9.6-9.5)}{(5/32-7/32)} = -1.6$$

and from Figure 7.2.4.A

$$\frac{\partial \%H_2}{\partial \eta} = \frac{(9.5-5.5)}{(1.0-0.1)} = 4.5$$

By substituting these values into the equation (7.3.2) yield;

$$\delta \%H_2 = -2\delta\zeta + 11.5\delta\epsilon - 1.6\,\delta d_p + 4.5\,\delta\eta \qquad (7.3.3)$$

7.3.5.A.2 Carbon Monoxide

By applying the same procedure as section 7.3.5.A.1, the following expression can be found for gas composition of carbon monoxide;

$$\delta \%CO = -3.8\delta\zeta + 27.5\delta\epsilon - 4.8\,\delta d_p + 14.7\,\delta\eta \qquad (7.3.4)$$

7.3.5.A.3 Carbon Dioxide

Again by applying the same procedure as section 7.3.5.A.1, the following expression can be found for gas composition of carbon dioxide;

$$\delta \%CO_2 = 1.3\delta\zeta - 14\delta\epsilon - 6.4\,\delta d_p - 9.2\,\delta\eta \qquad (7.3.5)$$

7.3.5.B Total Gasification Time

The total gasification time (T) is sensitive to changes in the parameter values. This fundamental relationship can be written mathematically as;

$$T = f(\zeta, \epsilon, d_p, \eta) \qquad (7.3.6)$$

By applying the chain rule of differentiation to the equation (7.3.6), it can be shown That;

$$\delta T = \left.\frac{\partial T}{\partial \zeta}\right|_{\epsilon, d_p, \eta} \delta\zeta + \left.\frac{\partial T}{\partial \epsilon}\right|_{\zeta, d_p, \eta} \delta\epsilon + \left.\frac{\partial T}{\partial d_p}\right|_{\zeta, \epsilon, \eta} \delta d_p + \left.\frac{\partial T}{\partial \eta}\right|_{\zeta, d_p, \epsilon} \delta\eta \qquad (7.3.7)$$

By applying the same procedure as section 7.3.5.A.1, the following expression can be found for changes in total burning time;

$$\delta T = -15\,\delta\zeta + 125\,\delta\epsilon + 320\,\delta d_p + 15\,\delta\eta \qquad (7.3.8)$$

Therefore, the following equations were obtained from the sections 7.3.5.A and 7.3.5.B:

$$\left.\begin{aligned}
\delta\%H_2 &= -2\,\delta\zeta + 11.5\,\delta\epsilon - 1.6\,\delta d_p + 4.5\,\delta\eta \\
\delta\%CO &= -3.8\,\delta\zeta + 27.5\,\delta\epsilon - 4.8\,\delta d_p + 14.7\,\delta\eta \\
\delta\%CO_2 &= 1.3\,\delta\zeta - 14.0\,\delta\epsilon - 6.4\,\delta d_p - 9.2\,\delta\eta \\
\delta T &= -15.0\,\delta\zeta + 125.0\,\delta\epsilon + 320\,\delta d_p + 15\,\delta\eta
\end{aligned}\right\} \quad (7.3.9)$$

Now, equation (7.3.9) shows how sensitive the gas composition and total burning time are to the parameter values. In this study, it was necessary to change the input parameter values of ζ, and η for the basic model in order to obtain the data corresponding to the experimental results (section 7.3.4).

As described in section 7.3.4, by changing the reactivity factor coefficients, one must also changes the heat transfer coefficient factor ζ simultaneously. These changes were from 1.0 to 0.1 for reactivity factor coefficients, and 1.0 to 3.0 for the heat transfer coefficient factor ζ. The change of particle diameter and void fraction was not necessary because these values were kept constant throughout the basic model and experimental studies.

By substituting these changes:

$$\delta\zeta = 1.0 - 3.0 = -2.0$$
$$\delta\eta = 1.0 - 0.1 = 0.9$$

$$\delta \epsilon = 0.0$$

$$\delta d_p = 0.0$$

into the equation (7.3.7), the following expression yields;

$$\%H_2 = -2.0x-2.0 + 11.5x0.0 - 1.6x0.0 + 4.5x0.9 = 8.0\%$$

$$\%CO = -3.8x-2.0 + 27.5x0.0 - 4.8x0.0 + 14.7x0.9 = 20.8\%$$

$$\%CO_2 = 1.3x-2.0 + 14.0x0.0 - 6.4x0.0 - 9.2x0.9 = -10.9\%$$

$$\delta T = -15.0x-2 + 125.0x0.0 + 320.0x0.0 + 15.0x0.9 = 43.5 \text{ sec.}$$

The above example shows the effect of the fuel (char/coke) reactivity on gas composition and gasification burning time. However, equation (7.3.9) shows that, the change in bed voidage (ϵ) has more effect on the composition of gases than the other input parameters (ζ, d_p, η), due to a larger coefficient in the of equation (7.3.9). Also, for the same reason the change in the particle diameters (d_p) has more effect on the burning time than the other input parameters (ζ, ϵ, η). Therefore, the flexibility of the input parameters allows control over desired gas composition and total burning time.

7.4 Comparison and Modification of the Model to Conform With the Experimental Data

Comparison of the computed results based on the model with the experimental data of the combustion pot has been made for different runs using metallurgical quality coke as feedstock (see Table 6.2.1 and 6.2.2).

The results of run No.1, as shown in Table 7.4.1 typify the results of all three runs in this study. This table compares the outlet gas compositions generated by the specific model (specific model is for a specific char/coke), the measured experimental data, a fixed bed gasifier, and the combustion of coke in a furnaces by Lewis (11). This table also shows that the gas compositions of the actual measured experimental data are not in good agreement with available fixed-bed gasifier data. However, the basic model generated data that is in good agreement with the fixed-bed gasifier data in the literature, as shown in Table 7.2.1. This discrepancy found between the two models is due to the difference in reactivity factor coefficients. Apparently, the basic model uses the same reactivity factor coefficients as the literature, but the experimental study uses a lower reactivity factor coefficients.

Figure 7.4.1.A and 7.4.1.B show the comparison of the outlet gas composition between the experimental run No.1 and the specific model with time. After a trial and error procedure, reactivity factor coefficients (η_1, η_2) of 0.1 were used in the specific model to afford agreement of the results

Table 7.4.1 Comparison of Gas Composition at the Outlet of the Bed Between Specific Model, Experimental Data, and other Available Experimental Data

Gaseous Component (%)	Experimental Results Run No. 1*	Specific Model*	Lewis (11)	Fixed Bed (50)
H_2	5.5	5.3	--	10
CO	15.1	14.8	13.5	29
CO_2	14.5	13.8	10.	3.5
CH_4	---	0.6	--	0.7
N_2	63.5	62.5	--	56.8
Other	1.4	3.0	2.5	--

* This data represents the results for 80% of total burning time.

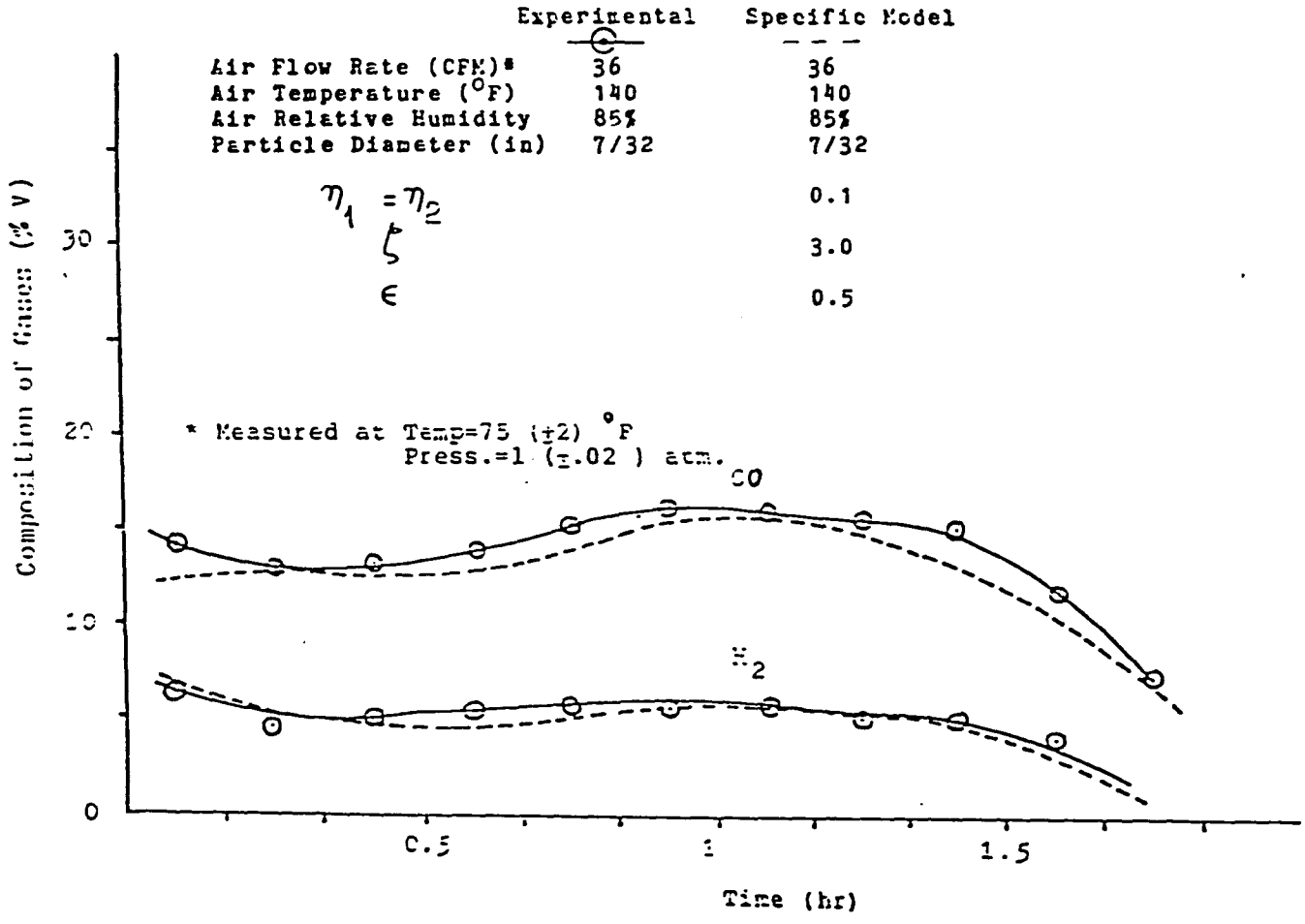

Figure 7.4.1.A Comparison of Experimental and Calculated Outlet Product Gases as a Function of Time

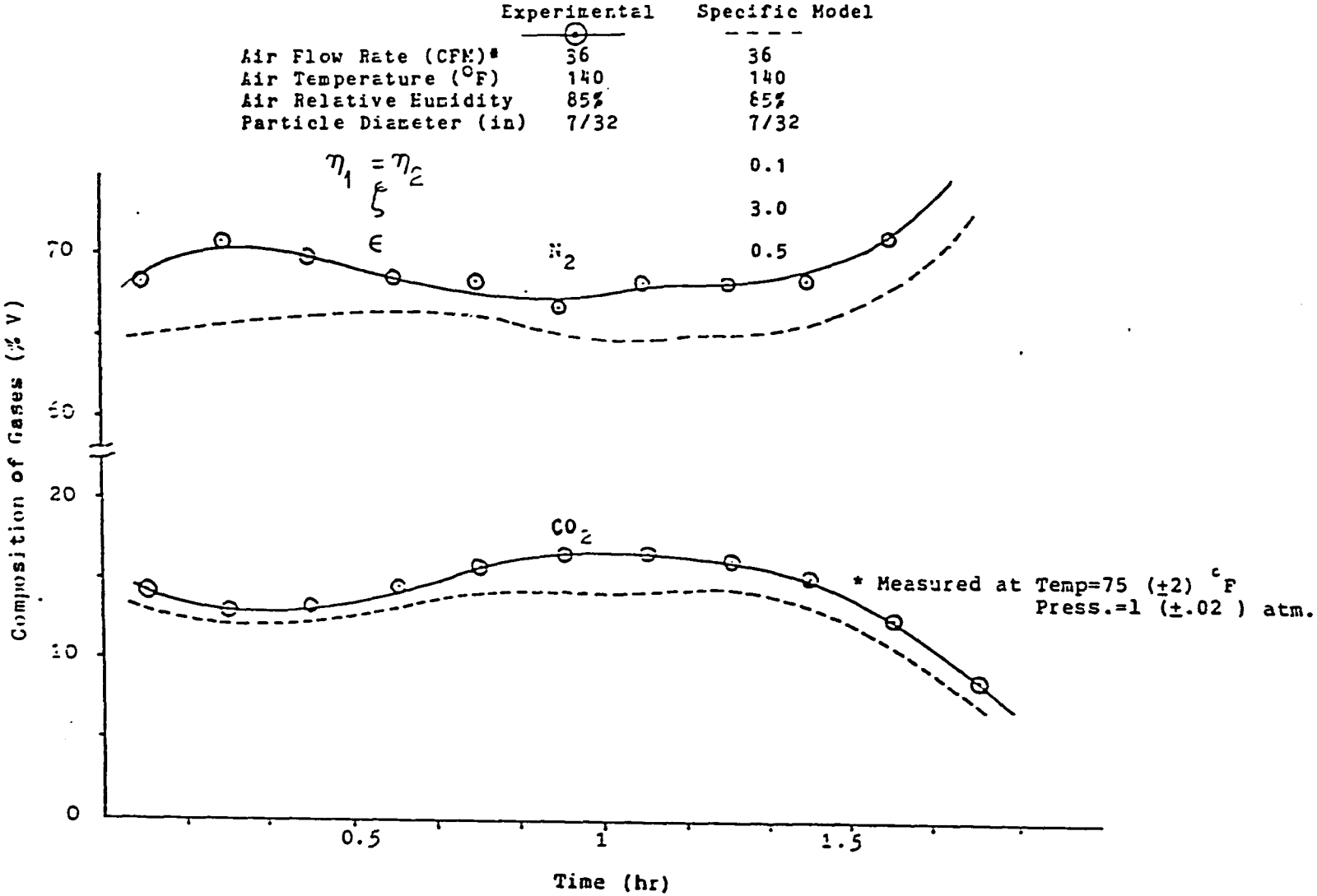

Figure 7.4.1.B Comparison of Experimental and Calculated Outlet Product Gases as a Function of Time

between the specific model and the experimental run No.1. Simultaneously, the gas-solid heat transfer coefficient factor was assumed to be 3.0. Figure 7.4.2 shows for reactivity factor coefficients (η_1, η_2) of 0.1 and 1.0, the overall reaction rates for C-H_2O, and C-CO_2 reactions are within a range of values collected by Wen et al. (25). Therefore, one can vary the reactivity factor coefficients in this model for different types of char/coke, as long as the overall initial rates are within the range of Wen's (25) collected data (Figure 7.4.2). The experimental data from run No.1 also agrees with data obtained (see Table 7.4.1) by Lewis (11). His experiment involved the gasification of coke, but, he encountered serious problems when sampling the gases.

Figure 7.4.3 shows the variation of local temperature at six different heights in the bed for experimental run No. 1. The path of the combustion zone is shown by the maximum of each curve (the maximum temperature) as it moves down through the bed with time. Figure 7.4.3 shows the combustion zone has reached its peak at 7.5" in depth with the maximum temperature of 2700 ^{o}F.

Figure 7.4.4 shows a comparison of the specific model's solid and gas temperature with local temperatures measured in the actual experiment at the location of 7.5" in depth. This Figure shows the profile of the measured local temperture located between the solid and gas temperatures profiles from

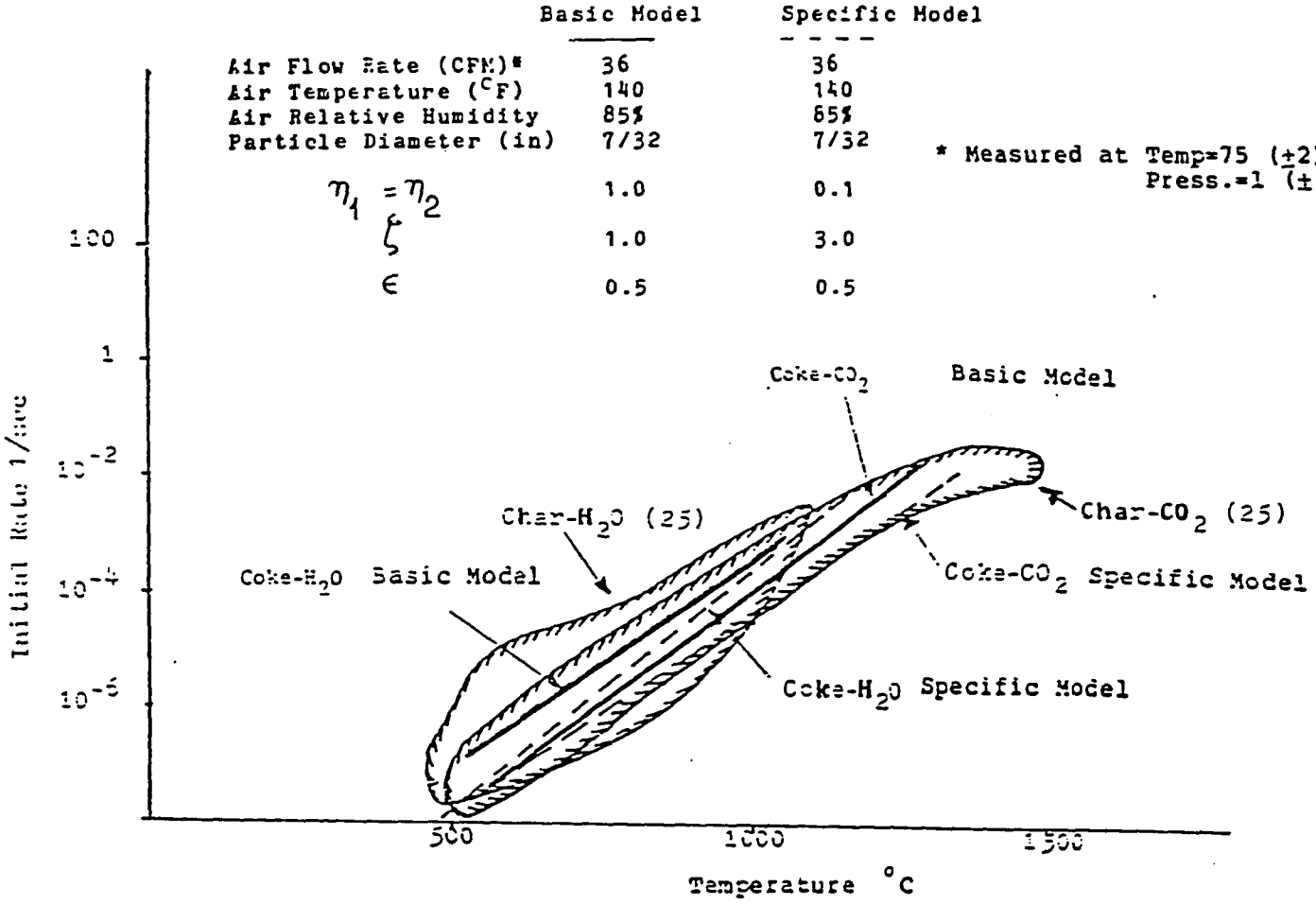

Figure 7.4.2 Comparison of Initial Rate of C-CO_2 and C-H_2O Between Collected Data for Different Type of Char by Wen (25) and the Data Generated from this Study as a Function of Temperature

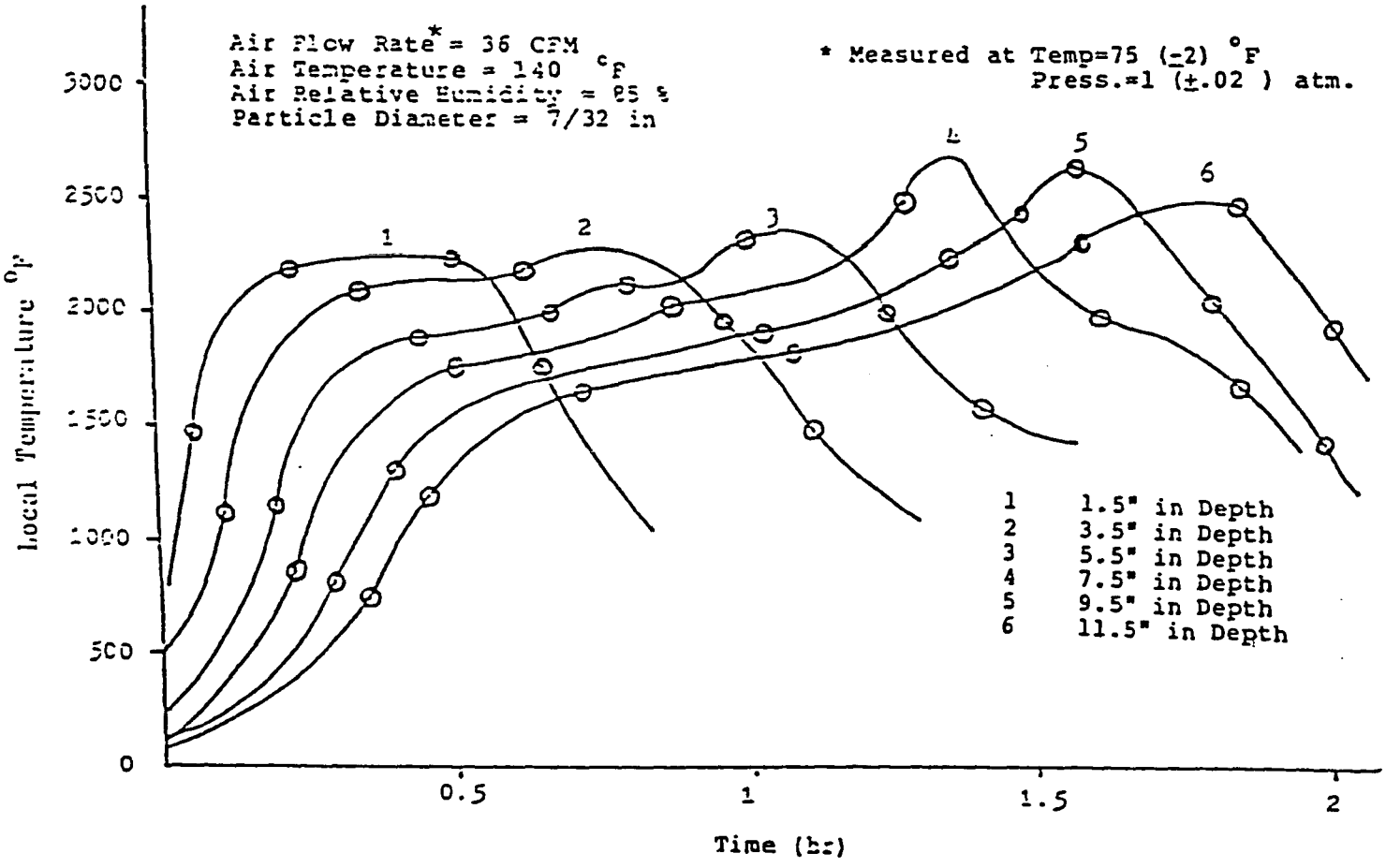

Figure 7.4.3 Variation of Experimental Local Temperature with respect to Time at Different Heights in the Bed

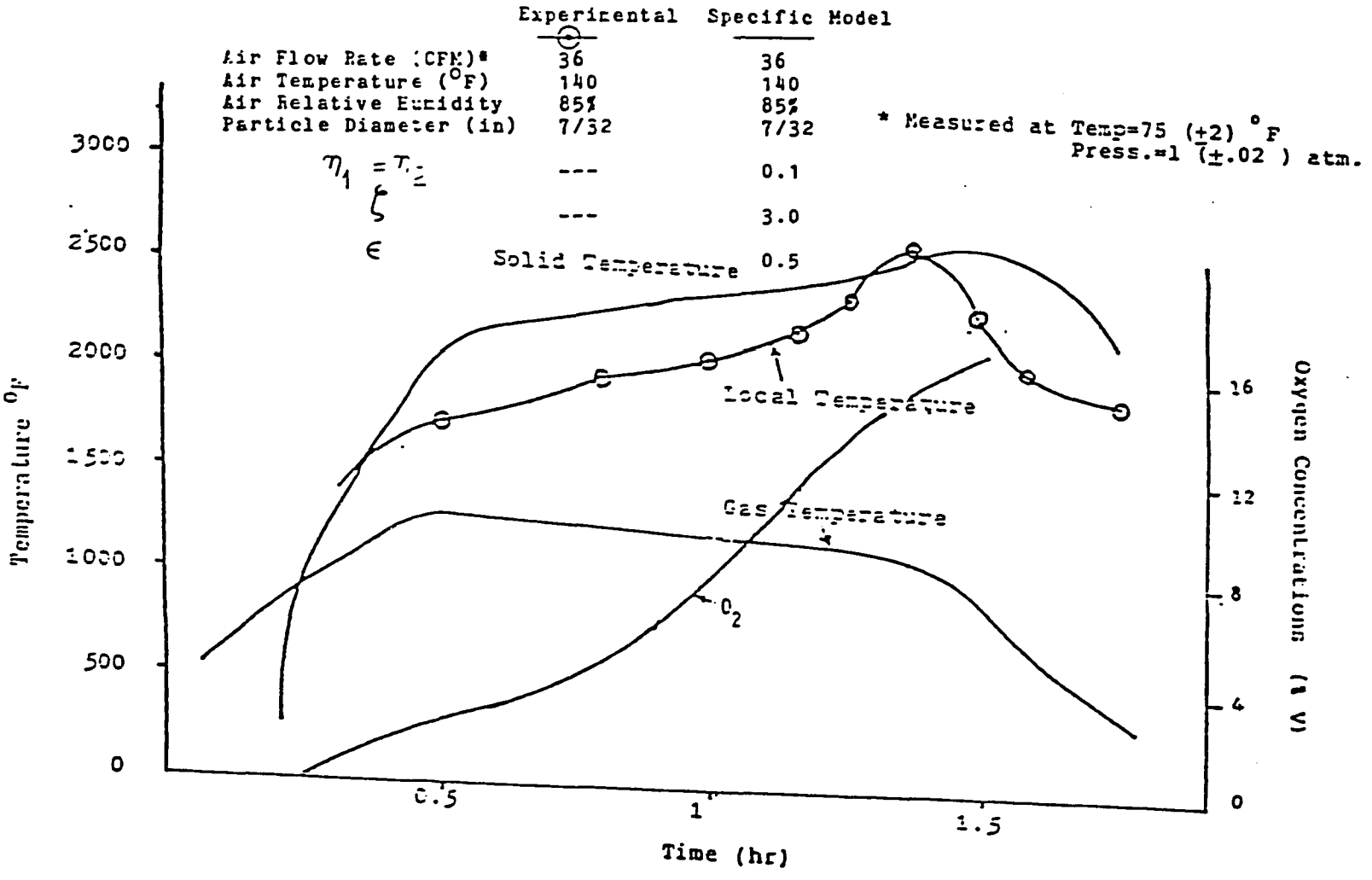

Figure 7.4.4 Comparison of Experimental and Calculated Temperature Profile at a Location (7.5") of the Bed as a Function of Time

the specific model. Figure 7.4.4 also shows that the solid temperature exceeds the gas temperature at time=15 min. Therefore, in order to evaluate this sudden increase in solid temperature, the oxygen concentration profile from the specific model was plotted with respect to time (Figure 7.4.4). This profile shows that the oxygen starts breaking through the bed and hits the solid particles at location of 7.5" at the time=15 min. The oxygen continues to increase its value to a maximum where the solid temperature has its maximum value. Therefore, the increase in solid temperature over the gas temperature is caused by the increase in oxygen concentration.

In order to obtain the gasification rate for the experimental run No.1 and the specific model, the location of maximum local temperature from run No.1 and and the location of the maximum solid temperature from the specific model were plotted versus time (Figure 7.4.5). The lines plotted in Figure 7.4.5 are offset from the origin to illustrate the time required for the coke to become fully ignited. This is known as the ignition period. These maximum temperatures define the location of the combustion zone. The gasification rates were calculated by multiplication of the slopes of Figure 7.4.5, the density of the solid, and $(1-\epsilon)$, and were found to be 25 $lb/hr\text{-}ft^2$ for run No.1 as compared to 25.5 $lb/hr\text{-}ft^2$ for specific model.

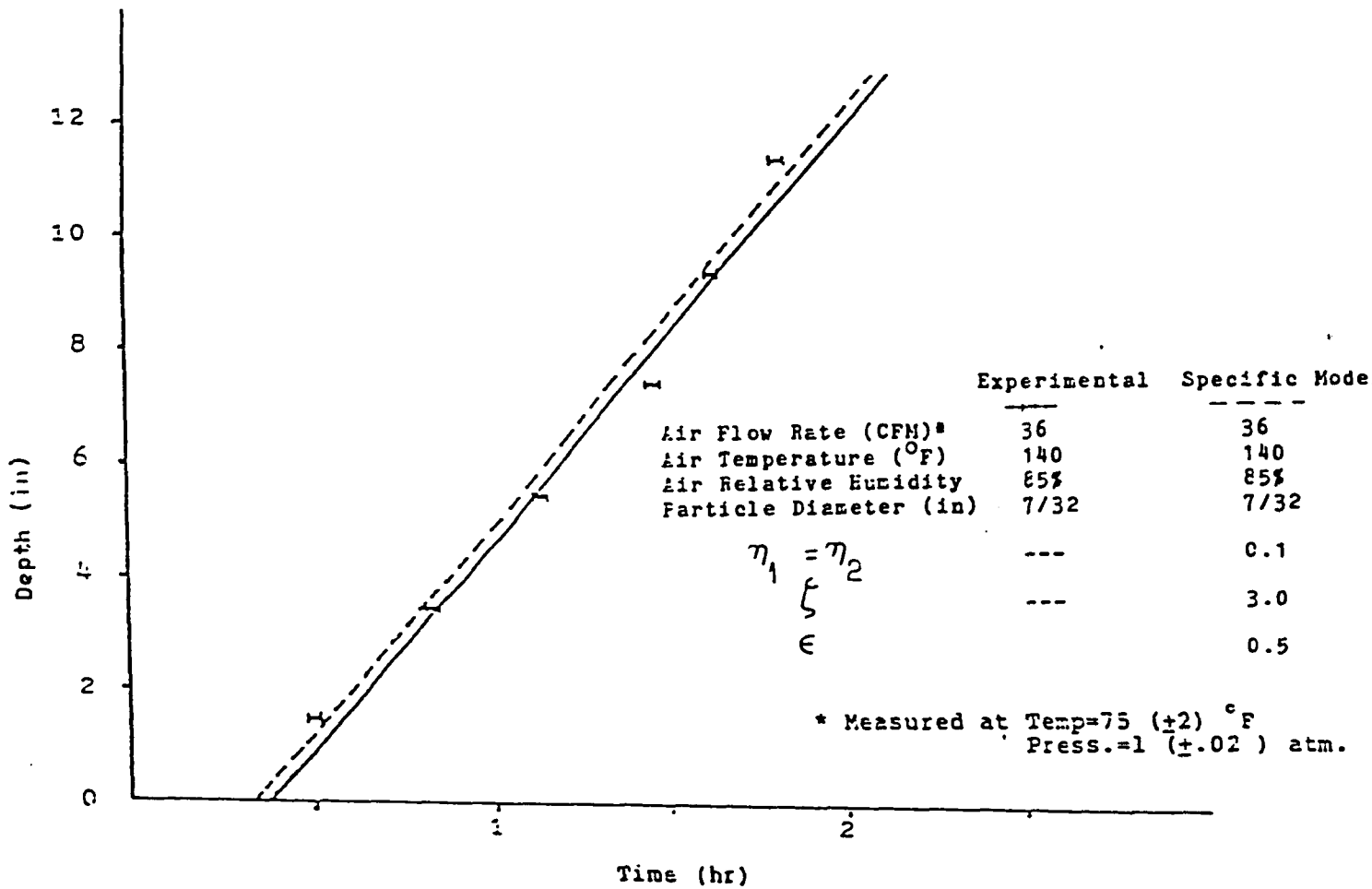

Figure 7.4.5 Location of Maximum Local Temperature from the Experimental System and Solid Temperature from the Specific Model as a Function of Time

Figures 7.4.6.A and 7.4.6.B show the comparison of the outlet gas composition between the experimental run No.2 and the specific model. In the specific model the values of η, and ζ were also chosen to be .1 and 3 respectively because of using the same fuel (coke) as experimental run No.1. Even though the comparison of the outlet gas composition between the experiment and the specific model are slightly different, they do not correlate with available literature. As mentioned earlier, the effect of reactivity of fuel (char/coke) could explain this discrepancy. The slight discrepancy between the experiment and the specific model could have been due to non-uniform burning of the fuel (coke) layer, particularly marked towards the end of the gasification. With non-uniform burning, unburnt coke remains on the walls of the combustion pot and the reacting gas flows past it. Therefore, the composition of the gas does not correspond to the uniform layer calculated by the specific model. This could explain the slight differences of the outlet gas composition between the experimental run and the specific model. In future studies non-uniform burning could possibly be avoided by continually levelling the layer of fuel (coke) during the experiment.

Figure 7.4.7 is the same as Figure 7.4.3 except it is for experimental run No.2. A maximum temperature is found to be 2300 ^{o}F as compared to 2700 ^{o}F for run No.1. This difference

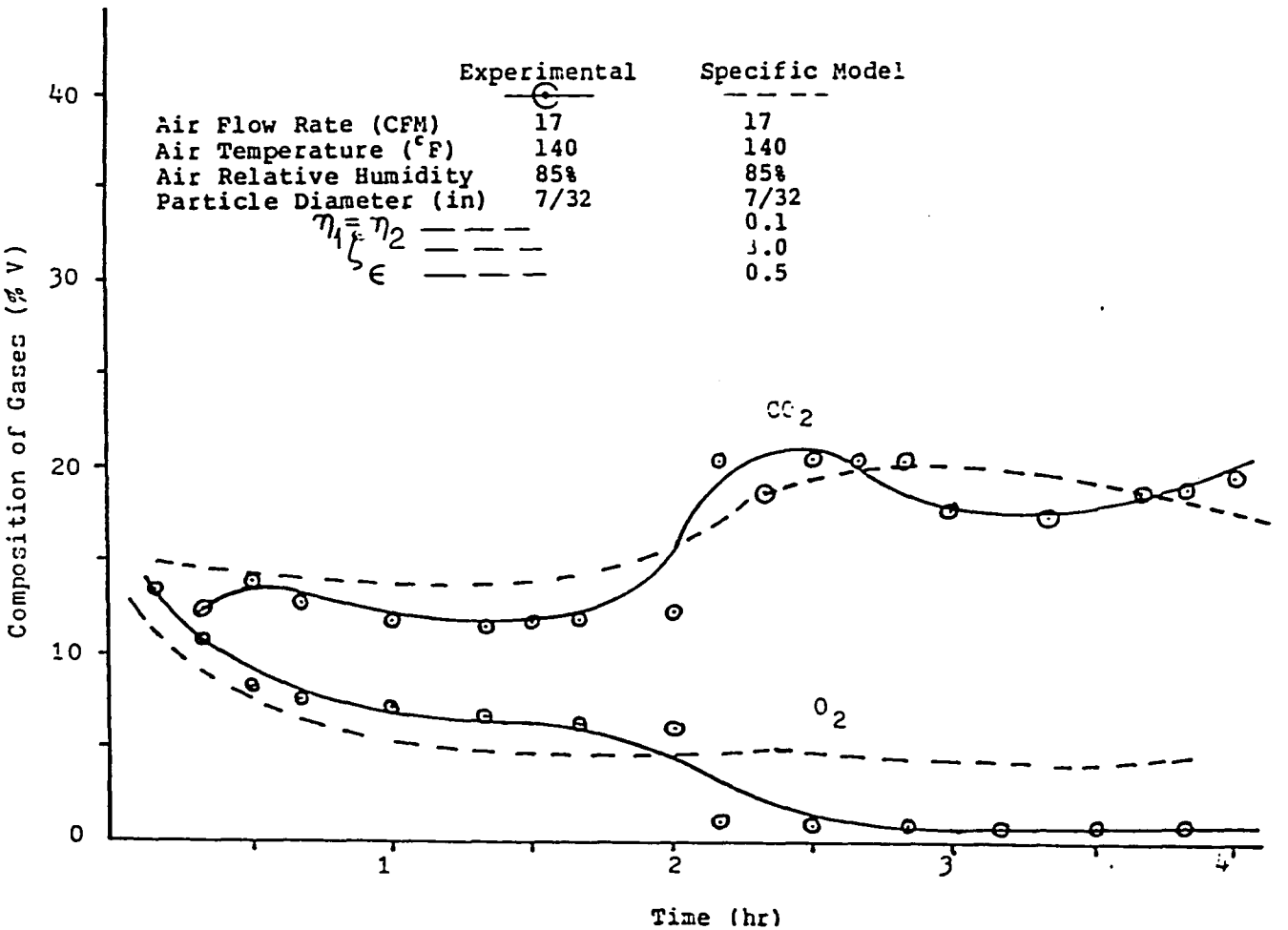

Figure 7.4.6.A Comparison of Experimental and Calculated Outlet Product Gases as a Function of Time

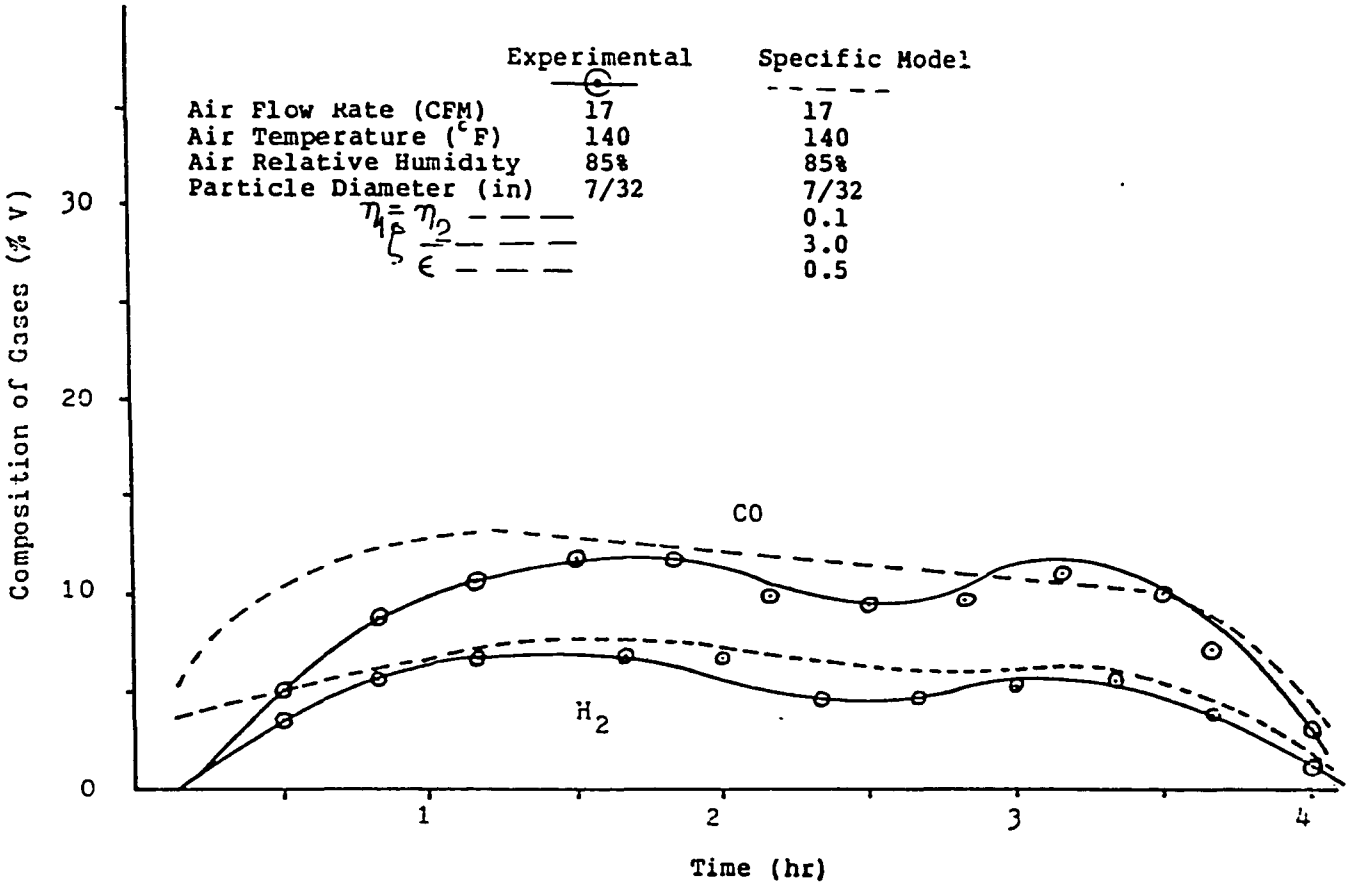

Figure 7.4.6.B Comparison of Experimental and Calculated Outlet Product Gases as a Function of Time

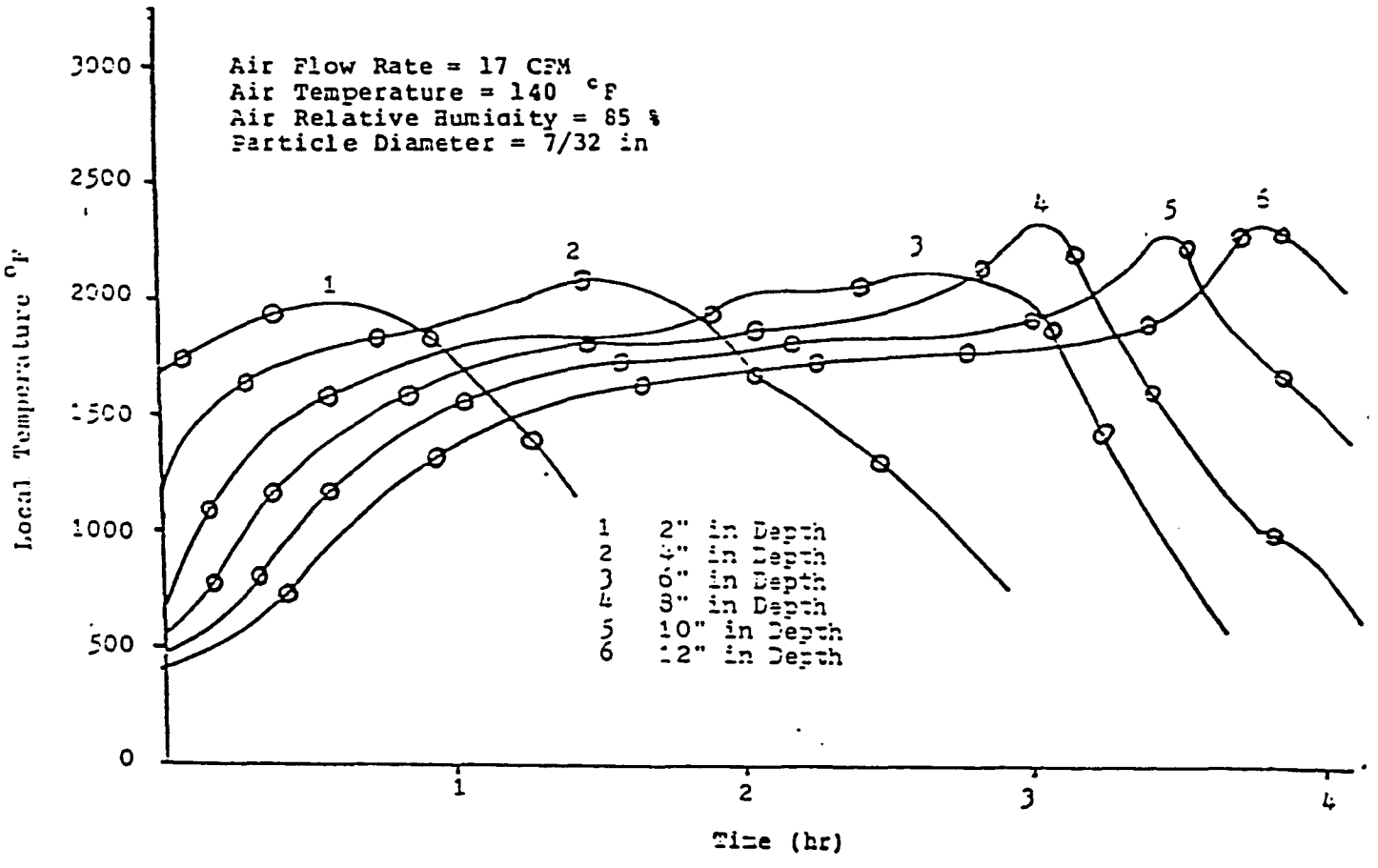

Figure 7.4.7 Variation of Experimental Local Temperature with respect to Time at Different Heights in the Bed

is due to different air flow rates; 36 CFM for run No.1 and 17 CFM for run No.2.

Figure 7.4.8 is the same as Figure 7.4.5 except it is for experimental run No. 2 and specific model with new air flow rate. The gasification rates was calculated from the slopes of Figure 7.4.8 and were found to be 9 $lb/hr-ft^2$ for experimental run No.2 as compared to 10 $lb/hr-ft^2$ for specific model run with the new air flow rate. The difference in gasification rate ($lb/hr-ft^2$) for experimental and specific model runs No.1 and 2 is summarized in Table 7.4.2.

Because the initial and boundary conditions were held constant except for the air flow rate, the decrease in the gasification rate may be attributed to the change in the air flow rate.

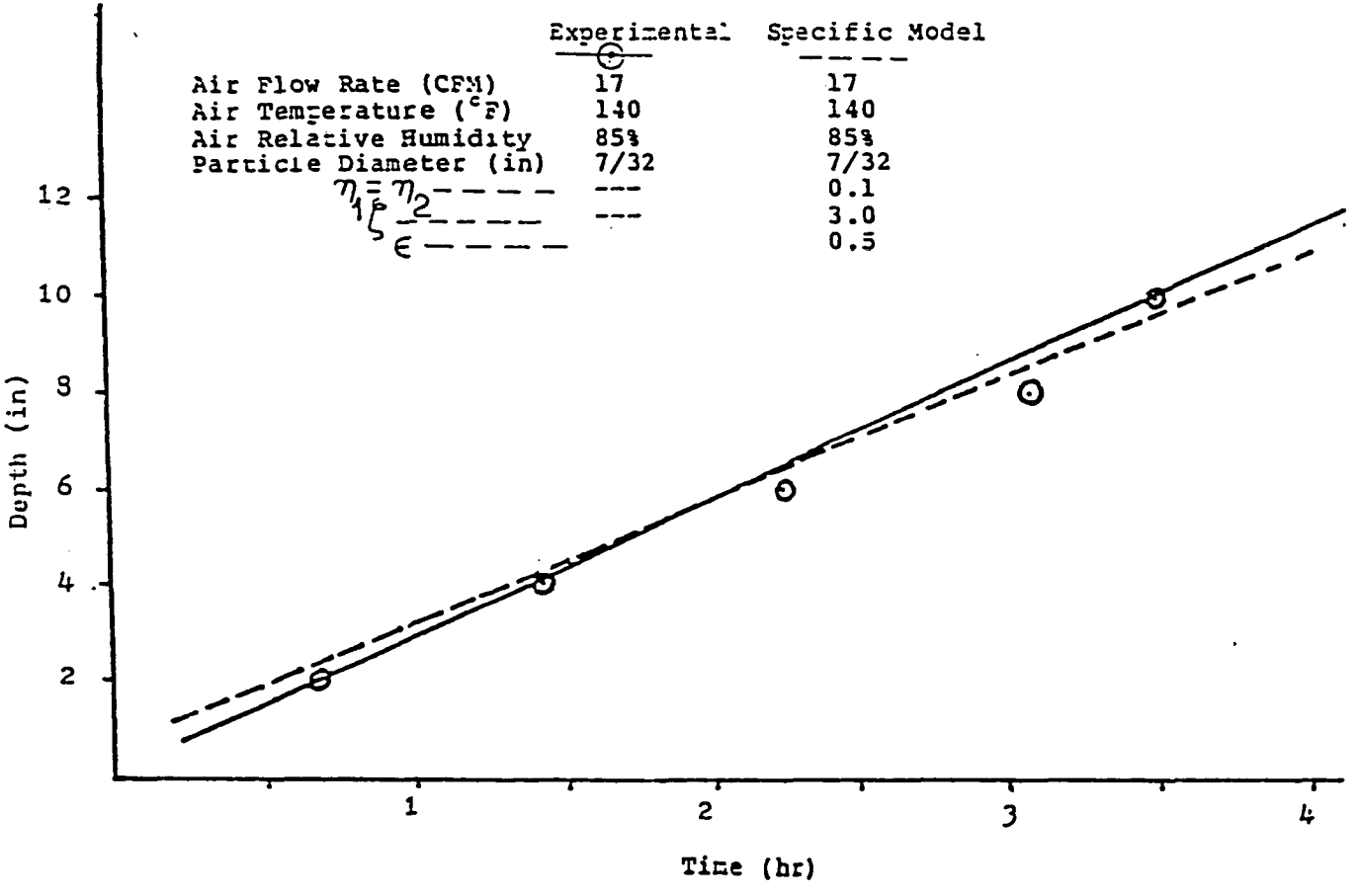

Figure 7.4.8 Location of Maximum Local Temperature from the Experimental System and Solid Temperature from the Specific Model as a Function of Time

Table 7.4.2 Effect of Air Flow Rate on the Gasification Rate ($lb/hr\ ft^2$)

Runs	1	2
Air Flow Rate (CFM)*	36	17
Experimental	25	9
Specific Model	25.5	10

*measured at Temp.=75 (± 2) $^{\circ}F$, and Press.=1. (± 0.02)atm.

8. CONCLUSIONS AND RECOMMENDATIONS

The purpose of this study was to analytically and experimentally simulate the char-gasification process occurring in the gasification component of a crossflow coal gasifier. The basic accomplishments of this study were the development of a computer model to simulate char-gasification and the construction and operation of a batch gasification facility. The result of these efforts have led to the following conclusions:

(1) A simple model (which is referred to as the basic model) for the char-gasification of the crossflow coal gasifier has been developed and validated by available fixed bed gasifier data from the literature. The model predicts the gas composition and temperature profile in the bed and they are in good agreement with available fixed bed gasifier data.

(2) A sensitivity analysis was performed to evaluate the model and ascertain the relative importance of each phenomenon (e.g the gas-solid heat transfer coefficient factor, void fraction, particle diameter, reactivity factors) in the model. The following conclustions were obtained from the sensitivity analysis:

(a) The gas compositions of CO and H_2 are much higher (150-200%), and CO_2 is much less (40-60%) for

fuel with high reactivity than for fuel with low reactivity.

(b) The gas-solid heat transfer coefficient factor has a strong influence on the solid and gas temperature and hence the performance of the gasifier.

(c) Fuel particle size has the major effect on the time for complete combustion and gasification. Small particles require less time for complete combustion and gasification than larger particles.

(d) The bed voidage has a slight effect on the time for complete combustion and gasification, but has a larger effect on the composition of gases.

(3) The experimental results show that the output gas composition obtained from the gasification of coke is heavily dependant on the reactivity of the fuel, which is, in turn, a function of fuel used.

(4) Since the chemical kinetics and the gas-solid heat transfer coefficient are dependant on the reactivity of char/coke, therefore, their values could be varied for different char/coke with different reactivities. Therefore, a specific model has been developed by modifiying parameters (heat transfer coefficient factor ζ, and reactivity factors (η_1 ,η_2)) in the basic model, in order to obtained the data for specific char/coke with specific reactivity. The data obtained from the specific model was validated by the data gathered from this experimental study using specific coke as a feedstock and were in good agreement.

(5) These results support the validity of the applicability of the model to a char-gasification of crossflow coal gasifier, and they provide a basis for the primary objective of the work, which is the study of the crossflow coal gasicication concept.

Although the proposed model provided insight into the reaction of gas and solid, the following considerations should be examined in future crossflow coal gasification research efforts:

1. to develop an expression for the water-gas shift reaction rate, rather than assuming equilibrium.
2. to investigate a correlation to estimate the gas-solid heat transfer coefficient for the gasification processes.
3. the effect of radiation heat transfer in the energy balance.
4. experimental data on temperature and concentration profiles for different types of cokes/chars are also needed to verify and refine the model development. Also to evaluate η, ζ for variety of cokes/chars ranks in order to use these values in the specific model.

BIBLIOGRAPHY

1. U.S. Department of the Interior Bureau of Mines, "Preliminary Economic Analysis of Lurgi Plant Producing 250 Million SCFD Gas from New Mexico Coal," Morgantown, West Virginia (1976).

2. Yoon,H., Wei,J., and Denn, M.M., "A Model for Moving-Bed Coal Gasification Reactors," AIChE J. 24, 885 (1978).

3. Yoon, H., Wei, J. and Denn, M.M., "Transient Bahavior of Moving-Bed Coal Gasification Reactors," AICHE J. 25, 429 (1979).

4. Yoon, H., Wei, J. and Denn, M.M., "Feasible Operating Regions for Moving Coal Gasification Reactors, "Ind. Eng. Chem. Process Des. Dev., Vol. 18, No.2 (1979).

5. Cho, Y.S., and Joseph, Y.S, "Heterogenous Model for Moving-Bed Coal Gasification Reactors," Ind. Eng. Chem. Process Des. Dev. 20, 314 (1981).

6. Desai, P.R., and Wen, C.Y., "Simulation of a METC Fixed Bed Gasifier," presented for the U.S. DOE under contract No. E4-76-S-21-8039.

7. Amundson, N.R., and Arri, L.E., " Char Gasification in a Countercurrent Reactor," AICHE J. 24,87 (1978).

8. Aris, L.E., and Amundson, N.R., " An Analytical Study of Single Particle Char Gasification," AICHE J. 24, 72 (1978).

9. Eapen, T., Blackadar, R. and Essenhigh, R. H., "Kinetics of Gasification in a Combustion Pot," Proceeding of the 16th Symposium on Combustion Institute, Pittsburgh, Pa., 515. (1977)

10. Karzhavina, N. "The Burning of Carbon III," Fuel, 220, 19 (1940)

11. Lewis, K. W., "Chemistry of Combustion in Coal-Fired Furnaces," Ind. Eng. Chem. XV, 502 (1923)

12. Sign, C. P. P. and Saraf, D. N., "Simulating of High-Temperature Water-Gas Shift Reactors," Ind. Eng. Chem. Process Des. Dev., 16, 313 (1977)

13. Choudhury, S.S., and Gangulo, P.C., "Effect of Carbonate Minerals on Volatile Matter of Coals, Fuel 57, 175 (1978).

14. Chaung, T.Z., and Wen, C.Y., "Entrainment Coal Gasification Modeling," Ind. Eng. Chem. Process Des. Dev. 18, 684 (1979).

15. Wen, C.Y., "Noncatalytic Heterogeneous Solid Fluid Reaction Models," Ind. Eng. Chem. , 60, 34 (1968).

16. Johnson, J.L., "Coal Gasification," Adv. Chem. Ser., 131, 145 (1974)

17. Walker, P.L., Jr., Rusinko, F., Jr., and Austin, L.G., "Gas Reactions of Carbons," Adv. Catalysis," 2, 134 (1959).

18. Dutta, S. and Wen, C.Y., "Reactivity of Coal and Char in Oxygen-Nitrogen Atmosphere," Ind. Eng. Chem. Process Des. Dev. 16, 31, (1977).

19. Wen., C.Y., and Wu. C.N.T., "An Analysis of Slow Reactions in a Porous Particle," AICHE J. 22, 1012 (1976).

20. Levenspiel, O., Chemical Reaction Engineering, John Wiley & Sons, N.Y. (1972).

21. Essenhigh, R.H., "Combustion of Coal" Coal Conversion Technology ed. by E.S. Lee and C.Y. Wen, Advisor-Wisley Publishing Co., (1979).

22. Advedesian, M.M., and Davidson, J.F., "Combustion of Carbon Particles in a Fluidised Bed," Trans, Inst. Chem. Eng., 51, 121 (1973)

23. Caram, H.S., and Amundson, N.R., "Diffusion and Reaction in a Stagnant Boundary Layer about a Carbon Ind. Eng. Chem. 16, 171 (1977).

24. Phillips, R., Vastala, F.J., and Walker, "Factors Affecting the Product Ratio of the Carbon-Oxygen Reaction. 1 and 2," Carbon, 7. 479 (1969), Carbon 8, 205 (1970).

25. Wen, C.Y., and Dutta, S., Coal Conversion Technology, edited by Wen and Lee, Adison-Wiley Publishing Co., (1979).

26. Arthur, J.R., "Reaction Between Carbon and Oxygen," Tran. Faraday Soc. 47, 164 (1951).

27. Wen, C.Y., and Tone, S. "Coal Conversion Reaction Engineering" ACS Symposium Series 72 (1978).

28. Burke, S.P., and Shuman, T.E.N., Proc. 3rd Ind. Conf. Bituminous Coal, 2, 485 (1931).

29. Field, M.A., Gill, D.W., Morgan, R.B. and Hawskley, P.B.W., 'Combustion of Pulverized Coal,' (1967).

30. Wen, C.Y., "Optimization of Coal Gasification Processes," R and D Report No. 66, Office of Coal Research PN-78 (1972).

31. Dutta, S., Wen, C.Y. and Belt, R.J., "Reactivity of Coal and Char in Carbon Dioxide Atmosphere," Ind. Eng. Chem. Process Des. Dev., 16, 20 (1977).

32. Reid, B.E. and Hanesia, D., "Kinetic Study of Carbon-Steam Reaction," Ind. Eng. Chem. Process Des. Dev. , 14 (1), 70 (1975).

33. Gray, M.D. and Kimber, M.G., "Reaction of Charcoal Particles with Carbon Dioxide and Water at Temperature up to 2800 K," Nature, 214, 797 (1967).

34. Dobner,S. "Modeling of Entrained Bed Gasification," EPRI, 15, (1976).

35. Yang, R.T. and Steinberg, M., "A Diffusion Cell Method for Studying Heterogeneous Kinetics in the Chemical Reaction," Ind. Eng. Chem. Fund. 16 (2), 235 (1977).

36. Blackwood, J.D. and Mcgrory, F., "The Cabon- Steam Reaction at High Pressure," Fuel, 11,16 (1958).

37. Gumz, W., Gas Procedures and Blast Furnances, Wiley, N.Y. (1950).

38. Wen, C.Y. and Huebler, J., "Kinetic Study of Coal Char Hydrogasification," Ind. Eng. Chem. Process Des. Dev., 4, 142 (1965).

39. Yoshida, K. and Kunii, D., "Gasification of Porous Carbon by Carbon Dioxide," J. Chem. Eng. (Japan), 2, 170 (1969).

40. Ergun, S., "Kinetics of the Reaction of Carbon Dioxide With Carbon," J. Phy. Chem. 60, 480 (1956).

41. Turkdogen, E.T. and J.V. Vinters, "Kinetics of Oxidation of Graphite and Charcoal in Carbon Dioxide," Carbon, 7, 101 (1969).

42. Austin, L.G. and Walker, P.L., "Effect of Carbon Monoxide in Causing Nonuniform Gasification of Graphite by Carbon Dioxide," AICHE J., 9, 303 (1963).

43. Fuchs, W.E. and Yovorsky, P.M., Preprint 170th National Division Fuel Chem., 20, 3, 115 (1975).

44. Birch, T.J., Hall, K.R. and Urie, R.W., "Gasification of Brown Coal with Hydrogen in a Continuous Fluidized-Bed," J. Inst. Fuel, 33, 422 (1960).

45. Linden, H.R. and Pyrocioch, E.J., "Pipeline Gas by High-Pressure Fluid-Bed Hydrogasification of Char," Ind. Chem., 52, 590 (1960).

46. Gupta, A.S., and Thodos, G., "Direct Analogy Between Mass and Heat Transfer to Beds of Spheres," AICHE J. 9, 751 (1963).

47. Argo, W.B. and Smith, J.M., "Heat Transfer in Packed Beds," Chem. Eng. Progress, 49, 444 (1953).

48. Shampine, F. L. and Richard, C. A., Numerical Computing, W. B. Saunders Co. (1973)

49. Gallagher, A. M., Master Thesis; W. V. U., Morgantown, W. VA (1986)

50. Wellman Gulusha, Sales Brochure, MacDowell-Wellman Co. (1976)

51. Hoffman, J. E., Coal Conversion, Energon Co., (1978)

52. Hahn, O. J. and Schrodt, J. T., "Low Btu Gas and Solid Desulfurized Fuel," A Kentuky Coal Utilization Research Program, Annual report, (1973)

53. Cho, Y. S. , "Modeling and Simulation of Lurgi-Type Gasifiers," M.S. Thesis, Washington University, St. Louis, (1980)

54. Klei, H. E., "Kinetics of the Activated Carbon-Steam Reaction," Ind. Eng. Chem., Process Des. Dev., 14, 47 (1975)

Appendices

Appendix I

Derivation of Overall Chemical Reaction Rate

Defining the reaction rate as:

$$\text{Rate} = \frac{1}{4\pi R_o^2} \frac{dm_A}{dt}$$

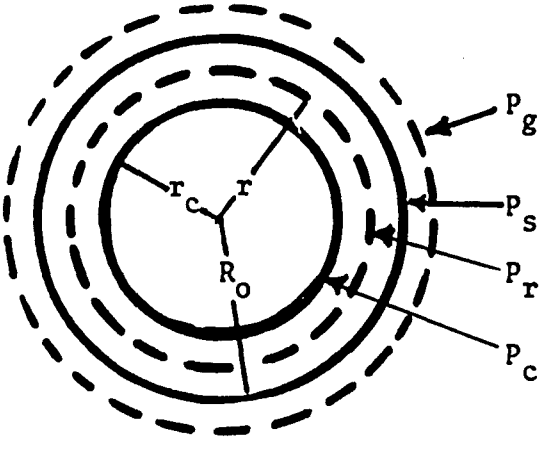

Figure I.1 Representation of Concentrations of Reactants and Products A(g) + B(s) ⟶ E(g) + F(s) for a Particles of Unchanged Size.

where

P_g = Gas film pressure

P_s = Surface pressure

P_r = Surface pressure of any radius r

P_c = Unreacted core pressure

In this model three steps were visualized occuring in succession during reaction.

Step 1. Diffusion of gaseous reactant A through the film surrounding the particle to the surface of the solid. Figure I.1 show that no reactant is present at the surface; hence the pressure driving force, given by $P_g - P_s$, is constant at all time during reaction of particles. Therefore, the rate equation based on exterior surface of particles yield to:

$$-\frac{1}{4\pi R_o^2}\frac{dm_A}{dt} = K_g (P_g - P_s) \qquad (I.1)$$

Step 2. Penetration and diffusion of gas A through the blanket of ash to the surface of the unreacted core. And by assuming the rate of reaction of A at any instant is given by its rate of diffusion to the reaction surface, or

$$-\frac{1}{4\pi r_c^2}\frac{dm_A}{dt} = D_e \left.\frac{dP_r}{dr}\right|_{r=r_c} \qquad (I.2)$$

Where D_e is the effective diffusion coefficient of gaseous reactant in the ash layer. And for motionless particles, the value of D_e can be found from the experession:

$$D_e = R_o K_{ash}$$

Therefore, the equation (I.2) yield to:

$$-\frac{1}{4\pi r_c^2}\frac{dm_A}{dt} = R_{ash} K_o \left.\frac{dP_r}{dr}\right|_{r=r_c} \qquad (I.3)$$

Step 3. Reaction of gaseous A with solid at r_c. And the rate of reaction in terms of shrinking radius is given by

$$-\frac{1}{4\pi r_c^2}\frac{dm_A}{dt} = K_s P_c \qquad (I.4)$$

Now, as with particles of constant size, the rate expression becomes:

From continuity equation, in the ash layer, we have

$$\frac{D_e}{r^2}\frac{d}{dr}\left(r^2\frac{dP_r}{dr}\right) = 0$$

or

$$\frac{R_o K_{ash}}{r^2}\frac{d}{dr}\left(r^2\frac{dP_r}{dr}\right) = 0 \qquad (I.5)$$

The solution yield to:

$$P_r(r) = \frac{A}{r} + B \qquad (I.6)$$

With boundary conditions of

$$P_r = P_s \qquad \text{at} \qquad r = R_o$$

and

$$P_r = P_c \qquad \text{at} \qquad r = r_c$$

After applying these boundary conditions to the equation (I.6), the solution to the equation (I.6) yield to:

$$P_r(r) = \frac{(P_s - P_c)}{(\frac{1}{R_o} - \frac{1}{r_c})r} - \frac{(P_s - P_c)}{(\frac{1}{R_o} - \frac{1}{r_c})r_c} + P_c$$

And

$$\left.\frac{dP_r}{dr}\right|_{r=r_c} = \frac{(P_s - P_c)}{r_c\,(1 - \frac{r_c}{R_o})} \qquad (I.7)$$

By defining $\xi = \frac{r_c}{R_o}$; and substituting into the equation (I.7), then

$$\left.\frac{dP_r}{dr}\right|_{r=r_c} = \frac{(P_s - P_c)}{R_o (1 - \xi)} \qquad (I.8)$$

By substituding equation (I.8) into the equation (I.3), it was found that;

$$-\frac{1}{4\pi r_c^2}\frac{dm_A}{dt} = \frac{K_{ash}(P_s - P_c)}{(1 - \xi)}$$

or

$$-\text{Rate} = \frac{K_{ash}(P_s - P_c)}{(1 - \xi)} \qquad (I.9)$$

Also equations (I.4) and (I.1) yields to:

$$-\text{Rate} = \xi^2 K_s P_c \qquad (I.10)$$

and

$$-\text{Rate} = K_g (P_g - P_s) \qquad (I.11)$$

From the equations (I.9), (I.10), and (I.11), it was found that:

$$P_c = \frac{P_g}{1 + \frac{K_s}{K_{ash}}(1-\xi) + \frac{K_s}{K_g}\xi^2} \qquad \text{(I.12)}$$

Now by substituting the expression P_c into the equation (I.10), it was found that:

$$\text{Rate} = \frac{P_g}{\frac{1}{K_g} + \frac{1}{K_{ash}}\left(\frac{1}{\xi} - 1\right) + \frac{1}{K_s \xi^2}} \qquad \text{(I.13)}$$

Appendix II

Rate Expressions

Surface reaction type, unreacted-core shrinking model (20,15)

$$\dot{R}''_i = \frac{(P_j - P_j^*)}{\frac{1}{K_g} + \frac{1}{K_{ash}}\left(\frac{1}{\xi} - 1\right) + \frac{1}{K_s \xi^2}} \quad gm/sec\text{-}cm^2$$

(II.1) Char-O_2 Reaction (14,34)

$$K_s = 8710.\ \exp(-17967/T_s)$$

$$K_g = 0.292\,\phi\left(\frac{4.26}{T_g}\right)\left(\frac{T_g}{1800}\right)^{1.75}/(P_t\, d_p)$$

ϕ = the mechanism factor based on the stoichiometric relation of CO and CO2, can be roughly estimated by the following equations (25)

$$\phi = \frac{(2Z + 2)}{(Z + 2)} \qquad \text{for } d_p < .005 \text{ cm}$$

$$\phi = ((2Z + 2) - Z(d_p - .005)/.095)/(Z + 2) \qquad \text{for } .005 < d_p < 0.1 \text{ cm}$$

And

$$\phi = 1.0 \quad \text{for } d_p > 0.1 \text{ cm}$$

where

$$Z = 2500 \exp(-6249/T_m)$$

$$P_j - P_j^* = P_{O_2}$$

(II.2) Char-Steam Reaction (29)

$$K_s = 247 \times \eta_1 \exp(-21060/T_s)$$

$$K_g = 10 \times 10^{-4} (T_m/2000)^{0.75} / (P_t \cdot d_p)$$

$$K_{eq} = \exp(17.644 - 30260/(1.8 \cdot T_s))$$

$$P_j - P_j^* = P_{H_2O} - \frac{P_{H_2} P_{CO}}{K_{eq}}$$

(II.3) Char-CO_2 Reaction (14,29)

$$K_s = 247 \times \eta_2 \exp(-21060/T_s)$$

$$K_g = 7.45 \times 10^{-4} (T_m/2000)^{0.75} / (P_t \cdot d_p)$$

$$P_j - P_j^* = P_{CO_2}$$

(II.4) Char-Hydrogen Reaction

This reaction is still in volumetric reaction regim even @ high temperature (1600 ^{o}K) (14), because it has low intrinsic reaction rate but high diffusion Characteristics.

$$K_s = 0.12 \exp(-17921/T_s)$$

$$K_g = 1.33 \times 10^{-3} \left(\frac{T_m}{2000}\right)^{0.75} / (d_p \cdot P_t)$$

$$K_{eq} = 5.0 \times 10^{-6} \exp(10200./T_s)$$

$$P_j - P_j^* = P_{H_2} - (P_{CH_4} / K_{eq})^{1/2}$$

APPENDIX III

```
*****************************************************************
*                                                               *
*                                                               *
*                                                               *
*    COMPUTER PROGRAM FOR CROSSFLOW COAL GASIFICATION           *
*                                                               *
*                          by                                   *
*                                                               *
*                 ESMAIL R. MONAZAM                             *
*                                                               *
*                          1986                                 *
*                                                               *
*                                                               *
*                                                               *
*****************************************************************


      IMPLICIT REAL*8(A-H,O-Z)
      EXTERNAL F
      EXTERNAL F1
      EXTERNAL CPH
      DIMENSION AA(12),B(12),C(12),HFO(12),RWORK1(44),IWORK1(22)
     1  ,FF(10),CP(12),HH(12),HG(12),X(6),CPG(12),Y1(2),ATOL1(2)
     1  ,RWORK(134),IWORK(27),ATOL(7),Y(7),YY1(350),YY2(350)
      COMMON /NON/AREA,BBB,AMWO2,AMWH2O,AMWH2,AMWCO,AMWCO2,AMWCH4
     1       ,RATE1,RATE2,RATE3,RATE5,PHI,CKWG,CSEQK,HS2G
      COMMON /XX/AMOIST,VM,FIXC,ASH,HVCOAL,FC,FH,FO,FN,FS,FASH,
     1          COAL,AIR,STEAM,TCOAL,TAIR,TSTEAM,XL,DIA,HSTEAM
      COMMON /CC/RATEO2,RATH2O,RATCO2,RATECO,RATEH2,RATCH4,YC
     1 ,RATEC,RP,PHOC,TG,TS,HCON1,CPS,HRT,A,E,HS1G,HWGSHF,SUM
      CALL INPUT
C CONVERTS UNITS OF COAL, STEAM AND AIR FEED RATES
C FROM LBS/HR TO GMS/SEC OR GMOLES/SEC.
C TEMPERATURES ARE IN DEG KELVIN.
C INPUTS AND OUTPUTS ARE IFPS UNITS, HOWEVER ALL THE
C CALCULATIONS ARE DONE IN CGS UNITS
C   RATE1  C+O2-----CO+CO2
C   RATE2  C+H2O----CO+H2
C   RATE3  C+CO2----2CO
C   RATE4  CO+H2O---CO2+H2
C   RH=RELATIVE HUMIDITY OF ENTRING AIR
C   AIRFLW=AIR FLOW RATE (CFM)
C   TAIR=TEMPERATURE OF ENTRING AIR
C   NONODE=NO. OF NODES IN VERTICAL SECTION
C   XL=BED LENGTH
C   DELY=INCREMENT OF LENGTH
C   DELT=INCREMENT OF TIME
C   PHOC=DENSITY OF SOLID
C   PHOASH=DENSITY OF ASH
```

```
C    DTPR=INCREMENT OF PRINTING TIME
C    YC=CORE RADIUS/TOTAL RADIUS
C    RC=CORE RADIUS
C    DP=PARTICLE DIAMETER
C    VOLUMP=PARTICLE VOLUME
C    E=VOIDE FRACTION
C    AREA=AREA OF THE PARTICLE
       RH=0.7
       AIRFLW=36.0D 0
       DP=0.25
       TAIR=140.0D 0
       CALL PRESUR(PSAT,TAIR)
       PV=PSAT*RH
       PAIR=(14.7-PV)
       SPECIF=PV/PAIR
       TGIN=5./9.*(TAIR-32.0)+273.33
       WRITE(6,215) PSAT,SPECIF
 215   FORMAT(3X,2F12.5)
       MOM=1
       NONODE=26
       XL=XL*30.48
       N=1
      TMASBD=0.0D 0
      KK1=1
      JJ=1
      KKK=1
      I=KK1
       DELY=XL/NONODE
       TMASB=0.0D 0
       DTPR=300.0D 0
       TPR=DTPR
      DELT=10.
      PHOC=1.40
      PHOASH=PHOC
      PHOCOA=1.4
      CON1=0.0005
      DO 443 J=1,NONODE
      YY2(J)=1.0D 0
 443  CONTINUE
      DP=DP*30.48/12.0
      RP=DP/2.0
      VOLUMP=4.0*3.14*RP**3.0/3.0
      TMASP=VOLUMP*PHOC
      RC=YC*RP
      E=0.50
      AV=6.0/DP
      A=(1.0-E)*AV
      EBS=0.01
      AREA=4.*3.14*RP**2
C    AMW'S ARE MOLECULAR WEIGHTS OF EVERY SPECIES
      AMWO2=32.0
      AMWH2O=18.0
      AMWH2=2.0
```

```
      AMWCO=28.
      AMWCO2=44.0
      AMWCH4=16.0
      AMWAIR=28.9
      AMWN2=28.0
      AMWC=12.0
C
C    BDIA=DIAMETER OF THE BED
C    ABED=AREA OF THE BED
C    AGAS=OCCUPIED AREA BY THE GAS
C    TMASH=MASS OF THE ASH IN EVERY PARTICLE
      BDIA=13.0/12.0
      PHOA=.072
      CURLE=0.8
      AMAIR=(AIR*PHOA*454.4)/(60.0*AMWAIR)
      ABED=3.14*BDIA**2/4.0
      ABED=ABED*30.48*30.48
      AGAS=ABED*E
      AIR=AMAIR/AGAS
      TOMASC=ABED*DELY*PHOC*(1.0-E)
      TMASIN=ABED*XL*PHOC*(1.0-E)
      TMASH=FASH*TMASIN
C
C    SETS INITIAL CONDITION FROM EXPERIMENTAL RESULT FOR SOLID
C    TEMPERATURE
C
C
      IF(MOM.EQ.2)GO TO 412
      GO TO 413
 412  DO 416 LL=1,NONODE
      YY1(LL)=320.0D 0
 416  CONTINUE
      GO TO 414
 413  CONTINUE
      CALL INTIAL(YY1)
 414  CONTINUE
      PT=0.0
      PT=(PT+14.7)/14.7
      TSOLAV=400.0
      TS=TSOLAV
      TG=TGP
      TG1=TGP
      DT=XL/NONODE
       NEQ=7
      AAA=0.0D 0
      DA=XL/NONODE
      HHH=.5*DA
      HMAX=.7*DA
      ABSERR=1.0D-06
      RELERR=1.0D-06
      A1=0.0D 0
      DA1=10.0D 0
      HH1=0.5*DA1
```

```
      HMAX1=0.7*DA1
      NEQ1=2
      TOUT1=A1
      TOUT=AAA
C
C
C
C 1=CO, 2=CO2, 3=H2, 4=O2, 5=H2O, 6=CH4
C
C    PT=TOTAL PRESSURE
C    TS=SOLID TEMPERATURE
C    TG= GAS TEMPERATURE
C    X(I)'S ARE GR-MOLES OF SPECIES I
C    XAV'S ARE AVG GR-MOLE OF SPECIES I
C    CCC'S ARE GR-MASS OF SPECIES I
C    TMOLG=TOTAL MOLES
C    P'S =PARTIAL PRESSURE OF EACH SPECIES
C
 811 CONTINUE
      PHOA=0.057
      AIR=AIRFLW*PHOA*454.4*1.2/(60.0*AMWAIR*AGAS)
C      WRITE(6,612) TOUT1
      IF(KK1.GE.NONODE) GO TO 42
      TOUT=0.0D 0
      KKK=1
      IF(YY2(KK1).LE.0.10) TMASB=TMASB+TOMAS C
      IF(YY2(KK1).LE.0.10) KK1=KK1+1
      I=KK1
      Y1(1)=YY1(I)
      Y1(2)=YY2(I)
      TG=TGIN
      TG1=TGIN
      TS=Y1(1)
      YC=Y1(2)
      XYZ=.1
      EBS=0.01
      X(1)=0.0D 0
      X(2)=0.0D 0
      X(3)=0.0D 0
      X(4)=0.21*AIR
      X(5)=SPECIF*AIR
      X(6)=0.0D 0
      YYN2=0.79*AIR
      IF(MOM.EQ.2) CALL GAS(CPH,X,AGAS,YYN2,TG,TG1)
      XX1=X(1)
      XX2=X(2)
      XX3=X(3)
      XX4=X(4)
      XX5=X(5)
      XX6=X(6)
      XAV1=XX1
      XAV2=XX2
      XAV3=XX3
```

```
      XAV4=XX4
      XAV5=XX5
      XAV6=XX6
C
C
      CCC1=X(1)*AMWCO
      CCC2=X(2)*AMWCO2
      CCC3=X(3)*AMWH2
      CCC4=X(4)*AMWO2
      CCC5=X(5)*AMWH2O
      CCC6=X(6)*AMWCH4
      CCC7=TG1
      TMOLG=0.0D 0
      DO 14 L=1,6
 14   TMOLG=TMOLG+X(L)
      TMOLG=TMOLG+YYN2
C  CALCULATES FRACTION OF O2, H2O, CO, CO2, H2, CH4 FOR
C  RATES CALCULATIONS
C
C
C  CALCULATES PARTIAL PRESSURE OF O2, H2O, CO, CO2, H2, CH4
C  FOR RATES CALCULATION.
C
C      WRITE(6,823) PCO,PCO2,PH2,POXY,PSTEAM,PCH4
823   FORMAT(1X,'PCO=',6F14.3)
C      WRITE(6,743) TG
 743  FORMAT(1X,'TG=',F15.5)
      TMASSC=TMASSC+Y(3)*12./44.+Y(4)*12./28.
      DO 109 KK=KK1,NONODE
      IF(YY2(I).LE.0.10)GO TO 121
101   CONTINUE
      TMOLGA=XAV1+XAV2+XAV3+XAV4+XAV5+XAV6+YYN2
      XCO=XAV1/TMOLGA
      XCO2=XAV2/TMOLGA
      XH2=XAV3/TMOLGA
      XO2=XAV4/TMOLGA
      XH2O=XAV5/TMOLGA
      XCH4=XAV6/TMOLGA
      XN2=YYN2/TMOLG
      PCO=PT*XCO
      PCO2=PT*XCO2
      PH2=PT*XH2
      POXY=PT*XO2
      PSTEAM=PT*XH2O
      PCH4=PT*XCH4
      AAA=TOUT
      A1=TOUT1
      HHH=0.5*DA
      HMAX=0.7*DA
      HH1=0.5*DA1
      HMAX1=0.7*DA1
      Y(1)=CCC1
      Y(2)=CCC2
```

```
      Y(3)=CCC3
      Y(4)=CCC4
      Y(5)=CCC5
      Y(6)=CCC6
      Y(7)=CCC7
      Y1(1)=YY1(I)
      Y1(2)=YY2(I)
      KKK=KKK+1
      MMM=1
      IF(KKK.GT.500000)STOP
      CALL COMBUS(TG,TS,PT,RP,POXY,YC,RATE1,PHI,DELT,PHOC)
      CALL CBSTM(TG,TS,PSTEAM,PH2,PCO,RP,PT,YC,RATE2,DELT
     1,PHOC)
      CALL CBCO2(TG,TS,PCO2,RP,PT,YC,RATE3,DELT,PHOC)
      CALL CBHY(TG,TS,PH2,PCH4,RP,PT,RATE5,DELT,PHOC,YC)
C
C
C      WRITE(6,723) RATE1,RATE2,RATE3,RATE4,RATE5
723   FORMAT(1X,'RATES=',5D17.7)
      RATE4=0.0D 0
C      WRITE(6,711)RATE41
 711  FORMAT(2X,'RATE4=',D20.8)
      RATEO2=-(AMWO2/AMWC)*RATE1/PHI
      RATH2O=-(AMWH2O/AMWC)*RATE2-AMWH2O*RATE4
      RATCO2=(2./PHI-1.)*(AMWCO2/AMWC)*RATE1-(AMWCO2/AMWC)*RATE3+
     1        AMWCO2*RATE4
      RATECO=2.*(1.-1./PHI)*(AMWCO/AMWC)*RATE1+(AMWCO/AMWC)*RATE2+
     1       2.0*(AMWCO/AMWC)*RATE3-AMWCO*RATE4
      RATEH2=(AMWH2/AMWC)*RATE2+AMWH2*RATE4-2.0*(AMWH2/AMWC)*RATE5
      RATCH4=(AMWCH4/AMWC)*RATE5
C
C      WRITE(6,623) RATEO2,RATH2O,RATCO2,RATECO,RATEH2,RATCH4
623   FORMAT(1X,6D17.7,'HERE=',1X)
      CPS=.32
      IF(TS.GT.1300.) CPS=0.25
      IF(TS.GE.1200. .AND.TS.LT.1300.) CPS=0.25
      IF(TS.GE.1100. .AND.TS.LT.1200.) CPS=0.27
      IF(TS.GT.1000. .AND.TS.LT.1100.) CPS=0.30
      CPC=(2.673+.002617*TS-116900./TS/TS)/(12.04*1.2)
      HC=CPC*12.0*(TS-298.)
      DO 25 M=1,12
      CALL CPH(M,TS,CP(M),HH(M))
      CALL CPH(M,TG,CPG(M),HG(M))
 25   CONTINUE
      HS2G=((2.-2./PHI)*HH(1)+(2./PHI-1.)*HH(2)-
     1      HH(8)/PHI)*RATE1/AMWC+
     2     (HH(1)+HH(4)-HH(9))*RATE2/AMWC
     3    +(2.0*HH(1)-HH(2))*RATE3/AMWC+
     4     (HH(5)-2.*HH(4))*RATE5/AMWC
      SUM=XAV1*CPG(1)+XAV2*CPG(2)+XAV3*CPG(4)+XAV5*CPG(9)+
     1    XAV6*CPG(5)+XAV4*CPG(8)+YYN2*CPG(3)
      HS1G=((2.0-2.0/PHI)*(HH(1)-HG(1))+(2.0/PHI-1.)*(HH(2)-
     1       HG(2))-(HH(8)-HG(8))/PHI)*RATE1/AMWC+
```

```
     2 ((HH(1)-HG(1))+(HH(4)-HG(4))-(HH(9)-HG(9))
     C   )*RATE2/AMWC
     3    +(2.0*(HH(1)-HG(1))-(HH(2)-HG(2)))*RATE3/AMWC
     4    +((HH(5)-HG(5))-2.0*(HH(4)-HG(4)))*RATE5/AMWC
      HWGSHF=RATE4*(HG(2)+HG(4)-HG(9)-HG(1))
      CPMIX=XCO*CPG(1)+XCO2*CPG(2)+XH2*CPG(4)+XO2*CPG(8)+XH2O*CPG(9)
     1      +YYN2*CPG(3)/TMOLGA+XCH4*CPG(5)
      TMOMIX=XCO*AMWCO+XCO2*AMWCO2+XH2*AMWH2+XO2*AMWH2+XH2O*AMWH2O+
     1       XN2*AMWN2+AMWCH4*XCH4
      HCON1=1.33E-03*CURLE*(TMOLGA*TMOMIX)**1.092*(CPMIX/TMOMIX)**.3333
     1      /(E*DP**0.575)
C      WRITE(6,332) AAA,DA,Y(7),A1,DA1
C
      CALL RFK(AAA,DA,F,NEQ,Y,HHH,HMAX,ABSERR,RELERR,IFLAG)
C      WRITE(6,332) AAA,DA,Y(7),A1,DA1
332   FORMAT(3X,5E15.7,/)
C
C
      CALL RFK(A1,DA1,F1,NEQ1,Y1,HH1,HMAX1,ABSERR,RELERR,IFLAG)
C
C      WRITE(6,332) AAA,DA,Y(7),A1,DA1
C
C      YY1(I)=Y1(1)
C      YY2(I)=Y1(2)
      IF(Y(1).LE.0.0D 0) Y(1)=1.0D-05
      IF(Y(2).LE.0.0D 0) Y(2)=1.0D-05
      IF(Y(3).LE.0.0D 0) Y(3)=1.0D-05
      IF(Y(4).LE.0.0D 0) Y(4)=1.0D-05
      IF(Y(5).LE.0.0D 0) Y(5)=1.0D-05
      IF(Y(6).LE.0.0D 0) Y(6)=1.0D-05
C
      IF(ISTATE.LT.0.0)GO TO 99
      X(1)=Y(1)/AMWCO
      X(2)=Y(2)/AMWCO2
      X(3)=Y(3)/AMWH2
      X(4)=Y(4)/AMWO2
      X(5)=Y(5)/AMWH2O
      X(6)=Y(6)/AMWCH4
      TGAV=(Y(7)+CCC7)/2.0D 0
C      WRITE(6,618) TG,TGAV,Y(7)
618   FORMAT(5X,'TG=',F8.3,3X,'TGAV=',F8.3,2X,'Y(7)=',F8.3)
      RAT7=(TGAV-TG)/TGAV
      IF(DABS(RAT7).GT.EBS)GO TO 97
 201  TSAV=(Y1(1)+YY1(I))/2.0D 0
      RAT8=(TSAV-TS)/TSAV
      IF(DABS(RAT8).GT.EBS)GO TO 298
202   YCAV=(Y1(2)+YY2(I))/2.0
      RAT9=(YCAV-YC)/YCAV
      IF(DABS(RAT9).GT.EBS)GO TO 199
 203  XAVE1=(X(1)+XX1)/2.0
C      WRITE(6,843) XAV1,XAVE1
 843  FORMAT(3X,'XAV=',D15.7,3X,'XAVE=',D15.7)
      RAT1=(XAVE1-XAV1)/XAVE1
```

```
      IF(DABS(RAT1).GT.EBS)GO TO 91
  204 XAVE2=(X(2)+XX2)/2.0
      RAT2=(XAVE2-XAV2)/XAVE2
      IF(DABS(RAT2).GT.EBS)GO TO 92
  205 XAVE3=(X(3)+XX3)/2.0
      RAT3=(XAVE3-XAV3)/XAVE3
      IF(DABS(RAT3).GT.EBS)GO TO 93
  206 XAVE4=(X(4)+XX4)/2.0
      RAT4=(XAVE4-XAV4)/XAVE4
      IF(DABS(RAT4).GT.EBS)GO TO 94
  207 XAVE5=(X(5)+XX5)/2.0
      RAT5=(XAVE5-XAV5)/XAVE5
      IF(DABS(RAT5).GT.EBS)GO TO 95
  208 XAVE6=(X(6)+XX6)/2.0
      RAT6=(XAVE6-XAV6)/XAVE6
      IF(DABS(RAT6).GT.EBS)GO TO 96
  209 IF(MMM.EQ.2)GO TO 101
      GO TO 98
   91 CONTINUE
      XAV1=XYZ*XAV1+(1.-XYZ)*XAVE1
      MMM=2
      GO TO 204
   92 CONTINUE
      XAV2=XYZ*XAV2+(1.0-XYZ)*XAVE2
      MMM=2
      GO TO 205
   93 CONTINUE
      XAV3=XYZ*XAV3+(1.-XYZ)*XAVE3
      MMM=2
      GO TO 206
   94 CONTINUE
      XAV4=XYZ*XAV4+(1.0-XYZ)*XAVE4
      MMM=2
      GO TO 207
   95 CONTINUE
      XAV5=XYZ*XAV5+(1.0-XYZ)*XAVE5
      MMM=2
      GO TO 208
   96 CONTINUE
      XAV6=XYZ*XAV6+(1.0-XYZ)*XAVE6
      MMM=2
      GO TO 209
   97 CONTINUE
      TG=XYZ*TG+(1.0-XYZ)*TGAV
      MMM=2
      GO TO 201
  199 CONTINUE
      YC=XYZ*YC+(1.0-XYZ)*YCAV
      MMM=2
      GO TO 203
  298 CONTINUE
      TS=XYZ*TS+(1.0-XYZ)*TSAV
      MMM=2
```

```
      GO TO 202
C
C  CALCULATES PARTIAL PRESSURE OF O2, H2O, CO, CO2, H2, CH4
C  FOR RATES CALCULATION.
C
C      WRITE(6,823) PCO,PCO2,PH2,POXY,PSTEAM,PCH4
 98   CONTINUE
      TMOLG=0.0
      DO 18 LL=1,6
  18  TMOLG=TMOLG+X(LL)
      TMOLG=TMOLG+YYN2
      XCO=X(1)/TMOLG
      XCO2=X(2)/TMOLG
      XH2=X(3)/TMOLG
      XO2=X(4)/TMOLG
      XH2O=X(5)/TMOLG
      XCH4=X(6)/TMOLG
      PCO=PT*XCO
      PCO2=PT*XCO2
      PH2=PT*XH2
      POXY=PT*XO2
      PSTEAM=PT*XH2O
      PCH4=PT*XCH4
      XX1=X(1)
      XX2=X(2)
      XX3=X(3)
      XX4=X(4)
      XX5=X(5)
      XX6=X(6)
      TS=Y1(1)
      TG=Y(7)
      CALL WGSHIF(TG,TS,PCO,PSTEAM,PCO2,PH2,PT,RATE4,CKWG,
     1            RATE4M,AGAS,XX1,XX2,XX3,XX5,PEXC,TMASH)
C  CALCULATES FRACTION OF O2, H2O, CO, CO2, H2, CH4 FOR
C  RATES CALCULATIONS
C
C
C  CALCULATES PARTIAL PRESSURE OF O2, H2O, CO, CO2, H2, CH4
C  FOR RATES CALCULATION.
C
C      WRITE(6,823) PCO,PCO2,PH2,POXY,PSTEAM,PCH4
C      WRITE(6,611) RATE41,X(1),X(2),X(3),X(5)
 611  FORMAT(2X,5D20.8)
      X(1)=X(1)-RATE4M
      X(2)=X(2)+RATE4M
      X(3)=X(3)+RATE4M
      X(5)=X(5)-RATE4M
      CCC1=X(1)*AMWCO
      CCC2=X(2)*AMWCO2
      CCC3=X(3)*AMWH2
      CCC4=X(4)*AMWO2
      CCC5=X(5)*AMWH2O
      CCC6=X(6)*AMWCH4
```

```
      CCC7=Y(7)
      TMOLGG=X(1)+X(2)+X(3)+X(4)+X(6)+YYN2+X(5)
      AMOLCO=X(1)/TMOLGG
      AMOCO2=X(2)/TMOLGG
      AMOLH2=X(3)/TMOLGG
      AMOLO2=X(4)/TMOLGG
      AMOCH4=X(6)/TMOLGG
      AMOLN2=YYN2/TMOLGG
      TM=(TS+TG)/2.0
      WGEQC=DEXP(-3.6893+7234./(1.8*TM))
      WGEQP=X(2)*X(3)/(X(5)*X(1))
C      WRITE(6,531) WGEQC,WGEQP
C      WRITE(6,178)I,AMOLCO,AMOCO2,AMOLH2,AMOLO2,Y1(2),AMOLN2,
C    C            TG,TS
      IF(TOUT1.EQ.TPR)GO TO 295
      GO TO 296
  295 CONTINUE
      IF(I.EQ.KK1)WRITE(6,612) TPR
  612 FORMAT(30X,'TIME=',F8.2,/)
      TGAS=9.0/5.0*(Y(7)-273.33)+32.0D 0
      TSOLID=9.0/5.0*(Y1(1)-273.33)+32.0D 0
C      WRITE(6,77) Y(4),Y(1),Y(2),Y(5),Y(7),Y1(1),Y1(2)
      WRITE(6,178)I,AMOLCO,AMOCO2,AMOLH2,AMOLO2,Y1(2),AMOLN2,
      C             TGAS,TSOLID
178    FORMAT(1X,'I=',I2,'MCO=',F8.6,'MCO2=',F8.6,'MH2=',F8.6,
     1 'MO2=',F8.6,'YC=',F8.6,'MN2=',
     1 F8.6,'TG=',F8.3,'TS=',F8.3)
77 FORMAT(2X,'MO2=',E12.4,'MCO=',E11.4,'MCO2=',E11.4,'MH2O='
     1 ,E11.4,'TG=',F8.3,'TS=',F8.3,'YC=',F8.6)
      TM=(TS+TG)/2.0
  531 FORMAT(5X,'WGEQC=',E11.4,4X,'WGEQP=',E11.4)
      IF(I.EQ.NONODE) WRITE(6,134) TMASLF
      IF(I.EQ.NONODE) TPR=TPR+DTPR
  296 CONTINUE
      XCARBC=1.0-Y1(2)**3.0
      TMASCR=TOMASC*XCARBC
      TMASBD=TMASBD+TMASCR
134   FORMAT(2X,'TOTAL MASS OF SOLID IN THE BED=',F15.6,2X,'LB')
      KKK=1
      YY1(I)=Y1(1)
      YY2(I)=Y1(2)
  121 I=I+1
      Y1(1)=YY1(I)
      Y1(2)=YY2(I)
      TMOLG=0.0D 0
      DO 22 LLL=1,6
      TMOLG=TMOLG+X(LLL)
   22 CONTINUE
      TMOLG=TMOLG+YYN2
      XX1=X(1)
      XX2=X(2)
      XX3=X(3)
      XX4=X(4)
```

```
      XX5=X(5)
      XX6=X(6)
      XAV1=XX1
      XAV2=XX2
      XAV3=XX3
      XAV4=XX4
      XAV5=XX5
      XAV6=XX6
      TG=Y(7)
      YC=YY2(I)
      TS=YY1(I)
      TOUT=TOUT+DA
109   CONTINUE
      TMASLF=TMASIN-TMASBD-TMASB
      TMASLF=TMASLF/454.4
C      WRITE(6,134) TMASLF
      TMASBD=0.0D 0
      TOUT1=TOUT1+DA1
      IF(TOUT1.GT.300.0)MOM=1
C      WRITE(6,189)
 189  FORMAT(5X,/,'START NEW INITIAL CONDITION',2X)
      GO TO 811
 42   WRITE(6,119) IWORK(11),IWORK(12),IWORK(13)
 119  FORMAT(/,2X,'NO. STEPS=',I4,2X,'NO. F-S=',I4,2X,
     1'NO. J-S=',I4)
      STOP
  99  WRITE(6,129) ISTATE
 129  FORMAT(///,10X,'ERROR HALT ..ISTATE=',I3)
      STOP
      END
```

```
      SUBROUTINE COMBUS(TG,TS,PT,RP,POXY,YC,RATE1,PHI,DELT,
                        PHOC)
      IMPLICIT REAL*8(A-H,O-Z)
      VOID=0.8
      DP=2.*RP
      TM=(TS+TG)/2.
      Z=2500.*DEXP(-6249./TM)
      IF(DP.LE.5.0E-3) GO TO 105
      IF(DP.LE.0.1) GO TO 306
      GO TO 43
  105  PHI=(2.*Z+2.)/(Z+2.)
      GO TO 40
  306  PHI=((2.0*Z+2.)-Z*(DP-.005)/0.095)/(Z+2.0)
      GO TO 40
   43 PHI=1.
   40 IF(POXY.LE.0.0) GO TO 55
      IF(TS.LT.273) GO TO 55
      BTTS=-17967./TS
      IF(DABS(BTTS).GT.49.) GO TO 33
      EBTTS=DEXP(BTTS)
      GO TO 49
   33 EBTTS=1.E-15
   49 AKS=8710.*EBTTS
      DIFF=(4.26/PT)*(TG/1800.)**1.75
      AKDIFF=(PHI*.292*DIFF)/(DP*TM)
      IF(YC.GE.0.95) GO TO 45
      AKDASH=AKDIFF*(VOID**2.5)
      AKOVER=1./(1./AKDIFF+1./(AKS*YC*YC)+(1./AKDASH)*(1./YC-1.))
      GO TO 50
   45 AKOVER=1./(1./AKDIFF+1./AKS)
   50 RATE1=AKOVER*POXY
      GO TO 66
   55 RATE1=0.0
   66 RETURN
      END
```

```
      SUBROUTINE CBSTM(TG,TS,PSTEAM,PH2,PCO,RP,PT,YC,RATE2
     1,DELT,PHOC)
      IMPLICIT REAL*8(A-H,O-Z)
      VOID=0.8
      DP=2.*RP
      IF(PSTEAM.LT.0.001) GO TO 105
      IF(PH2.LE.0.0) GO TO 305
      IF(PCO.LE.0.0) GO TO 305
      POWER=17.644-30260./(1.8*TS)
      IF(DABS(POWER).GT.16.) GO TO 105
      CSEQK=DEXP(POWER)
      IF(CSEQK.GT.10000.) GO TO 305
      EFFP=PSTEAM-PH2*PCO/CSEQK
      GO TO 6
305     EFFP=PSTEAM
6     IF(EFFP.LE.0.0) GO TO 105
      GO TO 306
105   RATE2=0.0
      GO TO 43
306   TM=(TS+TG)/2.
      IF(TM.LE.200.)GO TO 105
      AA=-21060./TS
      IF(DABS(AA).GT.25.)GO TO 105
      EAA=DEXP(AA)
      AKS=247.*EAA
      AKDIFF=(10.E-4)*(TM/2000.)**0.75/(DP*PT)
      IF(YC.GT.0.95) GO TO 45
      AKDASH=AKDIFF*(VOID**2.5)
      AKOVER=1./(1./AKDIFF+1./(YC*YC*AKS)+(1./AKDASH)*(1./YC-1.))
      GO TO 50
45    AKOVER=1./(1./AKDIFF+1./AKS)
50    RATE2=AKOVER*EFFP
43    RETURN
      END
```

```
      SUBROUTINE CBCO2(TG,TS,PCO2,RP,PT,YC,RATE3,DELT,PHOC)
      IMPLICIT REAL*8(A-H,O-Z)
      VOID=0.8
      DP=2.*RP
      IF(TS.LE.850.) GO TO 105
      IF(PCO2.LE.0.0) GO TO 105
      GO TO 100
  105 RATE3=0.0
      GO TO 200
  100 TM=(TS+TG)/2.
      IF(TM.LE.200.)GO TO 105
      BTS=-21060./TS
      IF(DABS(BTS).GT.25.)GO TO 105
      EBTS=DEXP(BTS)
      AKS=247.*EBTS
      AKDIFF=(7.45E-4)*(TM/2000.)**.75/(DP*PT)
      IF(YC.GE.0.95) GO TO 45
      AKDASH=AKDIFF*(VOID**2.5)
      AKOVER=1./(1./AKDIFF+1./(YC*YC*AKS)+(1./AKDASH)*(1./YC-1.))
      GO TO 50
   45 AKOVER=1./(1./AKDIFF+1./AKS)
   50 RATE3=AKOVER*PCO2
  200 RETURN
      END
```

```
      SUBROUTINE WGSHIF(TG,TS,PCO,PSTEAM,PCO2,PH2,PT,RATE4,CKWG,
     1                  RATE4M,AGAS,XX1,XX2,XX3,XX5,PEXC,TMASH)
      IMPLICIT REAL*8(A-H,O-Z)
C WATER GAS-SHIFT REACTION
      IF(TS.LE.1000.)GO TO 105
      TM=(TG+TS)/2.
      CKWG=DEXP(-3.6893+7234./(1.8*TM))
      PEXC=PCO-PCO2*PH2/(CKWG*PSTEAM)
      A=1.-CKWG
      B=XX2+XX3+CKWG*(XX1+XX5)
      C=XX2*XX3-CKWG*(XX1*XX5)
      D=B*B-4.0*A* C
      IF(D.LT.0.0)GO TO 105
C      IF(PEXC.LT.0.0)GO TO 25
      XX=(-B+DSQRT(D))/(2.0*A)
      GO TO 26
 105   RATE4M=0.0D 0
      GO TO 43
 25   XX=(-B-DSQRT(D))/(2.0*A)
 26   RATE4M=XX
 43   RETURN
      END
```

```
      SUBROUTINE CBHY(TG,TS,PH2,PCH4,RP,PT,RATE5,DELT,
                      PHOC,YC)
      IMPLICIT REAL*8(A-H,O-Z)
      IF(TS.LE.1200.0) GO TO 105
      VOID=0.8
      DP=2.0*RP
      TM=(TS+TG)/2.0
      IF(PH2.LE.0.001)GO TO 105
      IF(PCH4.LE.0.0) GO TO 305
      BTTS=18400.0/(1.8*TS)
      IF(DABS(BTTS).GE.25.0) GO TO 305
      AKEQ=(0.175/34713.)*DEXP(BTTS)
      PEQ=PCH4/AKEQ
      PEQMAX=PH2*PH2
      IF(PEQ.GE.PEQMAX)GO TO 105
      PEQMIN=PEQMAX/10000.0
      IF(PEQ.LE.PEQMIN)GO TO 305
      GO TO 6
  305   PEXC=PH2
      GO TO 7
    6 PEXC=PH2-DSQRT(PEQ)
    7 IF(PEXC.LE.0.001) GO TO 105
      BTS=-17921.0/TS
      IF(DABS(BTS).GE.25.0) GO TO 105
      AKS=0.12*DEXP(BTS)
      AKDIFF=(1.33D-03)*(TM/2000.0)**0.75/(DP*PT)
      IF(YC.GE.0.95) GO TO 306
      AKDASH=AKDIFF*(VOID**2.5)
      AKOVER=1./(1./AKDIFF+1./(YC*YC*AKS)+(1./AKDASH)*(1./YC-1.))
      GO TO 43
  306  AKOVER=1./(1./AKDIFF+1./AKS)
   43 RATE5=AKOVER*PEX C
      GO TO 100
  105  RATE5=0.0
  100 RETURN
      END
```

```
      SUBROUTINE CPH(J,TEMP1,CPG,H2)
      IMPLICIT REAL*8(A-H,O-Z)
C THIS SUBROUTINE CALCULATES MOLAR HEAT CAPACITY AND ENTHALPY OF
C GASES AT TEMPERATURE T
C HFO=HEAT OF FORMATION AT T=298 DEG K
C UNITS OF ENTHALPY ARE CAL/G-MOL
C UNITS OF CP ARE CAL/G-MOL K
C CP=A+B*T+C*T**2.    ***T=DEG K***
C 1=CO,2=CO2,3=N2,4=H2,5=CH4,6=C2H6,7=H2S,8=O2,9=H2O,10=NH3,
C 11=NO,12=SO2
C
C ************************************************************
C
      DIMENSION AA(12),B(12),C(12),HFO(12)
      DATA AA,B,C/7.8122D 00,4.3249D 00,7.7099D 00,6.183D 00,
     C7.9184D 00,1.375D 00,6.662D 00,7.3611D 00,7.9888D 00,
     C7.0405D 00,8.4623D 00,5.9262D 00,
     C-6.6683D 00,20.8089D 00,-5.5039D 00,4.7107D 00,-11.4172D
     C00,41.852D 00,5.134D 00,-5.3696D 00,-1.5063D 00,1.2091D
     C00,-10.4067D 00,14.4706D 00,
     C17.283D 00,-22.9459D 00,13.1214D 00,-10.9215D 00,63.7345D
     C00,-13.827D 00,-0.854D 00,20.5418D 00,6.6661D 00,18.33D
     C00,27.5488D 00,-7.397D 00/
      DATA HFO/-26417.0D 00,-94052.0D 00,0.0D 00,0.0D 00,
     C-17889.0D 00,-20236.0D 00,-4880.0D 00,0.0D 00,-57789.0D 00
     C,-10970.0D 00,21580.0D 00,-70947.0D 00/
      CPG=AA(J)+B(J)*(1.E-3)*TEMP1+C(J)*(1.E-6)*TEMP1*TEMP1
      A1=(TEMP1-298.)
      A2=(TEMP1**2-298.**2)/2.
      A3=(TEMP1**3-298.**3)/3.
      H2=HFO(J)+AA(J)*A1+B(J)*(1.E-3)*A2+C(J)*(1.E-6)*A3
      RETURN
      END
```

```
      SUBROUTINE INPUT
      IMPLICITE REAL *8(A-H,O-Z)
      COMMON /XX/AMOIST,VM,FIXC,ASH,HVCOAL,FC,FH,FO,FN,FS,FASH,
     1          COAL,AIR,STEAM,TCOAL,TAIR,TSTEAM,XL,DIA,HSTEAM
      AMOIST=0.8
      VM=1.5
      FIXC=84.1
      ASH=13.6
      HVCOAL=12071.0
      FC=0.832
      FH=.0027
      FO=.0104
      FN=.0102
      FS=.0078
      FASH=.133
      COAL=35.
      STEAM=50.
      AIR=36.
      TCOAL=77.
      TAIR=140.
      TSTEAM=312.
      XL=13./12.
      DIA=13./12.
      WRITE(6,11) AMOIST,VM,FIXC,ASH,HVCOAL
   11 FORMAT(1X,'****** PROXIMATE ANALYSIS ******',/,1X,
     1'MOISTURE=',F6.3,/,1X,'VOLATILE MATTER=',F6.3,/,1X,
     1'FIXC=',F6.3,/,1X,'ASH=',F6.3,/,1X,'HEATING VALUE='
     1,F8.2,/)
      WRITE(6,12) FC,FH,FO,FN,FS,FASH
   12 FORMAT(1X,'****** ULTIMATE ANALYSIS ******',/,1X,'CARBON=',
     1F6.4,/,1X,'HYDROGEN=',F6.4,/,1X,'OXYGEN=',F6.4,/,1X,
     1'NITROGEN=',F6.4,/,1X,'SULFUR=',F6.4,/,1X,'ASH=',F6.4,/)
      WRITE(6,13) COAL,AIR,STEAM,TCOAL,TAIR,TSTEAM
   13  FORMAT(1X,'COAL FEED RATE =',F10.3,2X,'LB/HR',/,1X,
     1'AIR FEED RATE=',F10.3,2X,'LB/HR',/,1X,'STEAM FEED RATE='
     1,F10.3,2X,'LB/HR',/,1X,'TEMP OF COAL=',F10.3,2X,'F',/,1X,
     1'TEMP OF AIR=',F10.3,2X,'F',/,1X,'TEMP OF STEAM=',F10.3,
     1 2X,'F',/)
      WRITE(6,14) DIA,XL
   14 FORMAT(1X,'DIAMETER OF GASIFIER=',F10.3,2X,'FT',/,1X,
     1'LENGTH OF THE BED=',F10.3,2X,'FT',/)
      RETURN
      END
```

```
      SUBROUTINE PRESUR(PV,TAIR)
      IMPLICIT REAL*8(A-H,O-Z)
      DIMENSION FF(10)
      FF(1)=-741.9242
      FF(2)=-29.721
      FF(3)=-11.55286
      FF(4)=-0.8685635
      FF(5)=0.1094098
      FF(6)=0.439993
      FF(7)=0.2520658
      FF(8)=0.0522
      TC=5./9.*(TAIR-32.)
      SUM=FF(1)
      DO 23 K=2,8
      SUM=SUM+FF(K)*(6.5D-01-0.01*TC)**(K-1)
   23 CONTINUE
      TT=1000.0D 0/(TC+273.2D 0)
      TCR=374.136
      PCR=3204.0 D0
      POWER=TT*(TCR-TC)*1.0D-05*SUM
      PV=PCR*DEXP(POWER)
      RETURN
      END
```

```
      SUBROUTINE INTIAL(YY1)
      IMPLICIT REAL*8(A-H,O-Z)
      DIMENSION YY1(100)
      F01=2440.0
      F2=2360.0
      F3=2290.
      F4=2220.0
      F5=2150.0
      F6=2080.0
      F7=2000.0
      F8=1940.0
      F9=1860.0
      F10=1780.0
      F11=1710.0
      F12=1640.0
      F13=1560.0
      F14=1500.0
      F15=1430.0
      F16=1360.0
      F17=1280.0
      F18=1220.0
      F19=1140.0
      F20=1080.0
      F21=1000.0
      F22=930.0
      F23=860.0
      F24=780.0
      F25=700.0
      F26=650.0
C
C CHANGE THE LOCAL TEMPERATURE FROM DEG F TO DEG K
C
      YY1(1)=5./9.*(F01-32.)+273.33
      YY1(2)=5./9.*(F2-32.)+273.33
      YY1(3)=5./9.*(F3-32.)+273.33
      YY1(4)=5./9.*(F4-32.)+273.33
      YY1(5)=5./9.*(F5-32.)+273.33
      YY1(6)=5./9.*(F6-32.)+273.33
      YY1(7)=5./9.*(F7-32.)+273.33
      YY1(8)=5./9.*(F8-32.)+273.33
      YY1(9)=5./9.*(F9-32.)+273.33
      YY1(10)=5./9.*(F10-32.)+273.33
      YY1(11)=5./9.*(F11-32.)+273.33
      YY1(12)=5./9.*(F12-32.)+273.33
      YY1(13)=5./9.*(F13-32.)+273.33
      YY1(14)=5./9.*(F14-32.)+273.33
      YY1(15)=5./9.*(F15-32.)+273.33
      YY1(16)=5./9.*(F16-32.)+273.33
      YY1(17)=5./9.*(F17-32.)+273.33
      YY1(18)=5./9.*(F18-32.)+273.33
      YY1(19)=5./9.*(F19-32.)+273.33
      YY1(20)=5./9.*(F20-32.)+273.33
      YY1(21)=5./9.*(F21-32.)+273.33
```

```
YY1(22)=5./9.*(F22-32.)+273.33
YY1(23)=5./9.*(F23-32.)+273.33
YY1(24)=5./9.*(F24-32.)+273.33
YY1(25)=5./9.*(F25-32.)+273.33
YY1(26)=5./9.*(F26-32.)+273.33
RETURN
END
```

```
      SUBROUTINE GAS(CPH,X,AGAS,YYN2,TG,TG1)
      IMPLICIT REAL*8(A-H,O-Z)
      DIMENSION CP(12),X(10),HH(12)
      TGP=1200.00
      TG=TGP
      TG1=TG
      TGR=333.33
      TGRCH4=298.0
      DO 912 J1=1,12
      CALL CPH(J1,TGP,CP(J1),HH(J1))
912   CONTINUE
      HO2P=HH(8)
      HN2P=HH(3)
      HCO2P=HH(2)
      HH2OP=HH(9)
      HO2R=HH(8)
      DO 914 JJ1=1,12
      CALL CPH(JJ1,TGR,CP(JJ1),HH(JJ1))
 914  CONTINUE
      HO2333=HH(8)
      HN2333=HH(3)
      DO 918 J11=1,12
      CALL CPH(J11,TGRCH4,CP(J11),HH(J11))
 918  CONTINUE
      HCH4R=HH(5)
      XXAIR=(2.0*HO2P-HCO2P-2.0*HH2OP+HCH4R+3.76*HN2333)/
     1      (HO2P+3.76*HN2P-HO2333)
      AIRFUL=XXAIR
      X(1)=1.0D-06
      X(2)=1.0/AGAS
      X(3)=1.0D-06
      X(4)=(XXAIR-2.)/AGAS
      X(5)=2.0/AGAS
      X(6)=1.0D-06
      YYN2=3.76*XXAIR/AGAS
      RETURN
      END
```

```
      SUBROUTINE F(AAA,Y,YDOT,NEQ)
      IMPLICIT REAL*8(A-H,O-Z)
      DIMENSION Y(NEQ),YDOT(NEQ)
      COMMON /NON/AREA,BBB,AMWO2,AMWH2O,AMWH2,AMWCO,AMWCO2,AMWCH4
     1        ,RATE1,RATE2,RATE3,RATE5,PHI,CKWG,CSEQK,HS2G
      COMMON /CC/RATEO2,RATH2O,RATCO2,RATECO,RATEH2,RATCH4,YC
     1  ,RATEC,RP,PHOC,TG,TS,HCON1,CPS1,HRT,A,E,HS1G,HWGSHF,SUM
C      WRITE(6,3)  SUM,HS1G,TG,TS,HCON1
 3    FORMAT(1X,'SUM=',E12.4,1X,'HEATRG=',E12.4,1X,'TG=',2E12.4,
     11X,'HCON=',E12.4)
      YDOT(1)=A/E*RATECO
      YDOT(2)=A/E*RATCO2
      YDOT(3)=A/E*RATEH2
      YDOT(4)=A/E*RATEO2
      YDOT(5)=A/E*RATH2O
      YDOT(6)=A/E*RATCH4
      YDOT(7)=(A/E*HCON1*(TS-TG)+A/E*HS1G+A/E*HWGSHF)/SUM
      RETURN
      END
```

```
      SUBROUTINE F1(A1,Y1,YDOT1,NEQ1)
      IMPLICIT REAL*8(A-H,O-Z)
      DIMENSION Y1(NEQ1),YDOT1(NEQ1)
      COMMON /NON/AREA,BBB,AMWO2,AMWH2O,AMWH2,AMWCO,AMWCO2,AMWCH4
     1       ,RATE1,RATE2,RATE3,RATE5,PHI,CKWG,CSEQK,HS2G
      COMMON /CC/RATEO2,RATH2O,RATCO2,RATECO,RATEH2,RATCH4,YC
     1 ,RATEC,RP,PHOC,TG,TS,HCON1,CPS,HRT,A,E,HS1G,HWGSHF,SUM
C      WRITE(6,623) RATEO2,RATH2O,RATCO2,RATECO,RATEH2,RATCH4
623   FORMAT(1X,6D17.7,'HERE',1X)
      YDOT1(1)=(A*HCON1/(1.0-E)*(TG-TS)-A/(1.-E)*HS2G)/(PHOC*CPS)
      YDOT1(2)=(-A/(3.0*(1.0-E)*PHOC*YC**2.)*(RATE1+RATE2+RATE3+
     1            RATE5))
      RETURN
      END
```

```
      SUBROUTINE RFK(A,DA,F,N,Y,H,HMX,ABSERR,RELERR,IFLAG)
C
C  Y : ON INPUT THE VECTOR OF INITIAL VALUES
C      ON OUTPUT  VECTOR OF COMPUTED SOLUTION AT A.
C  N : NUMBER OF FIRST ORDER EQUATIONS.
C  F : SUBROUTINE F(A,Y,YP,N) COMPUTES VECTOR OF DERIVATIVES YP
C       FOR A AND VECTOR Y Y OF DEPENDENT VARIABLES.
C  DA  : INTEGRATION IS FROM A TO A+DA.DA CAN BE NEGATIVE.
C  H   : INTIAL GUESS FOR STEP SIZE.WILL BE CHANGED TO MEET
C        TOLERANCE.
C  HMX : POSITIVE UPPER BOUND  ON STEP SIZE.
C  ABSERR : BOUNDS ON ABSOLUTE ERRORS.
C  RELERR : BOUNDS ON RELATIVE ERRORS.
C  IFLAG  : REPORTS SUCCESS(1) , FAILURES(2-4).
C
       IMPLICIT REAL *8(A-H,O-Z)
      DIMENSION Y(N),YTEMP(25),R(25)
      REAL*8 K1(25),K2(25),K3(25),K4(25),K5(25),K6(25)
      DATA U/9.0D-14/
C
C   TEST INPUT
C
       IF(RELERR.LT.0.0.OR.ABSERR.LT.0.0.OR.ABSERR+
     1 RELERR.EQ.0.0.OR.HMX.LE.0.0)GO TO 18
       B=A+DA
       IF (DABS(DA).LE.13.0*U*DMAX1(DABS(A),DABS(B))) GO TO 19
       HMAX=DMIN1(HMX,DABS(DA))
       IF(DABS(H).LE.13.0*U*DABS(A))H=HMAX
       KOUNT=0
       IADJUS=0
3      H=DSIGN(DMIN1(DABS(H),HMX),DA)
       IF(DABS(B-A).GT.1.25*DABS(H))GO TO 4
       HKEEP=H
       IADJUS=1
       H=B-A
C
C   START CALCULATION
C
4      CALL F(A,Y,K1,N)
       KOUNT=KOUNT+1
305      CONTINUE
       DO 6 I=1,N
6      YTEMP(I)=Y(I)+0.25*H*K1(I)
       ARG=A+0.25*H
       CALL F(ARG,YTEMP,K2,N)
       DO 7 I=1,N
7      YTEMP(I)=Y(I)+H*(K1(I)*(3.0/32.0)+K2(I)*(9.0/32.0))
       ARG=A+H*(3.0/8.0)
       CALL F(ARG,YTEMP,K3,N)
       DO 8 I=1,N
8      YTEMP(I)=Y(I)+H*(K1(I)*(1932.0/2197.0)-K2(I)*
     1 (7200.0/2197.0)+K3(I)*(7296.0/2197.0))
       ARG=A+H*(12.0/13.0)
```

```
      CALL F(ARG,YTEMP,K4,N)
      DO 9 I=1,N
9     YTEMP(I)=Y(I)+H*(K1(I)*(439.0/216.0)-8.0*K2(I)+
     1 K3(I)*(3680.0/513.0)-K4(I)*(845.0/4104.0))
      ARG=A+H
      CALL F(ARG,YTEMP,K5,N)
      DO 105 I=1,N
105    YTEMP(I)=Y(I)+H*(2.0*K2(I)-K1(I)*(8.0/27.0)-K3(I)*
     1 (3544.0/2565.0)+K4(I)*(1859.0/4104.0)-K5(I)*(11.0/40.0))
      ARG=A+.5*H
      CALL F(ARG,YTEMP,K6,N)
      DO 11 I=1,N
      TEMP=K1(I)*(25.0/216.0)+K3(I)*(1408.0/2565.0)+K4(I)*
     1 (2197.0/4104.0)-0.2*K5(I)
11    YTEMP(I)=Y(I)+H*TEMP
C
C  CHECK ACCURACY
C
      DO 12 I=1,N
12    R(I)=K1(I)/360.0-K3(I)*(128.0/4275.0)-K4(I)*
     1 (2197.0/75240.0)+K5(I)/50.0+K6(I)*(2.0/55.0)
      RATIO=0.0
      DO 13 I=1,N
      TR=DABS(R(I))/(RELERR*DABS(YTEMP(I))+ABSERR)
13    RATIO=DMAX1(RATIO,TR)
      IF(RATIO.GT.1.0) GO TO 15
      DO 14 I=1,N
14    Y(I)=YTEMP(I)
      A=A+H
      IF(IADJUS.EQ.1) GO TO 16
C
C      CHANGE STEP SIZE
C
      RATIO=DMAX1(RATIO,6.5536D-4)
15    RATIO=DMIN1(RATIO,409.60D+1)
      H=.8*H/DSQRT(DSQRT(RATIO))
      IF(DABS(H).LE.13.0*U*DABS(DA)) GO TO 19
      KOUNT=KOUNT+5
      IF (KOUNT.GE.2995) GO TO 17
      IF (RATIO.LE.1.0 ) GO TO 3
      IADJUS=0
      GO TO 305
16    IFLAG=1
      H=HKEEP
      RETURN
17    IFLAG=2
      WRITE (6,30)
  43  FORMAT (5X,'MORE THAN 3000 EVALUATION')
      RETURN
18    IFLAG=3
      WRITE (6,40)
  40  FORMAT (5X,'ILLEGAL INPUT')
      RETURN
```

```
19    IFLAG=4
      WRITE (6,50)
   50 FORMAT (5X,'STEP SIZE TOO SMALL')
      RETURN
      END
```

APPROVAL OF EXAMINING COMMITTEE

Eugene V. Cilento
Dr. Eugene V. Cilento

John T. Jurewicz
Dr. John T. Jurewicz

Massood Ramezan
Dr. Massood Ramezan

Charles F. Stanley
Dr. Charles F. Stanley

John W. Zondlo
Dr. John W. Zondlo

Nov 14 1986
Date

Eric K. Johnson
Dr. Eric K. Johnson (Chairman)